Characterisation of Substance P and Transient Receptor Potential Melastatin Channel Messenger RNA and Protein Expression in Acute and Chronic Neurological Disorders

Naomi L. Cook
BMedSc (Hons)

Discipline of Pathology,
School of Medical Sciences,
The University of Adelaide

December, 2009

A thesis submitted in partial fulfilment of the requirements for the degree of Doctor of Philosophy

Chapter 1

Introduction

1.1 Acute Neurological Disorders

Traumatic brain injury (TBI) represents a significant public health burden, and is the acute neurological disorder focused upon in the present thesis. This section will review current literature regarding the epidemiology, pathogenesis and treatment strategies of TBI. Particular emphasis will be placed on the role of magnesium and neuropeptides in TBI pathophysiology.

1.2 Traumatic Brain Injury

1.2.1 Epidemiology

Traumatic injury to the central nervous system (CNS) is the leading cause of death and disability in people under 40 years of age (Fleminger and Ponsford, 2005). Motor vehicle incidents account for the majority of severe TBI cases, whereas falls, sporting and recreation accidents and assault are responsible for most mild to moderate injuries (Tate et al., 1998). Worldwide incidence rates of TBI are estimated at 150-200 cases per 100,000 population per annum (León-Carrión et al., 2005), with incidence peaks in early childhood, late adolescence/early adulthood and in the elderly (Bruns Jr. and Hauser, 2003). In Australia, the highest incidence of TBI occurs in people aged 15-19 (284 per 100,000) and the lowest in the age group of 45-64 years (69 per 100,000) (Fortune and Wen, 1999). Males are at a higher risk of experiencing TBI than females in all age groups. There are an estimated 50,000 TBI-related deaths per annum in the USA (Bramlett and Dietrich, 2004). TBI therefore constitutes a significant socioeconomic burden. Despite attempts to develop a neuroprotective therapy for TBI, no effective treatment is currently available, and survivors are often left with debilitating neurologic deficits that require long-term rehabilitation (Vink and Nimmo, 2009).

1.2.2 Pathology

TBI can be defined as craniocerebral trauma associated with decreased level of consciousness, amnesia, other neurological or neuropsychological abnormalities, skull fracture, intracranial lesions or death (Hirtz et al., 2007). The neurological dysfunction resulting from TBI is due to both direct, immediate mechanical damage to brain tissue (the primary injury) and indirect, delayed (secondary) injury mechanisms

(Morales et al., 2005). Neuronal death in TBI is likely to involve both necrotic and apoptotic pathways (Liou et al., 2003). The primary event in TBI is irreversible and may comprise both focal and diffuse lesions, including contusions, lacerations and diffuse axonal injury (DAI) (Gentile and McIntosh, 1993). Preventative measures such as airbags, helmets, and road traffic initiatives (e.g. driver education campaigns) have been introduced in an attempt to reduce the incidence of primary injury (Khan et al., 2003).

In contrast, secondary injury involves series of complex biochemical changes that are triggered by the primary event and may continue for days to weeks after the insult (Roth and Farls, 2000). These changes include blood-brain barrier (BBB) disruption, oedema, ischaemia, hypertension, inflammation, excitotoxicity, oxidative stress and dysfunction of ion homeostasis, all of which can be deleterious to neuronal cells (Barone and Kilgore, 2006; Golding, 2002; Cormio et al., 1997; Gentile and McIntosh, 1993). To provide an example of the secondary injury cascade, shearing of nerve fibres at the time of insult results in massive ion fluxes across cell membranes, loss of membrane potential and rapid release of neurotransmitters from damaged neurons. This may result in excitotoxicity, which can evoke an inflammatory response, thereby stimulating further processes (such as the changes described above), eventually leading to cell death (Vink and Van Den Heuvel, 2004). Secondary injury is associated with significant morbidity and mortality following TBI (Gentile and McIntosh, 1993), but given that it manifests over time, this provides an opportunity to administer a pharmacological agent to impede or prevent further injury and thus improve outcome. Several injury processes relevant to TBI will be discussed in this section, including DAI, oedema, oxidative stress, mitochondrial dysfunction, inflammation and magnesium decline.

Diffuse Axonal Injury

DAI is a principal cause of coma following TBI, and significantly contributes to TBI-related morbidity and mortality (Li and Feng, 2009). Classically, DAI was categorised as a primary injury, whereby axons are torn and rupture at the time of insult (Adams et al., 1982). However, more recent evidence suggests that DAI is triggered at the time of injury by inertial forces and may evolve over a period of hours to days, progressing from focal disruptions to axons to impaired axonal transport, axolemmal swelling and, ultimately, axonal disconnection (Mazzeo et al., 2009; Büki and Povlishock, 2006; Stone et al., 2004). DAI is generally diagnosed at post-mortem by immunostaining for β-amyloid precursor protein (APP) (Gentleman et al., 1993), although recent imaging advances may allow its detection at an earlier stage (Li and Feng, 2009).

Oedema

Cerebral oedema is defined as an abnormal accumulation of fluid within the brain parenchyma, resulting in a volumetric enlargement (swelling) of brain tissue (Heo et al., 2005). Swollen tissues may exert harmful effects by increasing pressure in surrounding tissues, leading to ischaemia and additional oedema (Simard et al., 2007a). Swelling has particularly dele-

terious consequences in the brain, due to the fact that the volume of the intracranial cavity is fixed (Ayata and Ropper, 2002). The resulting rise in intracranial pressure (ICP) with cerebral oedema formation is a potentially lethal process (Kimelberg, 1995). Indeed, cerebral oedema plays an important role in the outcome of TBI victims: uncontrolled brain swelling with the accompanying rise in ICP is the leading cause of death in TBI patients (Marmarou et al., 2000).

Cerebral oedema is classified as cytotoxic and vasogenic, depending upon whether or not BBB permeability is increased (Verlooy and Van Reempts, 2005). The BBB is composed of a monolayer of endothelial cells forming tight junctions that prevent the direct interaction of the peripheral circulation with the CNS (Palmer, 2010). Cytotoxic oedema refers to the movement of water, Na^+ and Cl^- from the extracellular to the intracellular space, which results in cell swelling and predisposes cells to oncotic cell death. However, cytotoxic oedema does not involve increases in BBB permeability, nor does it contribute to the actual net increase in brain water (Simard et al., 2007a; Ayata and Ropper, 2002). Conversely, vasogenic oedema is associated with the degradation of tight junctions between endothelial cells of the BBB (Heo et al., 2005). Consequently, the BBB becomes more permeable to macromolecules and permits the movement of fluid from capillaries to the extravascular compartment (Simard et al., 2007a; Heo et al., 2005); hence vasogenic oedema causes a net increase in brain water content (Ayata and Ropper, 2002). In TBI, the increase in BBB permeability may occur by mechanical injury, autodestructive mediators or both (Unterberg et al., 2004). However, despite the potentially lethal consequences of oedema in TBI, there is currently no effective therapy to prevent its formation or progression. Treatments such as mannitol, corticosteroids, barbiturates, induction of hypothermia, drainage of the cerebrospinal fluid (CSF) and surgical decompression (Ayata and Ropper, 2002; Clausen and Bullock, 2001) have had limited success in managing rises in ICP (Vink and Van Den Heuvel, 2004).

Neurogenic inflammation is a local inflammatory reaction of neurons in response to infection, toxins or trauma, which is characterised by vasodilation, plasma extravasation and oedema (Turner et al., 2006; Ro et al., 2005; Black, 2002). Studies from our laboratory (Nimmo et al., 2004; Vink et al., 2003) have shown that neurogenic inflammation may be involved in the formation of vasogenic oedema and the functional deficits following diffuse TBI in rats, and that the neuropeptide, substance P (SP, discussed in Section 1.6), is a potent initiator of neurogenic inflammation. Further research from our laboratory (Donkin et al., 2009) has demonstrated that a SP receptor antagonist inhibits BBB breakdown and oedema formation, and significantly improves long-term functional outcome and motor deficits resulting from TBI. These important results may provide a novel pharmacological treatment for TBI.

Oxidative Stress

Reactive oxygen species (ROS) comprise a range of chemical entities, including hydroxyl radicals, peroxynitrite, superoxide anions, hydrogen peroxide, nitric oxide and singlet oxygen (Ellis, 2007; Chong et al.,

2005). ROS are highly reactive molecules, possessing one or more unpaired electrons in their outer orbits (Halliwell, 1992). While some ROS are normal by-products of cellular metabolism (Yu, 1994), their overproduction can lead to cell injury and tissue damage via reactions with proteins, lipids and nucleic acids, and cellular activation by ROS induces signalling cascades that lead to rises in intracellular Ca^{2+} concentrations (Massullo et al., 2006; Alexandrova and Bochev, 2005). When ROS are generated in excess of endogenous antioxidant mechanisms, the result is oxidative stress (Finkel and Holbrook, 2000).

Brain tissue is highly susceptible to damage by oxidative stress for a number of reasons. The brain has a high rate of oxygen metabolism, which increases the likelihood of excess ROS production (Chong et al., 2005). Furthermore, it contains high levels of polyunsaturated fatty acids, which are particularly vulnerable to damage by free radicals (Halliwell, 1992). Critically, the brain has relatively low antioxidant and repair capacities compared with other organs (Vink and Nimmo, 2009). All of these factors render brain tissue extremely sensitive to increases in ROS, and oxidative stress is indeed relevant to TBI. Studies demonstrate that the production of ROS is enhanced following TBI, and this is accompanied by an impairment of antioxidant defences (Ansari et al., 2008; Lima et al., 2008). TBI-induced oxidative stress can lead to cytoskeletal damage, mitochondrial dysfunction and altered signal transduction, which can be deleterious to neuronal and vascular cells (Ansari et al., 2008; Chong et al., 2005).

Mitochondrial Dysfunction

Mitochondria are organelles that are present in all cells and play a critical role in regulating cellular energy production via the electron transport chain (Mazzeo et al., 2009; Bayir and Kagan, 2008). Consequently, it would be expected that disruption to mitochondrial function would have serious adverse consequences to cells, particularly those with a high energy demand, such as neurons. Indeed, mitochondrial dysfunction is an important factor in TBI pathophysiology that can lead to energy depletion, free radical release and apoptosis, or programmed cell death (Vink and Nimmo, 2009). In experimental TBI, alterations in mitochondrial function have been reported within hours of injury and may persist for days (Robertson, 2004). Furthermore, in clinical TBI studies, patients with profound mitochondrial dysfunction have a poor outcome (Signoretti et al., 2008).

As discussed, TBI leads to conditions of oxidative stress. Oxidative stress directly contributes to mitochondrial dysfunction, promoting the release of cytochrome c from the inner membrane of the mitochondrion, which triggers an apoptotic cascade involving caspases and other pro-apoptotic proteins (Bayir and Kagan, 2008; Chong et al., 2005). Mitochondria also constitute an important intracellular source of ROS, which are produced during the synthesis of ATP (Kowaltowski et al., 2009). During states of electron transport chain dysregulation, as may occur following TBI, there is an increase in the production of ROS (Bayir and Kagan, 2008). Mitochondria have also been implicated in glutamate-mediated excitotoxic-

ity, by participating in the release of glutamate, Ca^{2+} sequestration and the generation of ROS (Nicholls and Budd, 2000).

Inflammation

The inflammatory response represents another important secondary injury process of TBI. TBI-induced inflammation may be beneficial in the short term, by removing cellular debris or promoting regeneration, however, in excess, inflammatory responses can have severe deleterious effects that lead to neurodegeneration (Vink and Nimmo, 2009; Maas et al., 2008). Inflammation can occur within the neural tissue, where activated microglia and astrocytes release cytokines, chemokines and ROS. There is also evidence that the complement system is activated following TBI (Stahel et al., 1998). Furthermore, disruption to the BBB in response to brain insult is associated with the transmigration of leukocytes to the area of damage, which themselves produce cytokines (Jain, 2008). Indeed, levels of the pro-inflammatory cytokines, tumour necrosis factor (TNF)-α and interleukin (IL)-1β are elevated following experimental TBI (Fan et al., 1996, 1995), and may act synergistically to exacerbate the neuroinflammatory response and excitotoxicity (Morganti-Kossmann et al., 2007). On the other hand, anti-inflammatory cytokines, such as IL-10 and transforming growth factor (TGF)-β, may exert neuroprotective effects in TBI (Knoblach and Faden, 1998) by suppressing the actions of TNF-α and IL-1β (Benveniste et al., 1995). Finally, IL-6 may act either to promote or inhibit inflammation in different situations, exemplifying the complexity of the neuroinflammatory pathways associated with TBI (Morganti-Kossmann et al., 2007).

Magnesium Decline

Magnesium has been implicated as a crucial component of the secondary injury cascade that follows TBI. A significant decline in serum ionised magnesium (Mg^{2+}) levels has been demonstrated in TBI patients, with the magnitude of Mg^{2+} decline correlating with severity of TBI (Kahraman et al., 2003). A decrease in brain intracellular free Mg^{2+} concentration has also been shown after TBI in rats, and this is associated with the development of neurological deficits (Heath and Vink, 1996; Vink et al., 1988). Another study (Saatman et al., 2001) examined the consequences of magnesium deficiency prior to TBI in rats, and found that the Mg^{2+}-deficient group had significantly greater cortical cell loss compared to the vehicle group, as well as cytoskeletal alterations in cortical and hippocampal neurons. These results suggest that magnesium deficit is associated with poor neurological outcome following TBI.

Accordingly, several groups have investigated whether Mg^{2+} administration reduces the mortality and morbidity associated with TBI. Saatman et al. (2001) found that post-TBI Mg^{2+} administration in rats significantly reduced cortical cell loss compared to the vehicle group. Another study (Bareyre et al., 1999) showed that magnesium chloride attenuated the neurological motor deficits in brain-injured rats. Research conducted in our laboratory with magnesium salts (Turner et al., 2004) has also demonstrated a neuroprotective effect of Mg^{2+} following TBI. Similar results have also been obtained by other

studies (Browne et al., 2004; Fromm et al., 2004; McIntosh et al., 1989). Therefore, there exists substantial evidence that Mg^{2+} decline plays a role in the secondary injury cascade of TBI and that administration of magnesium salts is neuroprotective in experimental TBI in rats. Mg^{2+} has been shown to improve neurological outcome when administered up to 24 hours after injury (Hoane and Barth, 2002), however the best results have been achieved when the therapeutic window is restricted to 12 hours (Vink and Cernak, 2000). The study by Heath and Vink (1996) found that the Mg^{2+} decline persisted for at least 4 days after injury. However, the concentration of Mg^{2+} in CNS injury has been shown never to fall below 0.2 mM (Vink et al., 1988). Thus, it is likely that the length of time for which free Mg^{2+} concentration is reduced, rather than the magnitude of decline, is the parameter that influences neurological outcome (Vink and Cernak, 2000).

Despite the positive results obtained using Mg^{2+} as a therapy for TBI in animal models, a recent Phase III clinical trial (Temkin et al., 2007) found that $MgSO_4$ given to patients for 5 days after traumatic brain injury was not neuroprotective and possibly even had a negative effect on outcome. Given that all patients (including the control group) received Mg^{2+} to restore depleted serum levels to normal, it is unclear whether this restoration of serum Mg^{2+} level was sufficient to confer positive effect in all patients irrespective of the treatment group. This result was in marked contrast to the clinical trial reported by Dhandapani et al. (2008) which reported that acute Mg^{2+} administration (less than 24 h) resulted in significant improvements in neurological outcome, post-operative brain swelling and 1-month mortality.

Importantly, pharmacological interventions that have improved motor outcome following TBI have increased levels of free Mg^{2+} in the brain (Vink and Cernak, 2000). Indeed, a study from our laboratory (Vink et al., 2004) found that treatment with a SP receptor antagonist after TBI in rats augmented intracellular Mg^{2+} concentration in the brain. The molecular and cellular mechanisms whereby Mg^{2+} improves neurological outcome in TBI are not completely understood, although several mechanisms have been proposed. Prior to discussing these, a section outlining the vital physiological role fulfilled by magnesium has been included.

1.2.3 Physiological Role of Magnesium

Functions

Magnesium (Mg) is the second most abundant intracellular cation after potassium (Ebel and Günther, 1980), and the fourth most common cation in mammals (Fawcett et al., 1999). The concentration of total Mg is between 14 - 20 mM in most cells (Romani, 2007), and the majority of cellular Mg is complexed with molecules such as adenine nucleotides, which bind to the cation with high affinity (Wolf, 2004). Therefore, only a small fraction (around 0.5 mM) of total Mg is present in its ionised form (Mg^{2+}) (Saris et al., 2000).

Mg^{2+} is required for the functioning of a large number of enzymes, therefore playing a vital role in cellular processes (Ebel and Günther, 1980). For example, almost all enzymes involved in transcription, translation and replication of nucleic acids require Mg^{2+}

as an essential cofactor for optimal activity (Black and Cowan, 1995). In addition, Mg^{2+} is necessary for all reactions that either consume or produce ATP, including glycolysis, oxidative phosphorylation and cellular respiration (Van Den Heuvel and Vink, 2004). Mg^{2+} also plays an important role in protein synthesis (Terasaki and Rubin, 1985), the cell cycle and normal neuronal functioning (Fawcett et al., 1999) and is often referred to as a physiological calcium blocker (Iseri and French, 1984). Indeed, cytosolic Mg^{2+} has recently been demonstrated to inhibit Ca^{2+} uptake by mitochondria (Szanda et al., 2009). Furthermore, Mg^{2+} maintains the stability, integrity and normal function of the cell membrane, and is essential for the activity of the membrane sodium-potassium pump (Na^+/K^+-ATPase) (Bara and Guiet-Bara, 1984). Mg^{2+} also modulates other ion transport pumps, carriers and channels, and therefore is likely to be involved in the regulation of signal transduction and the intracellular concentrations of ions such as K^+ and Ca^{2+} (Saris et al., 2000).

Neuroprotection in TBI

Since magnesium plays so many important physiological roles, it is clear that a decline in Mg^{2+} concentration, such as that resulting from TBI, will adversely affect normal cellular functioning, the maintenance of membrane potential and the capacity for cells to undergo repair (Vink and Cernak, 2000). Therefore, it is not surprising that several groups have investigated Mg^{2+} as a potential multifactorial therapy for TBI (reviewed in the previous section), since it is able to modulate many processes of the secondary injury cascade. With reference to these secondary injury factors, magnesium ions are able to modulate excitotoxic processes by blocking voltage- and ligand-gated Ca^{2+} channels, in particular the N-methyl-D-aspartate receptors (NMDAR) (Royo et al., 2003). Mg^{2+} treatment following TBI in rats has been shown to reduce apoptosis and the expression of p53-related (apoptosis-inducing) proteins (Lee et al., 2004) as well as modulating levels of Bax and Bcl-2, which are also regulators of apoptosis (Ravishankar et al., 2001). Mg^{2+} may also have protective effects on the BBB, thereby reducing the formation of vasogenic oedema (Van Den Heuvel and Vink, 2004). It has also been demonstrated that Mg^{2+} inhibits the formation of ROS (Blache et al., 2006). Finally, Mg^{2+} preserves mitochondrial membrane potential and has been shown to improve oxidative phosphorylation and decrease lactic acid production when administered post-TBI (Van Den Heuvel and Vink, 2004). Therefore, despite the disappointing results of Phase III clinical trials of $MgSO_4$ in TBI (Temkin et al., 2007), Mg^{2+} may still exert a beneficial neuroprotective effect for TBI patients as part of a combination drug treatment strategy.

Deficiency

The refinement and processing of magnesium-rich foods such as wholegrains and vegetables has resulted in a decrease in dietary Mg consumption over the last century (Eby and Eby, 2006). A number of diseases have been associated with low Mg^{2+} levels, including atherosclerosis (Maier et al., 2004; Maier, 2003), diabetes (Blache et al., 2006), metabolic syndrome

(Guerrero-Romero and Rodríguez-Morán, 2006), depression, headache, insomnia (Eby and Eby, 2006) and Guamanian amyotrophic lateral sclerosis and Parkinsonism-dementia complex (Hermosura et al., 2005).

In rats, Mg^{2+} deficiency impairs antioxidant defences (Blache et al., 2006) and evokes an inflammatory response (Malpuech-Brugère et al., 2000), including the release of pro-inflammatory cytokines and SP (Mazur et al., 2006). Indeed, within one week of Mg^{2+} deficiency, plasma SP concentration was elevated (Weglicki and Phillips, 1992), which was associated with the development of neurogenic inflammation (Weglicki et al., 1994). Furthermore, a SP receptor antagonist improved the functional recovery of Mg^{2+} deficient rats following cardiac ischaemia-reperfusion injury (Kramer et al., 1997). Thus, it has been proposed that Mg^{2+} deficiency contributes to cardiovascular pathology by promoting SP release, which exacerbates inflammatory events and enhances oxidative and nitrosative stress (Kramer et al., 2009). Considering that our laboratory has associated increased SP release with neurological deficits in TBI (Donkin et al., 2009), it is possible that low Mg^{2+} levels contribute to neuronal pathology in TBI in a similar way.

Homeostasis and Transport

Mg^{2+} homeostasis is achieved via the intestinal absorption of dietary Mg^{2+} balanced with renal excretion/reabsorption of Mg^{2+} (Goytain and Quamme, 2005b; Ebel and Günther, 1980). On a cellular level, Mg^{2+} concentration is strictly regulated by mechanisms controlling Mg^{2+} entry, efflux and intracellular buffering (Romani, 2007). Mg^{2+} influx is dependent upon an electrochemical gradient generated by intracellular negative charges, which drives Mg^{2+} into the cell through specific Mg^{2+} transporters (Wolf, 2004). However, despite the physiological significance of Mg^{2+}, only a few proteins have actually been identified as fulfilling the role of mammalian Mg^{2+} carriers (Goytain and Quamme, 2005b).

Of the few mammalian Mg^{2+} transporters described to date, two are members of the transient receptor potential melastatin (TRPM) family. TRPM6 and TRPM7 channels have been shown to play important roles in regulating Mg^{2+} entry into cells, and are described in more detail in Section 1.5. Other Mg^{2+} transporters, including SLC41A1 and SLC41A2, have recently been characterised (Goytain and Quamme, 2005a; Sahni et al., 2007). SLC41A1 mRNA level was shown to be upregulated in Mg^{2+}-deficient tissues, and the authors suggest this transporter may be involved in epithelial Mg^{2+} homeostasis (Goytain and Quamme, 2005a).

Since Mg^{2+} is driven into cells via an electrochemical gradient, cells require an extrusion mechanism to counteract the constant influx of Mg^{2+}. Several lines of evidence suggest that a Na^+/Mg^{2+} antiporter maintains intracellular Mg^{2+} concentration at low levels by expelling Mg^{2+} in exchange for extracellular Na^+ (Wolf, 2004; Günther and Vormann, 1995; Zhang and Melvin, 1995). While the Na^+/Mg^{2+} antiporter is functionally well characterised (Wolf, 2004), there is currently no method of specifically tagging the protein and therefore its identification and molecular characterisation remains elusive (Politi and Preston, 2003).

1.2.4 TRPM Channels and Acute Brain Injury

As reviewed in Section 1.2.2, there are a number of secondary injury factors that contribute to neuronal cell death after TBI. Excitotoxicity resulting from unregulated Ca^{2+} influx through NMDAR is one established mechanism of delayed cell death following CNS injury (MacDonald et al., 2006) and is highly relevant to TBI (Barone and Kilgore, 2006; Arundine and Tymianski, 2004). However, despite evidence for a role of NMDAR in acute CNS injury, antiexcitotoxic therapies (AET) have not been clinically effective in preventing delayed neuronal cell death (Sacco et al., 2007; MacDonald et al., 2006).

Several other secondary injury processes including oxidative stress, oedema formation, apoptosis and necrosis also require, to some extent, the influx of cations into neurons (Simard et al., 2007b). Therefore, non-selective cation channels have gained attention as potential contributors to neuronal death. In particular, recent evidence has implicated transient receptor potential (TRP) channels, specifically, members of the melastatin (TRPM) subfamily, as playing direct roles in Ca^{2+}-mediated neuronal death (Simard et al., 2007b). The TRPM channel family is discussed in further detail in Section 1.5.2, but is mentioned briefly here with relevance to cell death.

The ubiquitously expressed TRPM7 consists of an ion channel fused to a protein kinase domain (Runnels et al., 2001). TRPM7 is permeable to several divalent cations (Monteilh-Zoller et al., 2003) and plays an important role in regulating vertebrate Mg^{2+} homeostasis (Schmitz et al., 2003). Recent studies have implicated TRPM7 in the anoxic death of neuronal cells (Aarts et al., 2003), and activation of TRPM7 during ischaemia is proposed to be a key factor contributing to excitotoxicity and other deleterious processes (MacDonald et al., 2006).

Aarts et al. (2003) used an in vitro model of cultured cortical neurons exposed to oxygen-glucose deprivation (OGD) to study mechanisms of neuronal cell death. Their studies showed that AET prevented neuronal death when OGD exposure was less than 1 hour, but was ineffective when OGD was continued for 1.5 - 2 hours, even in the presence of blockers of excitatory amino acid receptors, Ca^{2+} channels, Na^{+} channels and all other known ionic entry pathways associated with neurotoxicity. These studies therefore revealed the presence of a lethal, anoxia-activated cation current, which was subsequently shown to be carried by TRPM7 (Aarts and Tymianski, 2005a,b; Aarts et al., 2003). Interestingly, inhibition of TRPM7 blocked Ca^{2+} influx, precluded cell death of neurons exposed to up to 3 hours of OGD (even in the absence of AET) and prevented the generation of ROS. These significant findings indicate that TRPM7 is a critical mediator of neuronal cell death. More recently, (Wei et al., 2007) demonstrated that reducing levels of extracellular divalent cations resulted in TRPM7 disinhibition that was lethal to cells.

TRPM2 is a non-selective cation channel that is activated by oxidative stress and is highly permeable to Ca^{2+} (Perraud et al., 2005). TRPM2 has also been shown to be a mediator of cell death, possibly by providing a pathway for Ca^{2+} influx or by generating ROS (Aarts and Tymianski, 2005a; Hara

et al., 2002). In addition, TRPM2 mRNA level has been shown to increase following transient middle cerebral artery occlusion in rats (Fonfria et al., 2006a). However, no study to date has examined the mRNA or protein expression of TRPM2 or TRPM7 channels following TBI; this is one of the aims of the present thesis.

1.3 Chronic Neurological Disorders

Parkinson's Disease (PD) is the chronic neurological disorder focused upon in the present thesis. PD is increasing in prevalence as the population ages and represents a significant public health issue. This section will review current literature regarding the epidemiology, pathogenesis and treatment strategies of PD, and will discuss the role of magnesium, TRPM channels and neuropeptides in PD pathophysiology.

1.4 Parkinson's Disease

1.4.1 Epidemiology

PD is the second most common neurodegenerative disease after Alzheimer's Disease (AD) and affects approximately 1 % of the population over 60 years of age (De Lau and Breteler, 2006). As the population continues to age and life expectancy increases, the prevalence of PD has been reported to increase (Yamawaki et al., 2009; Chan et al., 2001). This is not surprising, given that the strongest risk factor for PD is age (Driver et al., 2009). Indeed, the onset of PD is rare under 50 years of age and increases sharply after age 60, with up to 4 % of the population over 80 years affected by the disease (Yao and Wood, 2009).

The estimated age- and gender-adjusted annual PD incidence rate is 13.4 cases per 100,000 population (Van Den Eeden et al., 2003). However, this figure can vary depending on the methodological strategy employed, with a review of European PD incidence data by Von Campenhausen et al. (2005) reporting an incidence of between 11 to 19 per 100,000 population per annum, and a prevalence of 108 to 257 per 100,000. In Australia, prevalence estimates vary from 145 per 100,000 population (Peters et al., 2006) to (crude prevalence) 780 per 100,000 (Chan et al., 2005). The risk of developing PD is reported to be higher in men than women (Van Den Eeden et al., 2003), with oestrogen suggested to be a neuroprotective factor (Bourque et al., 2009), although this requires further clarification.

1.4.2 Pathology

The neuropathological characteristics of PD consist of the progressive degeneration of dopaminergic neurons in the substantia nigra pars compacta (SNpc), and the presence of eosinophilic, intracytoplasmic protein aggregates called Lewy bodies (Thomas and Beal, 2007), and thread-like Lewy neurites in cellular processes (Braak et al., 2003). Lewy bodies and Lewy neurites contain α-synuclein and may become widespread in advanced PD; depositions mainly appear in the olfactory bulb, brainstem, SN and cortex, but may also occur in other regions (Schapira, 2008). Other catecholaminergic neurons are also affected in PD; in the locus coeruleus, the extent of neuronal degeneration may exceed that in the SN (Levy et al., 2009).

It has been proposed that clinical PD

symptoms are preceded by a latent period of dopaminergic cell death, which lasts for approximately 8 years (Schapira, 2009). Clinical symptoms usually appear following the loss of over 50 % of dopaminergic neurons from the SNpc, which leads to a reduction of striatal dopamine (DA) levels of more than 80 % (Hald and Lotharius, 2005). DA is a key neurotransmitter in the CNS, and is involved in movement, emotion and learning (Nishii et al., 1998). DA is particularly important in the basal ganglia (BG). The BG form a collection of nuclei with connections to the motor and prefrontal cortices, and function to co-ordinate movement and cognition (Graybeil et al., 1994). The BG encompasses the striatum (which itself is composed of the caudate, putamen and accumbens nuclei), the SN (pars compacta and reticulata), globus pallidus and subthalamic nucleus (Gerfen, 1992).

Without adequate levels of striatal DA, the BG cannot function properly, resulting in the classical motor symptoms of PD: resting tremor, rigidity, bradykinesia and postural instability (Braak and Del Tredici, 2008). Resting tremor is the first symptom in the majority of PD patients and is typically asymmetrical at disease onset, with a frequency of 3 - 5 Hz. Rigidity is defined as increased resistance during joint movement. Bradykinesia refers to difficulties in carrying out fine motor tasks, while postural instability is the gradual development of poor balance and can increase the risk of falls (Samii et al., 2004).

In addition, a number of debilitating non-motor symptoms are associated with PD, including olfactory deficit, sleep disorder, cognitive changes and depression, some of which may present before the onset of motor symptoms (Löhle et al., 2009). These non-motor features of PD arise from the loss of non-dopaminergic neurons, including the cholinergic nucleus basalis of Meynert, the serotoninergic neurons of the raphe nucleus, small cortical neurons and the hypocretin-containing neurons of the hypothalamus (Chaudhuri and Schapira, 2009; Lang and Lozano, 1998a).

1.4.3 Aetiology

PD is a complex neurodegenerative disorder without cure; despite intensive research, its pathogenesis remains poorly understood. Familial forms of the disease have recently been linked to mutations in specific genes. In non-familial PD, genetic susceptibility and environmental exposures are likely to be involved in disease onset and course (De Reuck et al., 2005). Furthermore, molecular and cellular processes such as inflammation, oxidative stress and mitochondrial dysfunction, which are influenced by genetic and environmental factors, have been proposed to contribute to neuronal cell death; these will be discussed below.

Genetic Factors

Mutations in a number of genes, for example, α-synuclein (Park1), DJ1 (Park 7) and PTEN-induced kinase 1 (PINK1, Park 6), have been associated with the development of familial PD (Huang et al., 2004). These gene mutations have been proposed to affect protein aggregation (α-synuclein), oxidative stress (DJ1) and mitochondrial function (PINK1) (Schapira, 2009). However, familial, inherited forms of PD account for less than 10 % of all PD cases, with the majority of cases being sporadic (idiopathic) in nature

(Thomas and Beal, 2007). The discovery of genetic factors linked to the rare forms of PD has increased our understanding of the pathogenesis of the disease and the mechanisms leading to cell death (Huang et al., 2004).

The identification of mutations in the leucine-rich repeat kinase 2 (LRRK2, Park8) gene is particularly interesting, because they occur with relatively high frequency in both familial and sporadic PD patients. The Gly2019Ser mutation, where serine is substituted for glycine at position 2019, was present in 1.6 % of idiopathic PD patients (Gilks et al., 2005) and 5 % of familial cases (Nichols et al., 2005). The protein encoded by the LRRK2 gene, dardarin, contains a tyrosine kinase catalytic domain (Paisán-Ruiz et al., 2004), and is the first kinase to be associated with PD. However, the exact function of dardarin is unknown (Di Fonzo et al., 2005).

Furthermore, candidate susceptibility genes have been identified that may be positively or inversely associated with the onset of sporadic PD. Genetic variations of proteins involved in the metabolism of xenobiotics, dopamine transport, energy supply, signalling and many others, may, in conjunction with environmental triggers, increase susceptibility to PD (Elbaz and Tranchant, 2007; Huang et al., 2004).

Environmental Factors

The first environmental agent to be identified that selectively destroys dopaminergic neurons in the SN was 1-methyl-4-phenyl-1,2,3,6-tetrahydropyridine (MPTP). The neurotoxicity of MPTP was discovered when a group of drug users were exposed to synthetic heroin containing MPTP and subsequently developed symptoms resembling PD (Langston et al., 1999; Langston and Ballard, 1983). Since then, MPTP has become a useful tool in studying animal models of PD; MPTP crosses the BBB where it is converted to its toxic metabolite, 1-methyl-4-phenylpyridinium (MPP^+), which interferes with mitochondrial function (Smeyne and Jackson-Lewis, 2005). The chemical structure of MPTP is similar to environmental toxins, such as pesticides, which have also been associated with the development of PD (Costello et al., 2009; Elbaz and Tranchant, 2007; Lai et al., 2002a).

Other environmental exposures have been reported to lower the risk of idiopathic PD. Cigarette smoking, coffee and tea drinking have all been shown to have protective effects against PD. Both caffeine and nicotine may have protective effects on dopaminergic neurons, but due to the heterogeneous composition of coffee and cigarettes, it is unclear exactly how these effects are elicited (Elbaz and Tranchant, 2007). One study reported that non-smokers were significantly younger at onset and diagnosis of PD and start of levodopa treatment than smokers (De Reuck et al., 2005), while another study found the risk of PD was 60 % lower in smokers than non-smokers (Hernan et al., 2002). The inverse association between smoking and PD was confirmed in another report (Kandinov et al., 2009), which also showed a protective effect of drinking more than 3 cups of tea per day in delaying onset of PD motor symptoms. The study by Kandinov et al. (2009) also included a retrospective study on coffee consumption and PD, and found that more

than 3 cups of coffee per day advanced the onset of PD. This is in contrast to a prospective study (Ross et al., 2000) of over 8,000 men in the USA with 30 years of follow up. In this study, the incidence of PD was inversely related to coffee intake, with age-adjusted incidence ranging from 10.4 per 100,000 in the no coffee group to 1.9 per 100,000 in the group drinking at least 830 mL coffee per day. This is consistent with another study, where the incidence of PD was 30 % lower in coffee drinkers compared to non-coffee drinkers (Hernan et al., 2002).

Finally, long-term exposure to metals, such as manganese and copper, has also been linked to the development of parkinsonism (Lai et al., 2002a).

Inflammation

Following an insult to the CNS, a neuroinflammatory response is initiated, which may include the activation of glial cells and secretion of pro-inflammatory cytokines, chemokines, free radicals and growth factors. While some of these molecules may be neuroprotective by promoting repair processes, others may be detrimental by exacerbating oxidative stress and triggering apoptotic cascades (Tansey et al., 2007).

With regard to PD, chronic neuroinflammation is considered to be a significant pathophysiological feature that may actively and continuously participate in the degeneration of dopaminergic neurons (Hartmann et al., 2003). In particular, clinical and experimental studies have demonstrated a strong microglial response in the parkinsonian SN.

Microglia are the principal immune cells of the CNS, and upon activation from a variety of stimuli, rapidly transform to antigen-presenting cells in order to defend the immunological integrity of the CNS (Zecca et al., 2008). During the early stages of activation, microglia upregulate complement receptors, cell adhesion molecules and major histocompatibility complex molecules, and release cytokines to recruit lymphocytes to the site of injury (Orr et al., 2002). If the inflammatory stimulus is not removed, activated microglia release toxic molecules such as pro-inflammatory cytokines and prostaglandins, ROS and RNS. Free radicals are toxic to invading pathogens, however, the production of superoxide radical from microglia is thought to be a major source of oxidative stress that leads to dopaminergic cell death (McGeer and McGeer, 2004).

In PD patients, reactive microglia are present in the SN, putamen and cerebral cortex, with the extent of microglial activation in the SN correlating with the degree of α-synuclein deposition (Schapira, 2009). In the intrastriatal 6-OHDA model of experimental PD, a significant inflammatory response was observed, including widespread microglial activation in the striatum and SN (Cicchetti et al., 2002). However, it is currently unclear whether activated microglia play a protective or detrimental role in the survival of dopaminergic neurons (Godoy et al., 2008).

Interestingly, Langston et al. (1999) demonstrated that MPTP was able to elicit inflammatory reactions and neuronal cell death many years after exposure. In several patients exposed to MPTP, post-mortem examination revealed gliosis in the SN, with activated microglia clustering around the surviving neurons. These results suggest

that an initial toxic insult to the brain can evoke long-term neuroinflammatory processes that promote neuronal cell death in a self-perpetuating manner.

A number of other studies have investigated the role of inflammatory processes in PD. Mogi et al. (1994a,b) found that levels of the pro-inflammatory cytokines, TNF-α, IL-1β and IL-6, were elevated in the striatum and CSF of PD patients. These cytokines are likely to contribute to neurodegeneration (Allan and Rothwell, 2001). Indeed, Godoy et al. (2008) demonstrated a direct association between elevations in IL-1β and progression of dopaminergic neuronal death. In addition, some pro-inflammatory cytokines can upregulate inducible nitric oxide synthase (iNOS) and cyclooxygenase 2 (COX2), which are associated with inflammation and release free radicals, causing further tissue damage (Hirsch and Hunot, 2009). In another study by Zecca et al. (2008), neuromelanin, a by-product of DA synthesis, activated microglia and caused significant SN dopaminergic neuron death in rodents. The results of recent experimental PD studies suggest that anti-inflammatory agents may elicit neuroprotective effects (reviewed in Long-Smith et al., 2009). Taken together, these results provide strong evidence supporting a role for neuroinflammation in PD pathogenesis.

Of further significance, in an epidemiological study, Chen et al. (2003) found that chronic use of non-steroidal anti-inflammatory drugs (NSAIDs) reduced the risk of PD by up to 45 %. However, this may require clarification, as another study (Ton et al., 2006) did not observe any neuroprotective benefit from the use of NSAIDs.

An astroglial reaction has also been reported in the 6-OHDA animal model of PD (Rodrigues and Gomide, 2001). The exact role of astrocytes in PD neuroinflammation requires further investigation, however, it has been suggested that these cells may exert a neuroprotective effect by releasing neurotrophic factors such as glial-derived neurotrophic factor (Hirsch and Hunot, 2009).

Disruption to the BBB is an important factor contributing to neuronal cell death in TBI, and previous studies from our laboratory have demonstrated that neurogenic inflammation and SP release contribute to BBB breakdown and functional deficits in experimental TBI (Donkin et al., 2009). Recently, it has been suggested that a compromised BBB may also contribute to PD pathophysiology. Indeed, research from our laboratory (E. Thornton, PhD thesis) implicates neurogenic inflammation and SP release in cell death and progression of PD. Whether this is a primary factor that initiates dopaminergic cell death in the SN, or a consequence of it, is unclear. A current hypothesis (Ionov, 2008) suggests that damage to SN dopaminergic neurons increases BBB permeability, which in turn allows histamine and other molecules to enter the brain and promotes further neuronal cell death in a positive feedback loop that may involve SP. However, it is also possible that an initially compromised BBB is unable to prevent putative PD toxins from entering the brain, rendering neurons susceptible to damage (Zlokovic, 2008). Importantly, activated glial cells release factors that can increase BBB permeability (Stone et al., 2009). In any case, a dysfunctional BBB is likely to have severe consequences for neurons by allowing immune cells, toxins, cytokines, complement, metal ions and

other molecules to enter the brain (see Figure 1.1), promoting neuroinflammation and potentially the progression of PD.

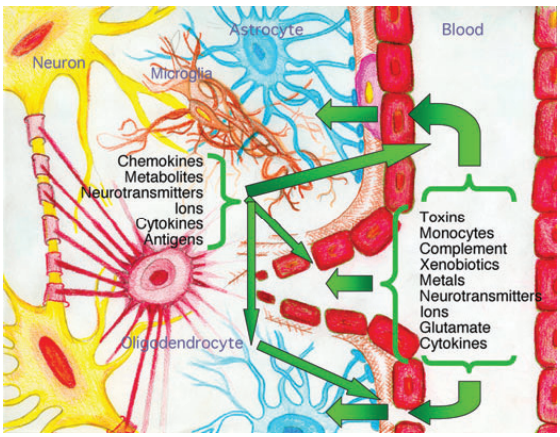

Figure 1.1: Consequences of BBB disruption. When the BBB is compromised, toxins, metal ions and inflammatory mediators, which would normally be excluded, may enter the brain. Furthermore, neurotransmitters and other molecules are more likely to leave the brain. In PD, a dysfunctional BBB could exacerbate neuroinflammatory injury processes, leading to neuronal cell death. Figure published in Carvey et al., 2009.

Oxidative Stress

As outlined in Section 1.2.2, oxidative stress is a state in which ROS are produced in excess of endogenous antioxidant mechanisms. ROS are highly reactive molecules that can damage cellular macromolecules and induce rises in intracellular Ca^{2+} levels. Brain tissue is particularly vulnerable to damage by oxidative stress due to its high rate of oxygen metabolism, relatively low antioxidant and repair capacities, and high levels of polyunsaturated fatty acids, which are particularly prone to damage by ROS (Chong et al., 2005; Halliwell, 1992).

Several lines of evidence support a role of oxidative stress in PD pathophysiology. Indeed, oxidative damage to lipids, proteins and nucleic acids has been reported in the brains of PD patients (Zhang et al., 1999), with a concomitant decrease in glutathione and other cellular antioxidant defences (Martin and Teismann, 2009).

There are several possible sources of oxidative stress in PD, including DA itself. Since the oxidation of DA generates ROS (see Figure 1.2), dopaminergic neurons in the SN are likely to be in a general state of oxidative stress and thus highly susceptible to damage (Thomas and Beal, 2007). In the early stages of PD, DA turnover is increased, which may exacerbate this process by generating excess free radicals. Furthermore, the autooxidation of DA yields reactive quinones and semi-quinones, which themselves may produce ROS (Koutsilieri et al., 2002). However, since the most effective treatment for the motor symptoms for PD, levodopa (see Section 1.4.4), elevates striatal DA levels in PD patients without accelerating disease progression, it is also possible that the metabolism of DA is not a significant source of cytotoxic ROS in PD (Chan et al., 2009).

High levels of iron have been reported in the brains of PD patients (Gerlach et al., 1994; Riederer et al., 1989), which may promote neurotoxicity by catalysing reactions that lead to the production of ROS. Unbound, ferrous iron (Fe^{2+}) reacts with hydrogen peroxide (H_2O_2), acting as an electron donor to produce ferric iron (Fe^{3+}) and hydroxyl radicals ($OH^{\bullet}$). It has been reported that the release of Fe^{2+} from ferritin complexes can be induced by 6-OHDA and DA and results in increased lipid peroxidation (Double et al., 1998). In addition, Fe^{2+} can promote DA autooxidation, therefore, the elevation in Fe^{2+} in PD may exacerbate oxidative stress

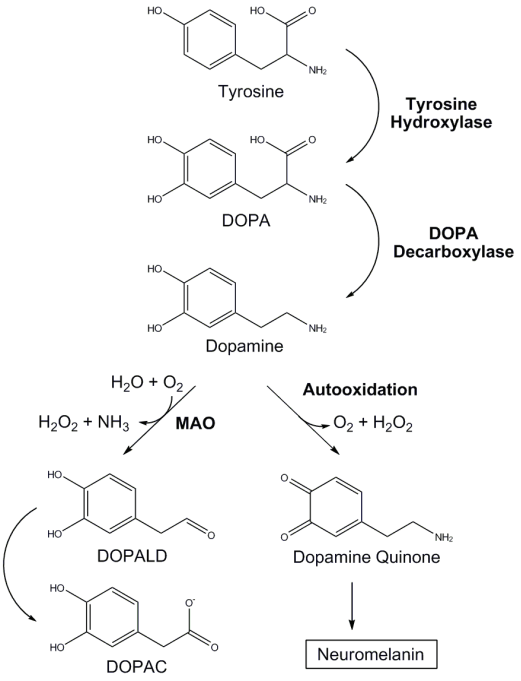

Figure 1.2: Synthesis and metabolism of DA. Tyrosine is converted to dihydroxyphenylalanine (DOPA) by tyrosine hydroxylase in a rate-limiting step. DOPA-decarboxylase converts DOPA to DA. DA is metabolised by monoamine oxidase (MAO) to yield dihydroxyphenylacetic acid (DOPAC) and H_2O_2. Autooxidation of DA produces H_2O_2 and DA-quinone, which may be converted to neuromelanin or covalently bind to proteins (not shown). In the presence of Fe^{2+}, H_2O_2 can produce highly reactive hydroxyl radicals ($OH^{\bullet}$) (Hald and Lotharius, 2005). DOPALD, dihydroxyphenylacetaldehyde. Figure prepared by Andrew Emmerich.

in dopaminergic neurons (Stone et al., 2009; Molina-Holgado et al., 2007). Furthermore, α-synuclein is more likely to aggregate and form deposits under conditions of high Fe^{2+} and oxidative stress (Barnham et al., 2004). In a recent study, Salazar et al. (2008) found an increase in the expression of the divalent metal transporter 1 (DMT1) in PD animals, which was associated with excess iron accumulation, oxidative stress and neuronal degeneration. Interestingly, a mutation in the DMT1 gene, leading to inhibition of iron transport, was neuroprotective against MPTP and 6-OHDA toxicity. Thus, targeting iron accumulation may provide therapeutic benefit in PD.

Reactive nitrogen species (RNS) have also been implicated in the degeneration of dopaminergic neurons. Nitric oxide (NO) is an important cellular signalling molecule, however, it can react with ROS to form molecules such as peroxynitrite, which can be highly toxic to cells. In addition, NO can modify cysteine residues in proteins in a process called S-nitrosylation, which affect such processes as gene transcription, signal transduction and apoptosis (Tsang and Chung, 2009).

Given that oxidative and nitrosative stress are likely pathogenetic factors in PD, antioxidants may be expected to reduce the neurotoxicity inflicted by excess free radicals. However, antioxidants have not been conclusively proven as neuroprotective in PD. A number of studies (reviewed in Lai et al., 2002a) have reported benefits in using Vitamins A, C and E in reducing PD risk, whereas other studies have not observed positive results with antioxidants. However, more recent investigations into the DJ-1 (Park 7) gene mutations associated with rare cases of familial PD have revealed that DJ-1 may be a neuroprotective factor against oxidative stress in the brain, and studies are ongoing to discover whether DJ-1 could be a promising pharmacological target in the future (Kahle et al., 2009).

High levels of ROS may also be generated during the inflammatory response, which, as discussed, is a significant event in PD (Stone et al., 2009). However, the major source of oxidative stress in PD is likely to be mito-

chondrial; this will be the focus of the next section.

Mitochondrial Dysfunction

As mentioned previously, mitochondria are ubiquitous cellular organelles that are critical in regulating cellular energy production via the electron transport chain (Mazzeo et al., 2009; Bayir and Kagan, 2008). Disruption to normal mitochondrial function can result in serious adverse consequences to cells, including energy failure, disruption to cellular homeostasis, generation of free radicals and activation of cell death pathways (Banerjee et al., 2009). Maintenance of mitochondrial dynamics is particularly relevant to cells with a high energy demand, such as neurons (Van Laar and Berman, 2009), and strong evidence indicates that mitochondrial dysfunction may play a central role in dopaminergic cell death in PD.

The toxic ion MPP^+, which causes irreversible parkinsonism, is an inhibitor of complex I (NADH-quinone oxidoreductase), a mitochondrial respiratory chain protein (Büeler, 2009; Langston et al., 1999). When MPP^+ accumulates in dopaminergic neurons, it causes cell death by inhibiting complex I activity and thus impairing mitochondrial function (Yao and Wood, 2009). Other environmental toxins, including the pesticides paraquat and rotenone, are also specific complex I inhibitors that lead to dopaminergic cell death. Accordingly, these compounds have been suggested to be environmental risk factors for PD (Banerjee et al., 2009).

Recent findings from studies of gene mutations associated with familial PD have provided further evidence implicating mitochondrial dysfunction in PD pathogenesis. Mutations in at least five genes (α-synuclein, Parkin, PINK1, DJ-1 and LRRK2) may have direct or indirect roles in mitochondrial dysfunction that may lead to cell death in PD (Banerjee et al., 2009; Yao and Wood, 2009; Büeler, 2009). Furthermore, mutations or polymorphisms in mitochondrial DNA can increase the risk of PD (Thomas, 2009). However, a detailed discussion of these mutations is beyond the scope of the present review.

The interplay between oxidative stress and mitochondrial dysfunction has been discussed in relation to TBI, but is reiterated here because it is also relevant to PD. Mitochondria are a significant source of ROS, which are produced during the synthesis of ATP (Kowaltowski et al., 2009) and at particularly high levels when the electron transport chain is disrupted (Bayir and Kagan, 2008). Furthermore, oxidative stress is directly implicated in mitochondrial dysfunction. ROS promote the release of cytochrome c from the inner membrane of the mitochondrion, which triggers an apoptotic cascade involving caspases and other pro-apoptotic proteins (Bayir and Kagan, 2008; Chong et al., 2005). Given that oxidative stress is enhanced in PD, these pathways are likely to significantly contribute to cell death in dopaminergic neurons. Finally, mitochondria may also participate in the release of glutamate and Ca^{2+} sequestration, leading to excitotoxicity (Nicholls and Budd, 2000).

In conclusion, neuroinflammation, oxidative stress and mitochondrial dysfunction have been suggested as interrelated molecular pathways with significant roles in PD pathophysiology (Malkus et al., 2009;

Thomas, 2009). Other mechanisms, not discussed here, have also been implicated in the disease, including dysfunctional gene regulation and protein handling (involving the ubiquitin-proteasome system), abnormal metabolism in the cerebral cortex (Ferrer, 2009), protein misfolding and aggregation (Tan et al., 2009), and Ca^{2+} dysregulation/excitotoxicity (Chan et al., 2009). It is clear that PD is an extremely complex neurodegenerative disease, possibly involving many interacting pathophysiological pathways. Effective anti-parkinsonian treatments in the future are thus likely to constitute a multifactorial approach (Maguire-Zeiss et al., 2008). The current treatment strategies for PD will be the next topic of discussion.

1.4.4 Treatments

As mentioned, there is no cure for PD and the currently available symptomatic therapies do not address the ongoing cell loss associated with the disease (Thomas, 2009).

Since the motor symptoms associated with PD arise from the degeneration of dopaminergic neurons and hence a loss of DA, drugs that target DA deficiency can improve the quality of life of PD patients (Stacy, 2009). DA is unable to cross the BBB, therefore its orally active precursor, levodopa (L-3,4-dihydroxyphenylalanine, L-DOPA), is administered, often in conjunction with dopa-decarboxylase and catechol-*O*-methyltransferase inhibitors to reduce its degradation in the periphery. Levodopa is subsequently converted to DA within dopaminergic neurons, thereby restoring DA levels in the striatum.

Other dopaminergic drugs may also be used to treat PD motor symptoms, including dopamine receptor agonists, which activate pre- and post-synaptic DA receptors, and MAO-B inhibitors, which prevent the metabolism of DA (Schapira, 2008).

While levodopa is the most effective pharmacological treatment for the motor symptoms of PD, importantly, it does not slow the progression of the disease, and many patients experience levodopa-related complications, such as wearing off and dyskinesias (Schapira and Olanow, 2004; Lang and Lozano, 1998b). Wearing off is related to a reduction in DA storage capacity and refers to a shorter, inadequate response to levodopa, resulting in the return of motor symptoms. Dyskinesias are involuntary movements that develop at a rate of approximately 10 % per year, with a higher rate in younger PD patients (Schapira et al., 2009; Stacy, 2009). It is estimated that 50 % of PD patients develop motor fluctuations after 5 years of levodopa therapy (Lang and Lozano, 1998b).

For PD patients with severe motor complications from DA replacement therapy, a surgical treatment option may be considered. Deep brain stimulation (DBS) has been shown to reduce motor symptoms and thus enrich the quality of life of PD patients, and can be targeted to various regions of the brain (Andrade et al., 2009).

However, despite advances in treatment options for PD patients, a neuroprotective agent that slows or prevents the progression of PD is urgently required, in addition to an effective therapy to ameliorate the non-motor symptoms (Schapira, 2008). Recent findings from our laboratory suggest that neurokinin-1 receptor (NK-1R) antagonists may constitute novel neuroprotective or symptomatic

therapies for PD; this research will be discussed in the next section.

1.4.5 Substance P and PD

SP is a neuropeptide with a number of physiological functions, including neurotransmission and nociception (Snijdelaar et al., 2000), which will be discussed further in Section 1.6. It is highly expressed in brain regions relevant to PD, including the SN, globus pallidus (GP), caudate nucleus and putamen (Raffa, 1998). The highest concentration of SP within the CNS is in the SN (Barker, 1996); high levels of NK-1 receptors are also present on dopaminergic neurons in the SN (Lévesque et al., 2007). SP is thought to be an important modulator of BG function (Chen et al., 2004). Indeed, SP can directly stimulate the release of DA from striatal dopaminergic neurons (Humpel et al., 1991). However, it is also interesting to note that DA appears to be essential to maintain striatal SP levels (Cruz and Beckstead, 1989), and DA receptor agonists were shown to increase the striatonigral synthesis of SP (Bannon et al., 1987). The potential role of SP in the pathogenesis of PD has thus been examined in a number of studies, with several reports demonstrating changes in SP expression in PD patients compared to controls, as well as in experimental PD animals.

Nisbet et al. (1995) found no significant difference in preprotachykinin (PPT, the gene encoding SP) mRNA levels between clinical PD and control basal ganglia tissue. However, SP immunoreactivity has been shown to decrease in the SN, GP and putamen of clinical PD cases compared to controls (Sivam, 1991; Tenovuo et al., 1984; Mauborgne et al., 1983). In patients with greater than 50 % DA reduction in the caudate nucleus, SP expression was decreased by 80 % in the medial GP compared to controls, but, conversely, increased three-fold when DA loss was greater than 80 % (De Ceballos et al., 1993). Furthermore, NK-1R expression was reduced in the GP of PD patients (Fernandez et al., 1994).

In the rodent 6-OHDA model of experimental PD, a number of studies using *in situ* hybridisation have reported significant reductions in PPT mRNA level in the striatum of PD animals compared to controls (Winkler et al., 2003; Gresch and Walker, 1999; Zeng et al., 1994; Nisenbaum et al., 1994; Gerfen et al., 1990). SP immunoreactivity has been shown to decrease in the ventral striatum of 6-OHDA lesioned rats (Voorn et al., 1987), while in another study, tissue levels of SP were reduced in the striatum and SN of PD animals (Lindefors et al., 1989).

Interestingly, the administration of high doses of SP to 6-OHDA lesioned rats increased levels of DA in the striatum, nucleus accumbens and frontal cortex (Krasnova et al., 1999), reversing the neurotoxic effects of 6-OHDA. In another study, rats exposed to a DA agonist after treatment with 6-OHDA had increased SP mRNA levels (Van De Witte et al., 1998). Further studies have shown that treatment with SP alleviates the functional and behavioural deficits induced by unilateral 6-OHDA lesion (Nikolaus et al., 1997; Mattioli et al., 1992).

Finally, in MPTP-treated monkeys, PPT mRNA level was significantly decreased compared to controls in the caudate nucleus, putamen (Wade and Schneider, 2001; Morissette et al., 1999; Herrero et al., 1995) and pedunculopontine nucleus (Gomez-Gallego

et al., 2007). In the study by Wade and Schneider (2001), PPT mRNA level was reduced in symptomatic, but not asymptomatic, MPTP-treated monkeys, suggesting that reduced SP expression could be directly related to the onset of PD symptoms.

Therefore, there is substantial evidence from both experimental and clinical studies suggesting that SP expression is reduced in PD. This suggests that depletion of SP in the BG may be a key event in PD pathogenesis (Chen et al., 2004; Barker, 1991). Whether this is be a primary pathology, a consequence of the DA denervation leading to a reduction in the capacity to produce tachykinins, or as a result of prolonged L-DOPA treatment is unclear (De Ceballos et al., 1993; Sivam, 1991). However, it is most likely that reduced SP levels are a direct loss of DA input to the striatum. This hypothesis is supported by reports demonstrating a reduction in SP expression in experimental PD animals which is restored to sham levels following L-DOPA administration (M. Hassall, Honours thesis; Zeng et al. 1994). These results suggest a positive feedback loop whereby DA promotes the release of SP and vice versa (Humpel et al., 1991; Bannon et al., 1987).

Recent studies from our laboratory (E. Thornton, PhD thesis) have revealed an alternative potential role of SP in PD pathogenesis. In the striatal 6-OHDA model of early PD in rats, there were increases in SP protein expression in the 6-OHDA lesioned rats compared to shams; these results are in contrast to the decreases in SP generally seen in previous studies. The administration of SP agonists or the angiotensin converting enzyme (ACE) inhibitor, captopril, which prevents the degradation of SP, exacerbated the motor deficits resulting from PD and increased dopaminergic cell death. However, when animals were treated with the SP receptor antagonist, N-acetyl-tryptophan (NAT) (Cascieri et al., 1994; MacLeod et al., 1993), these functional deficits were attenuated to levels observed in sham animals. These results indicate that SP may contribute to dopaminergic cell death in the early stages of PD. Importantly, these recent findings from our laboratory investigated SP expression in the early stages of PD, while the previously published articles mentioned above used late-stage animal models of PD or post-mortem clinical cases, where the majority of dopaminergic cell loss has already occurred.

To date, no studies have used quantitative, real-time RT-PCR to characterise the gene expression of SP in clinical PD, nor in 6-OHDA models of experimental PD; these aims will be addressed in the present thesis.

1.4.6 TRPM Channels and Magnesium in PD

Two complex neurodegenerative disorders, Amyotrophic Lateral Sclerosis and Parkinsonism-Dementia Complex of Guam (ALS-G and PD-G, respectively) have been found with a relatively high incidence on islands of the Western Pacific. Epidemiological assessments have identified the following possible environmental causes of these diseases: toxins from the cycad plant, deficiencies in Ca^{2+} and Mg^{2+}, and high exposure to aluminium, manganese and other toxic metals (Plato et al., 2003; Cox and Sacks, 2002).

A study by Hermosura et al. (2005) has reported a missense mutation in the TRPM7 gene, $TRPM7^{T1482I}$, in a subgroup of ALS-G

and PD-G patients but not in matched controls. The protein encoded by this variant (where threonine is replaced by isoleucine at position 1482) displays a higher sensitivity to inhibition by levels of intracellular Mg^{2+}. Thr1482, which lies between the channel and kinase domains of TRPM7, is evolutionarily conserved between many species, and phosphorylation of threonine in this position is likely to be important for channel function. Isoleucine cannot be phosphorylated, therefore, the mutant allele found in ALS-G and PD-G patients could potentially confer a functional deficit. Since TRPM7 is important in maintaining homeostasis of Mg^{2+} and Ca^{2+}, the authors propose that the higher sensitivity to Mg^{2+} of the TRPM7 variant, combined with the Mg^{2+}- and Ca^{2+}-deficient environment, could result in severe cellular deficiencies of these metal ions, which may contribute to the aetiology of diseases such as ALS-G and PD-G (Nilius et al., 2007; Hermosura et al., 2005).

Indeed, Mg^{2+} appears to be associated with the onset and progression of PD. Epidemiological studies have revealed that PD patients have slightly reduced Mg^{2+} levels in hair (Forte et al., 2005) and significantly decreased Mg^{2+} concentrations in the CSF (Bocca et al., 2006). In the study by Bocca et al. (2006), CSF Mg^{2+} concentrations were negatively associated with the severity and duration of the disease. In another study (Yasui et al., 1992), levels of Mg^{2+} were significantly decreased in several areas of the brain, including the BG.

A subsequent study (Oyanagi et al., 2006) investigated the effects of a low Mg^{2+} and/or low Ca^{2+} diet in rats over two generations, in order to simulate the actual conditions of human life on Guam, where several generations live in the same environment. The authors report that, over generations, a continuous Mg^{2+} deficiency (one-fifth of the normal level) led to a significant loss of dopaminergic neurons of the SN. These effects were only observed in rats exposed to a low Mg^{2+} diet constantly from the foetal and newborn stages to the prime of life, and were more pronounced in the Mg^{2+}-deficient group than the Mg^{2+}- and Ca^{2+}-deficient group.

Other recent studies also indicate a significant role for Mg^{2+} in PD. Hashimoto et al. (2008) found that Mg^{2+} was able to inhibit MPP^{+}-induced toxicity to rat dopaminergic neurons *in vitro*. In a very recent report, Muroyama et al. (2009) showed that mice fed a Mg^{2+}-deficient diet exhibited depression and anxiety-related behaviour, and these mice were more susceptible to reduced striatal DA levels following administration of MPTP compared to control mice.

Aside from a role in disease onset, Mg^{2+} administration has been shown to reduce levodopa-induced dyskinesia in MPTP-treated monkeys (Chassain et al., 2003), suggesting an interaction between neurotransmitter release and Mg^{2+} (Vink et al., 2009). In another study (Golts et al., 2002), Mg^{2+} inhibited the aggregation of α-synuclein.

A further study by Hermosura et al. (2008) has recently identified a missense mutation in the gene of the Ca^{2+}-permeable ion channel, TRPM2, in ALS-G and PD-G patients. The *TRPM2*^{P1018L} mutation produces ion channels with leucine replacing proline at position 1018. These TRPM2 channel variants are not active, that is, they do not maintain sustained ion influx, resulting in the attenuation of intracellular Ca^{2+}

rises in response to H_2O_2. This mutation could contribute to the pathophysiology of neurodegenerative disorders by interfering with Ca^{2+}-dependent downstream signalling pathways, particularly in cells such as microglia, in which TRPM2 is important for normal function (Kraft et al., 2004).

Interestingly, the expression of TRPM2 channels was upregulated in astroglia in response to oxidative stress (Bond and Greenfield, 2007), which was accompanied by an inhibition of protein synthesis. These results may also have relevance to the pathogenesis of neurodegenerative diseases, where dysregulation of Ca^{2+} homeostasis and protein handling can exacerbate disease progression.

To date, no studies have attempted to characterise the gene or protein expression of TRPM channels in relation to neurodegenerative disorders; this is one of the aims of the current thesis. The TRPM channel family will be discussed in detail in the next section.

1.5 The Transient Receptor Potential Channel Family

1.5.1 Overview

The TRP channel family was discovered during genetic screening of *Drosophila Melanogaster* for proteins involved in photoreceptor signal transduction. A *Drosophila* mutant was identified, which exhibited transient, rather than sustained, receptor potentials in response to continuous light. The subsequent cloning of the *trp* gene initiated a search for *Drosophila* homologues in other species, and led to the identification of the TRP superfamily, comprising a group of non-selective cation channels with diverse functions (Dietrich et al., 2006; Chubanov et al., 2005; Moran et al., 2004; Montell and Rubin, 1989).

There are now over 30 known members of the TRP channel family (Pedersen et al., 2005) that are divided into seven families on the basis of amino acid homologies: classical or canonical (TRPC), vanilloid receptor (TRPV), melastatin or long (TRPM), the mucolipins (TRPML), the polycystins (TRPP), the ankyrin transmembrane protein 1 (TRPA), and the no mechanoreceptor potential C (TRPN) (Pedersen et al., 2005; Moran et al., 2004). Each subfamily except TRPN contains a mammalian representative (Ramsey et al., 2006).

The mammalian TRP proteins are characterised by 6 transmembrane (TM) segments with a pore-forming region between the fifth (S5) and sixth (S6) TM segments (Ramsey et al., 2006) (See Figure 1.3).

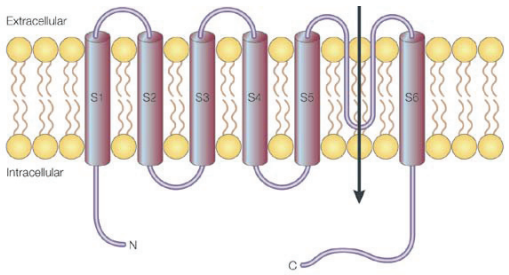

Figure 1.3: General structure of TRP channels. TRP channels are composed of 6 transmembrane segments (S1-S6) with a pore-forming region between S5 and S6 (indicated by an arrow), and intracellular N and C termini. Adapted from Clapham et al., 2001.

1.5.2 The Transient Receptor Potential Melastatin Family

The recently emerging TRPM channel family was named after the first discovered member, melastatin (TRPM1), which was iden-

tified in metastatic and benign melanomas and cloned in the late 1990s (Harteneck, 2005; Kraft and Harteneck, 2005; Duncan et al., 1998).

There are eight distinct members of the TRPM family, designated TRPM1-TRPM8. Phylogenetic analysis of mammalian TRPM channels divides the proteins into four subgroups (TRPM1 and TRPM3; TRPM6 and TRPM7; TRPM4 and TRPM5; TRPM2 and TRPM8) (Harteneck, 2005), although it has been suggested that TRPM2 and TRPM8 do not share enough structural or functional properties to be grouped together (Massullo et al., 2006).

TRPM proteins contain six TM segments flanked by cytoplasmic N-terminal and C-terminal sequences. The N-terminal region contains four 'TRPM homology domains', which are not representative of known structural motifs and whose functions are yet to be determined (Fleig and Penner, 2004). The C-terminal sequences are highly variable in length and structure (Kraft and Harteneck, 2005), and contain a coiled-coil region (a bundle of alpha-helices wound into a superhelix (Lupas, 1996)) that is believed to direct subunit assembly of TRPM channels into multimers (Jiang, 2007). Indeed, TRPM channels are thought to function as homotetramers, that is, four subunits which assemble to form a single pore (Massullo et al., 2006). The C-terminal sequences contain an enzymatic domain in TRPM2, TRPM6 and TRPM7, and all TRPM proteins contain a TRP motif (Jiang, 2007), a highly conserved sequence of 25 amino acids, which includes a group of six invariant amino acids (EWKFAR) known as the TRP box (Lepage and Boulay, 2007) (see Figure 1.4).

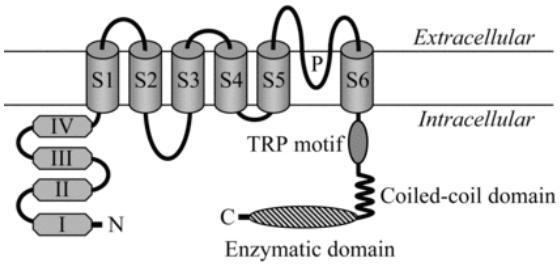

Figure 1.4: Structural diagram of TRPM channels. Diagram shows four highly homologous TRPM domains (I to IV) at the N-terminus (N), six transmembrane segments (S1-S6) with a pore region between S5 and S6 (P), a TRP motif, and a coiled-coil domain at the C-terminus (C). The enzymatic domain refers to the α-kinase domain in TRPM6 and TRPM7, and the NUDT9 protein homologous domain in TRPM2. Adapted from Jiang, 2007.

Biochemical and electrophysiological studies of TRPM proteins have revealed that the TRPM subfamily is a heterogeneous group of ion channels with diverse expression patterns, ion permeabilities, activation mechanisms and physiological functions. Four of its members, TRPM7, TRPM6, TRPM3 and TRPM2, will be discussed in more detail.

1.5.3 TRPM7

In 2001, Nadler and colleagues described and characterised TRPM7 as a widely expressed protein required for cell viability (Nadler et al., 2001). It was originally named LTRPC7 (Long TRP Channel 7), and is also known as TRP-PLIK (phospholipase interacting kinase) (Clapham et al., 2001), and ChaK1 (channel kinase 1) (Matsushita et al., 2005).

Permeability

TRPM7 has been characterised as a non-selective cation channel, conducting Ca^{2+} and monovalent ions (Runnels et al., 2001), however, other studies have described

TRPM7 as a highly selective divalent cation channel (Monteilh-Zoller et al., 2003; Nadler et al., 2001).

TRPM7 is permeable to Mg^{2+} (Schmitz et al., 2003; Nadler et al., 2001), which is rare among known ion channels (Miller, 2006). TRPM7 is also a major input pathway for other divalent metal ions, including nutritionally essential trace metals and toxic metal ions. Its affinities for metal ions, in descending order, are: Zn^{2+}, Ni^{2+}, Ba^{2+}, Co^{2+}, Mg^{2+}, Mn^{2+}, Sr^{2+}, Cd^{2+}, Ca^{2+} (Harteneck, 2005; Monteilh-Zoller et al., 2003). TRPM7 is more permeable to Mg^{2+} than Ca^{2+}, in contrast to other TRP channels (Chubanov et al., 2005). While trace metal ions are necessary for the catalytic function of enzymes and normal cellular function, their accumulation above trace levels is highly toxic (Monteilh-Zoller et al., 2003). For example, Zn^{2+}, Cu^{2+} and Fe^{2+} are required for the normal function of neurons, but in excess may contribute to the aggregation of amyloid-β (Aβ), the pathological hallmark of AD (Bush, 2006). Therefore, precise regulation of ion channels such as TRPM7 is vital to maintain normal physiological states.

Protein Kinase Activity

One of the most significant features of TRPM7 is that it contains both an ion channel and a protein kinase domain (Nadler et al., 2001; Runnels et al., 2001). This finding sparked immediate interest among researchers because the combination of ion channel and protein kinase was previously unknown (Schmitz et al., 2004). There are only three known ion channels that possess their own kinase domain: TRPM7, TRPM6 and TRPM2. These unique proteins are often referred to as 'chanzymes' in reference to their fused ion channel and protein kinase (enzyme) domains (Montell, 2003). TRPM7 and TRPM6 contain serine/threonine protein kinase domains resembling elongation factor 2 kinase and other atypical α-kinases (Dietrich et al., 2006; Kraft and Harteneck, 2005; Scharenberg, 2005). The catalytic domain of α-kinases contains several conserved motifs that are distinct from the characteristic sequence motifs of conventional protein kinases. However, despite the absence of sequence homology, α-kinases have a fold that is very similar to conventional protein kinases. α-kinases are so named due to evidence suggesting that they phosphorylate amino acids located within α-helices; this is in contrast to conventional protein kinases, which phosphorylate amino acids located within loops, turns, or irregular structures (Drennan and Ryazanov, 2004; Ryazanova et al., 2004).

The first substrate of the TRPM7 kinase domain to be identified was annexin I, a Ca^{2+}- and phospholipid-binding protein originally described as a mediator of the anti-inflammatory actions of glucocorticoids (Dorovkov and Ryazanov, 2004). The biological function of annexin I phosphorylation by TRPM7 is currently unknown (Schmitz et al., 2005). TRPM7 has also been shown to phosphorylate the myosin IIA heavy chain, suggesting a role in actomyosin contractility and cell adhesion (Clark et al., 2006). Other substrates of TRPM7 include the serine and threonine residues of myelin basic protein and histone H3 (Ryazanova et al., 2004), and the TRPM7 kinase domain can also undergo autophosphorylation (Clark et al.,

2006; Ryazanova et al., 2004; Runnels et al., 2001). The TRPM7 kinase domain appears to be specific for ATP, and cannot use GTP as a phosphate donor during phosphorylation, in contrast to many other protein kinases, and it requires a physiological Mg^{2+} concentration of 4-10 mM to be active (Ryazanova et al., 2004).

The role of the TRPM7 kinase domain and phosphorylation in relation to ion channel function remains unclear (Harteneck, 2005; Fleig and Penner, 2004; Ryazanova et al., 2004; Schmitz et al., 2003). TRPM7 channel activation was originally suggested to be dependent on the phosphotransferase activity of the intrinsic kinase domain (Runnels et al., 2001). However, Schmitz et al. (2003) demonstrated that TRPM7 channels containing point mutations that disrupt kinase activity formed functional channels. Another study (Matsushita et al., 2005) showed that mutations in the two autophosphorylation sites of TRPM7 also resulted in functional channels. Therefore, it is likely that TRPM7 channel activity is dissociated from the activity of the intrinsic kinase domain.

Regulation of TRPM7 Activity

TRPM7 has a low, constitutive activity in resting cells that is likely to fulfil a homeostatic role of providing a constant flow of Mg^{2+} and Ca^{2+} into the cell (Fleig and Penner, 2004). TRPM7 channel activity is inhibited by free intracellular Mg^{2+} and Mg.ATP complexes, and is strongly activated when intracellular Mg^{2+} and Mg.ATP concentrations are depleted (Demeuse et al., 2006; Matsushita et al., 2005; Jiang et al., 2003; Kozak and Cahalan, 2003; Nadler et al., 2001). A recent study has demonstrated that TRPM7 expression in endothelial cells is also influenced by extracellular Mg^{2+} concentrations (Baldoli et al., 2009).

It has been reported that Mg^{2+} is not unique in its inhibitory effects on TRPM7 channel activity, as other metal ions such as Ba^{2+}, Sr^{2+}, Zn^{2+} and Mn^{2+} cause complete inhibition of TRPM7 current (Kozak and Cahalan, 2003). Another study has demonstrated that polyvalent cations, such as spermine and Gd^{3+} (gadolinium ions) block monovalent TRPM7 current in a dose- and voltage-dependent manner (Kerschbaum et al., 2003; Hermosura et al., 2002). A recent article (Parnas et al., 2009) has identified carvacrol as a novel inhibitor of mammalian TRPM7 channels.

Biochemical characterisation of the protein kinase activity of TRPM7 revealed that, among all the divalent metal ions that TRPM7 permeates, only Mg^{2+} directly modulates its kinase activity *in vivo* (Ryazanova et al., 2004). Interestingly, when free Mg^{2+} levels are increased, TRPM7 kinase activity is increased, in contrast to channel activity, which is diminished in response to increases in Mg^{2+} (Schmitz et al., 2003). In another study, TRPM7 kinase activity was enhanced by Mg^{2+}, inhibited by Zn^{2+} and unaffected by Ca^{2+}, while channel activity was inhibited by all three cations (Matsushita et al., 2005).

TRPM7 may also be regulated by G-protein-coupled receptors (GPCR), either via the cyclic AMP (cAMP) and protein kinase A (PKA) pathway (Takezawa et al., 2004), or the phospholipase C (PLC)-mediated hydrolysis of phosphatidylinositol 4,5-bisphosphate (PIP_2) to form diacylglycerol (DAG) and inositol 1,4,5-triphosphate (IP_3) during the sec-

ond messenger cascade (Suh and Hille, 2005; Runnels et al., 2002) (see Figure 1.5).

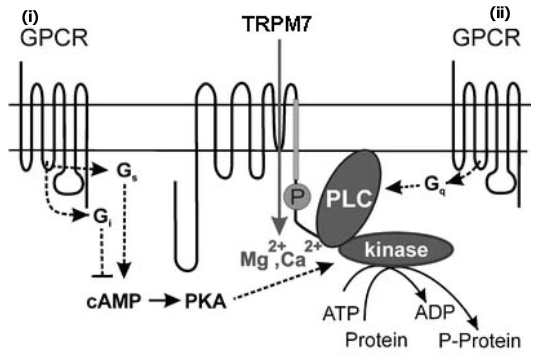

Figure 1.5: Mechanisms of regulation of TRPM7 channels by G-protein-coupled receptors. (i) TRPM7 is upregulated via the cyclic AMP (cAMP) and protein kinase A (PKA) pathway (Takezawa et al., 2004). (ii) TRPM7 is activated by PIP_2 (P) and inhibited by phospholipase C (PLC)-mediated hydrolysis of PIP_2 (Runnels et al., 2002). Roles of the different G-protein-coupled receptor subunits are as follows - G_s (stimulatory): activates adenylate cyclase to increase cAMP; G_i (inhibitory): inhibits adenylate cyclase; G_q: stimulates PLC (Strosberg and Nahmias, 2007). Diagram adapted from Harteneck, 2005.

Kozak et al. (2005) proposed that TRPM7 current is regulated by a screening mechanism of the negatively charged head groups of PIP_2, and that TRPM7 current is activated by elevated internal pH, regardless of the presence of intracellular Mg^{2+}. This is consistent with another study (Jiang et al., 2005), which showed that the inward current of TRPM7 is dramatically enhanced by a decrease in extracellular pH, with a 10-fold increase at pH 4.0 and a 1–2-fold increase at pH 6.0. These results suggest that TRPM7 may play a role in pathological conditions such as inflammation, infection and ischaemia, in which high concentrations of protons may be generated, leading to an acidic (pH $<$ 6.0) state.

Role in Cell Viability

Several lines of evidence demonstrate that TRPM7 is necessary for cell survival and plays a central role in magnesium homeostasis. Genetic deletion of TRPM7 in DT-40 chicken lymphocytes resulted in non-viable cells (Nadler et al., 2001), suggesting an important role of TRPM7 in cellular physiology, since lethality is rarely observed in ion channel knockout models (Butcher, 2004). A study by Elizondo et al. (2005) showed that the zebrafish *touchtone/nutria* phenotype, resulting from mutations in the TRPM7 gene, display growth retardation and serious alterations in skeletal development, indicating that TRPM7 is required for normal growth and development. In a further study (Schmitz et al., 2003), TRPM7-deficient cells were Mg^{2+}-deficient and growth arrested, but the viability and proliferation of these cells were rescued by supplementation of extracellular Mg^{2+}. The addition of high levels of other cations was ineffective in substituting for the loss of TRPM7, suggesting that TRPM7 regulates Mg^{2+} homeostasis in eukaryotic cells. These findings were unexpected, since previous hypotheses supported the concept that Mg homeostasis was mediated via Mg^{2+} efflux rather than influx (Wolf, 2004). However, a recent study by Jin et al. (2008) found that although TRPM7 is required for the proper development of mouse thymocytes, it does not mediate Mg^{2+} influx in T cells and may not be essential for Mg^{2+} homeostasis in mice.

Role in Synaptic Transmission

A report by Krapivinsky et al. (2006) demonstrated that TRPM7 is present in the mem-

brane of synaptic vesicles in sympathetic neurons, interacts with synaptic vesicle proteins and is required for the normal release of the neurotransmitter acetylcholine. The quantal sizes (amount of neurotransmitter released), amplitudes and decay times of the excitatory post-synaptic potentials changed in parallel with TRPM7 level (Montell, 2006). This is a significant finding, since the identity and role of ion channels involved in neurotransmitter release has previously been unknown.

Synaptic vesicles release neurotransmitters by fusing to the plasma membrane and releasing their contents into the intercellular space (Krapivinsky et al., 2006). It has been suggested that charged neurotransmitters are not free and mobile in synaptic vesicles, but associate with an 'ion-exchange matrix', possibly composed of proteoglycans (Montell, 2006; Reigada et al., 2003). In order for the neurotransmitter to be released, a counterion is required to displace the neurotransmitter from the matrix. The results obtained by Krapivinsky et al. (2006) suggest that TRPM7 may be the channel that supplies positively charged counterions to release acetylcholine.

Role in Central Nervous System Pathology

Neuronal Cell Death Despite the clearly established role of glutamate receptors in the pathophysiology of acute CNS injury, therapies targeting these processes have not been proven clinically effective (Forder and Tymianski, 2009).

One in vitro model for studying ischaemic neuronal injury consists of exposing cultured cortical neurons to oxygen-glucose deprivation (OGD), which is reported to mediate cell death through NMDAR activation (Choi et al., 1987). As discussed in Section 1.2.4, treatment with glutamate receptor antagonists in this model prevents neuronal death when OGD exposure is less than 1 hour, but is ineffective when OGD is continued for 1.5 - 2 hours, even in the presence of blockers of: excitatory amino acid receptors, Ca^{2+} channels, Na^{+} channels and all other known ionic entry pathways associated with neurotoxicity (Aarts et al., 2003). These studies, therefore, revealed the presence of a lethal, anoxia-activated cation current, which was named I_{OGD}. I_{OGD} is an outwardly rectifying, Ca^{2+}-permeable, non-selective cation channel, which is blocked by Gd^{3+}. Notably, inhibitors of I_{OGD} were able to prevent the death of neurons that would have occurred from OGD, despite the presence of AET (Aarts and Tymianski, 2005a,b).

Further investigations (Aarts et al., 2003) demonstrated that suppression of TRPM7 blocked I_{OGD} in response to chemical anoxia and addition of PIP_2, i.e. that I_{OGD} was mediated by TRPM7. Inhibition of TRPM7 also blocked Ca^{2+} uptake, precluded cell death of neurons exposed to up to 3 hours of OGD (even in the absence of AET) and prevented activation of I_{OGD} by ROS. These significant findings indicate that TRPM7 is a critical mediator of acute neuronal death that is activated by oxidative stress, in parallel to excitotoxic signal pathways (Figure 1.6). This may be explained by the fact that TRPM7 provides a pathway for toxic metals to enter cells (Monteilh-Zoller et al., 2003), or it may simply be due to Ca^{2+} overload toxicity resulting from TRPM7 activation (Aarts and Tymianski, 2005a). Future studies are required

to determine the exact mechanism whereby Ca^{2+} entry via TRPM7 channels causes neuronal death.

A recent report (Wei et al., 2007) has extended these findings by demonstrating that lowering levels of extracellular divalent cations can lead to TRPM7 disinhibition that is lethal to cells. This is relevant to the initial phase of ischaemia, where extracellular divalents are reduced, leading to an increase in monovalent ion permeation into cells. Wei et al. (2007) propose that TRPM7 carries this monovalent current and contributes to intracellular Na^{+} loading and associated toxicity. Of further significance, TRPM7 expression was recently demonstrated to increase following experimental stroke (Jiang et al., 2008).

Finally, TRPM2 channels (discussed in more detail in Section 1.5.6) are also able to mediate cell death. It has been suggested that the involvement of TRPM7 and TRPM2 in oxidative stress and cell death may be via the formation of heteromeric complexes (Aarts and Tymianski, 2005b).

Alzheimer's Disease The progressive neurodegenerative disorder, AD, is the most common cause of cognitive deterioration in the elderly (Lio et al., 2003). The neurodegenerative process of AD involves an oxidative stress component, in which Aβ plays a critical role (Barnham et al., 2004). TRPM7 may be involved in AD pathogenesis in a number of ways. Firstly, the production of ROS triggered by Aβ results in TRPM7 activation (Yamamoto et al., 2007), which may lead to cell death as detailed in Figure 1.6. TRPM2 may also be involved in this process. Moreover, since TRPM7 is permeable to Zn^{2+}, and Zn^{2+} imbalances contribute to neuronal toxicity, disruptions to Zn^{2+} homeostasis due to impairment of TRPM7 function could be a factor in AD (Yamamoto et al., 2007). Finally, TRPM7 may contribute to familial AD (FAD), which is caused by autosomal dominant mutations in the presenilin 1 and 2 genes (Larner and Doran, 2007). A study by Landman et al. (2006) showed that the activity of the TRPM7 channel was inhibited by FAD-associated pathogenic presenilin 1 mutations. This was proposed to be mediated through an imbalance of PIP_2 metabolism, since supplementation of PIP_2 ameliorated the observed ion channel dysfunction. The authors suggest that modulation of PIP_2 may serve as a new therapeutic target in FAD.

ALS-G and PD-G Considering the vital role fulfilled by TRPM7 with regard to cell viability and Mg^{2+} homeostasis, mutations in TRPM7 could be expected to result in severe pathological consequences (Nilius et al., 2007). Indeed, as discussed in Section 1.4.6, Hermosura et al. (2005) reported a missense mutation in the TRPM7 gene, Thr1482Ile, in a subgroup of ALS-G and PD-G patients but not in matched controls. The protein encoded by this variant displayed a higher sensitivity to inhibition by levels of intracellular Mg^{2+}. In conjunction with the Mg^{2+}- and Ca^{2+}-deficient environment in the Western Pacific, this could result in severe cellular deficiencies of these metal ions, which may contribute to the pathophysiology of these neurodegenerative disorders. The same group (Hermosura et al., 2008) recently reported a missense mutation of the TRPM2 gene in ALS-G and PD-G patients, which resulted in inactive TRPM2 channels.

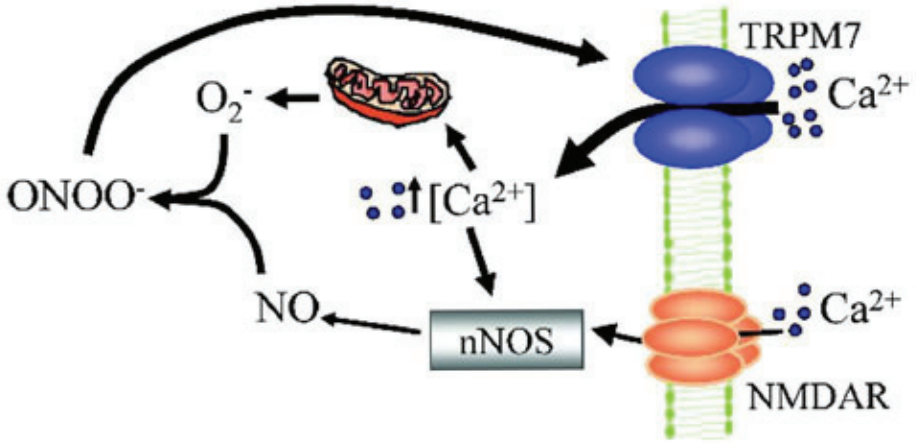

Figure 1.6: TRPM7 Channel Activation During Ischaemia. Diagram shows positive feedback loop of free radical production generated by TRPM7 channel activation during ischaemia. Activation of NMDA receptors during ischaemia causes Ca^{2+} influx, which stimulates neuronal nitric oxide synthase (nNOS), generates nitric oxide (NO) and releases superoxide O^{2-} from mitochondria. NO and O^{2-} combine to form the highly reactive species peroxynitrite $ONOO^{-}$, which in turn activates TRPM7, resulting in further entry of Ca^{2+} and generating more reactive oxygen and nitrogen species. The decrease in extracellular Ca^{2+} also disinhibits acid-sensing ion channels (not shown), indirectly resulting in more membrane depolarisation and contributing to the removal of the Mg^{2+} block of NMDAR, further promoting the positive feedback loop (Aarts and Tymianski, 2005a; MacDonald et al., 2006). Diagram adapted from Aarts and Tymianski, 2005a.

Given the involvement of TRPM2 and TRPM7 channels in mediating cell death and in the pathogenesis of PD-G and ALS-G, in addition to the recently discovered role of TRPM7 in neurotransmitter release, it is likely that future studies will continue to investigate these proteins in the setting of CNS disease.

1.5.4 TRPM6

TRPM6 was discovered by Ryazanova et al. (2001) during screening for homologues of elongation factor-2 kinase. The TRPM6 protein is the longest member of the TRP channel family (Bödding, 2007) and is the closest relative of TRPM7, with which it shares approximately 50 % homology at the amino acid level (Topala et al., 2006). While TRPM7 is ubiquitously expressed, TRPM6 is mainly expressed in the kidney and small intestine (Schlingmann et al., 2002), where it fulfils a role in epithelial Mg^{2+} (re)absorption (Voets et al., 2004). TRPM6 expression has also been reported in the brain (Fonfria et al., 2006b), with TRPM6 transcripts detected in the BG, cerebrum, forebrain and cerebellum (Kunert-Keil et al., 2006), as well as in cultured cortical neurons (Aarts et al., 2003). However, no studies to date have measured TRPM6 protein or mRNA levels in relation to CNS disease, and the role of TRPM6 in brain function is poorly understood.

Properties

TRPM6 is permeable to Mg^{2+} and Ca^{2+}, and is tightly regulated by intracellular concentration of Mg^{2+} (Voets et al., 2004). Intracellular ATP has been shown to inhibit TRPM6 channel activity (Thébault et al., 2008). In a

very recent report, Cao et al. (2009) identified the repressor of estrogen receptor activity (REA) as a dynamic regulator of TRPM6 channel activity. REA inhibited TRPM6 in a phosphorylation-dependent manner in human embryonic kidney (HEK) 293 cells, while 17β-estradiol stimulated TRPM6 current via a rapid (non-transcriptional) pathway.

As discussed, TRPM6 contains an atypical serine/threonine protein kinase domain fused to the TRPM channel region (Montell, 2003; Runnels et al., 2001). The exact function of the TRPM6 kinase domain remains to be elucidated, however, the receptor for activated C-kinase 1 (RACK1) has been shown to interact with the TRPM6 protein kinase domain to inhibit channel activity (Cao et al., 2008). It has been proposed that the TRPM6 kinase domain may function as an intracellular Mg^{2+} sensor that prevents Mg^{2+} overload (Van Der Wijst et al., 2009). In addition, TRPM6 is able to phosphorylate TRPM7, but not *vice versa* (Schmitz et al., 2005).

Multimerisation with TRPM7

Several studies demonstrate that TRPM6 and TRPM7 form functional heteromeric channel complexes (Chubanov et al., 2005, 2004; Schmitz et al., 2005). It was initially reported that TRPM6 expressed alone was not detectable on the cell surface and could not produce functional currents, that is, it required co-expression with TRPM7 (Schmitz et al., 2005; Chubanov et al., 2004). However, another study (Li et al., 2006) showed that TRPM6 forms homomeric channels on its own, as well as heteromeric channels with TRPM7, and that TRPM6, TRPM7 and TRPM6/TRPM7 channels are biophysically and pharmacologically distinguishable, as determined by their differing permeabilities, pH sensitivities, and single channel conductance. Further evidence that TRPM6 and TRPM7 perform different roles in vivo is provided by the observation that the TRPM6 channel was not able to compensate for a deficiency of TRPM7 (Chubanov et al., 2004).

Despite the evidence that TRPM6 and TRPM7 form functional heteromers, it is unknown whether TRPM6 participates in Ca^{2+}-mediated neuronal death along with TRPM7. As mentioned, the role of TRPM6 in CNS physiology remains to be elucidated.

Hypomagnesaemia with Secondary Hypocalcaemia

Hypomagnesaemia with secondary hypocalcaemia (HSH) is an autosomal recessive disorder characterised by low serum levels of Mg^{2+} and Ca^{2+}, which causes neurological symptoms such as muscle spasms and tetany (Jalkanen et al., 2006; Schlingmann et al., 2002). Mutations in the TRPM6 gene have been identified as the cause of HSH (Jalkanen et al., 2006; Schlingmann et al., 2002; Walder et al., 2002). These include the Ser141Leu missense mutation, which has been shown to interfere with TRPM6/TRPM7 heteromultimerisation, thus disrupting Mg^{2+} uptake machinery (Chubanov et al., 2004). The same group also reported a point mutation in the TRPM6 gene (Pro1017Arg), which causes a functional defect in the putative pore-forming region of TRPM6/TRPM7 channel complexes, resulting in HSH.

The results of a very recent article (Walder et al., 2009) suggest a role for TRPM6 in normal development. The authors devel-

oped a TRPM6 knockout mouse to further investigate the role of TRPM6 in Mg^{2+} homeostasis. Interestingly, the TRPM6-deficient mice usually did not survive to weaning, and most of those that did survive had neural tube defects (spina bifida occulta). These results were somewhat unexpected; although mutations in the human TRPM6 gene have been implicated in HSH, they were not previously known to cause mortality. It is unclear whether the observed defects were a result of the absence of the TRPM6 ion channel or kinase domain, since TRPM6 knockout mice were lacking both. However, given that TRPM7 is also required for normal growth and development, it is possible that in cells expressing both TRPM6 and TRPM7, these proteins interact and play a significant role in Mg^{2+}-dependent processes during development.

1.5.5 TRPM3

TRPM3 is the closest relative of TRPM1, and was one of the last TRP channels to be characterised (Clapham et al., 2001). TRPM3 is expressed in the human brain, kidney, testis, eye and spinal cord (Lee et al., 2003). Fonfria et al. (2006b) characterised TRPM channel distribution profiles across a wide range of human tissues and found the highest levels of TRPM3 in the brain and pituitary, suggesting that TRPM3 may have a significant role in CNS physiology. Within the brain, TRPM3 transcripts have been detected in the dentate gyrus, SN, cerebrum, forebrain and lateral septal nuclei, with a high expression in epithelial cells of the choroid plexus (Crispino et al., 2008; Kunert-Keil et al., 2006; Deo et al., 2006; Oberwinkler et al., 2005). At the cellular level, TRPM3 transcripts have been identified in mouse cultured cortical neurons (Aarts et al., 2003) and rat trigeminal neurons (Nealen et al., 2003). TRPM3 protein has recently been detected in primary hippocampal neurons (Crispino et al., 2008).

Alternative splicing of the TRPM3 gene encodes a number of TRPM3 variants. In the mouse, 5 different splice variants have been identified, designated TRPMα1 - TRPMα5 (Oberwinkler et al., 2005), while at least six human variants have been reported (Lee et al., 2003). The physiological consequences of such a large number of splice variants is not known, however, they potentially form the basis of a large functional diversity of TRPM3 channels (Oberwinkler and Philipp, 2007). For example, mouse variants of TRPM3 result in ion channels with different selectivity profiles: TRPM3α1 is permeable to monovalent, but not divalent, cations, while TRPM3α2 is highly permeable to divalent cations, including Ca^{2+} and Mg^{2+} (Oberwinkler, 2007; Oberwinkler et al., 2005).

When expressed in HEK293 cells, TRPM3 formed constitutively active channels permeable to Ca^{2+} and Mn^{2+}; currents were enhanced by a reduction in extracellular osmolarity (Grimm et al., 2003). TRPM3 is activated by D-erythro-sphingosine (Grimm et al., 2005), pregnenolone sulphate (Wagner et al., 2008) and Ca^{2+} store depletion (Lee et al., 2003). Like TRPM7 and TRPM6, TRPM3 is inhibited by rises in intracellular Mg^{2+} concentration (Oberwinkler, 2007). Based on the channel's known properties and localisation, TRPM3 is proposed to be involved in osmoregulation and renal Ca^{2+} homeostasis, and cation homeostasis in the CSF (Oberwinkler and Philipp, 2007; Grimm et al., 2003). Recently, TRPM3 was shown

to be expressed in pancreatic β-cells and may be involved in insulin secretion (Wagner et al., 2008). However, the physiological role of native TRPM3 channels, including their function in the brain, is incompletely understood. Interestingly, the human TRPM3 gene is located on human chromosome 9q-21.12, which has been linked to such diseases as HSH, and ALS with frontotemporal dementia (Lee et al., 2003). TRPM3 may therefore be another candidate gene for HSH, in addition to TRPM6, and further investigations of the contribution of TRPM3 in the CNS are warranted. To date, the characterisation of transcript or protein levels of TRPM3 in neurological disorders has not been attempted; this is one of the aims of the present thesis.

1.5.6 TRPM2

Properties and Localisation

TRPM2 is a non-selective cation channel, which is highly permeable to Ca^{2+}, and expressed in a wide range of human tissues, including immune cells, pancreatic β-cells, intestine and brain (Lange et al., 2008; Heiner et al., 2006; Eisfeld and Lückhoff, 2007; Nagamine et al., 1998). Specifically within the brain, TRPM2 is expressed in several regions, including cortex, cerebellum, medulla and hippocampus (Eisfeld and Lückhoff, 2007), with a unique truncated isoform of TRPM2 being present in the striatum (Uemura et al., 2005). Similar to its relatives TRPM6 and TRPM7, TRPM2 is a chanzyme, possessing both an ion channel and protein kinase domain (Scharenberg, 2005; Perraud et al., 2001). The TRPM2 protein kinase domain is highly homologous to nucleoside diphosphate-linked moiety X-type motif 9 (NUDT9), a mitochondrial adenosine diphosphoribose (ADPR) hydrolase, and is therefore known as the NUDT9 homology (NUDT9-H) domain (Kühn et al., 2005; Perraud et al., 2004, 2001). TRPM2 has intrinsic ADPR hydrolase activity, that is, it hydrolyses ADPR into AMP and ribose-5-phosphate (Kraft and Harteneck, 2005), but this is less effective than dedicated Nudix (nucleoside diphosphate-linked X) enzymes (Perraud et al., 2004, 2003).

Activation

TRPM2 can be activated in response to oxidative or nitrosative stress (Hara et al., 2002; Wehage et al., 2002), ADPR (Perraud et al., 2001; Sano et al., 2001), cyclic ADPR (Kolisek et al., 2005), nicotinamide adenine dinucleotide (NAD) (Sano et al., 2001), H_2O_2 (Hara et al., 2002; Wehage et al., 2002), silent information regulator 2 (SIR2) metabolites (Grubisha et al., 2006), and arachidonic acid (Hara et al., 2002). Intracellular and extracellular Ca^{2+} enhances TRPM2 currents (Starkus et al., 2007; McHugh et al., 2003), while calmodulin regulates the sensitivity of TRPM2 to Ca^{2+} (Tong et al., 2006).

Perraud et al. (2005) proposed that ADPR may activate TRPM2 via a mitochondrial biochemical pathway, whereby oxidative or nitrosative stress causes the production of ADPR in mitochondria, which is released into the cytosol and acts as a diffusible second messenger to induce TRPM2 gating. However, despite the evidence that oxidative stress stimulates TRPM2, Naziroğlu and Lückhoff (2008) recently showed that antioxidants did not prevent activation of TRPM2 channels by H_2O_2. Inhibitors of TRPM2 include flufenamic acid, a non-steroidal anti-

inflammatory compound (Hill et al., 2004), clotrimazole (Hill et al., 2006), intracellular ATP (Sano et al., 2001) and AMP (Kolisek et al., 2005).

Role in Cell Death

As mentioned in Section 1.5.3, TRPM2 plays a role in cell death. Several groups have shown that activation of TRPM2 by ROS, such as H_2O_2, results in cell death via unregulated Ca^{2+} influx (Hara et al., 2002; Fonfria et al., 2005). Of relevance to brain injury, TRPM2 may contribute to the pathophysiology that occurs following transient ischaemia: TRPM2 mRNA level was found to increase in a time-dependent manner in the transient middle cerebral artery occlusion model in rats (Fonfria et al., 2006a). The same group also showed that H_2O_2 and Aβ peptide caused significant Ca^{2+} influx and cell death in striatal neurons endogenously expressing TRPM2 (Fonfria et al., 2005). These finding suggest that TRPM2 activation may contribute to neuronal cell death in pathophysiological circumstances in which ROS are generated abundantly (Yamamoto et al., 2007; Fonfria et al., 2005).

It has been proposed that TRPM2 forms heteromeric channels with TRPM7 (Aarts and Tymianski, 2005b), but this has yet to be confirmed at the protein level (Hermosura and Garruto, 2007). TRPM2/TRPM7 heteromeric channels may provide a pathway for excess Ca^{2+} influx. Interestingly, Aarts et al. (2003) found that TRPM7 gene silencing resulted in a decrease in mRNA level of TRPM2, suggesting the transcripts may be co-regulated (Chinopoulos and Adam-Vizi, 2006), however, TRPM2 silencing did not affect TRPM7 (Fonfria et al., 2005). TRPM2 silencing did, however, induce a protective response against oxidative stress in neurons (Kaneko et al., 2006) and haematopoietic cells (Zhang et al., 2003) exposed to H_2O_2. Perraud et al. (2003) suggested that TRPM2 may be involved in a clearance pathway to remove cells irreversibly damaged by exposure to oxidants.

Since TRPM2 is a non-selective cation channel, it is permeable to Ca^{2+} and other ions. Therefore, another way in which TRPM2 could contribute to cell death is by conducting transition metal ions, such as Zn^{2+} and Mn^{2+}. Transition metals entering the cell via TRPM2 and other channels, can stimulate free radical production and increase oxidative stress, further activating TRPM2 channels and allowing large influxes of Ca^{2+}, causing even more ROS to be produced (Hermosura and Garruto, 2007). This is particularly relevant to neurodegeneration because the abnormal accumulation of such metals is associated with neurological disorders like AD (Bush, 2006).

Genetic Variants of TRPM2

As discussed in Section 1.4.6, Hermosura et al. (2008) recently reported a missense mutation of the TRPM2 gene in ALS-G and PD-G patients, which resulted in TRPM2 channels that were unable to sustain ion influx. Another study has identified a genetic variant of TRPM2 with an increased risk of bipolar disorder (Xu et al., 2009).

Synopsis TRPM proteins are a diverse and intriguing family of ion channels. The ubiquitously expressed TRPM7 is essential for

cell survival and may participate in regulating Mg^{2+} homeostasis, by providing a pathway for Mg^{2+} entry into cells. TRPM6 may also contribute to Mg^{2+} homeostasis, and genetic variants of TRPM6 result in the autosomal recessive disorder, HSH. TRPM7, TRPM6 and TRPM3 channels are all strongly activated when intracellular Mg^{2+} is depleted. Both TRPM7 and TRPM2 have been implicated in anoxic neuronal death, by allowing the unregulated influx of Ca^{2+} into cells, and both channels are activated by oxidative stress. TRPM3 is highly expressed in the brain, but its functional properties and physiological role are poorly understood. Previous studies have identified oxidative stress, unregulated Ca^{2+} influx, inflammation and Mg^{2+} decline as important components of the TBI injury cascade that lead to cell death. As discussed, TRPM channels have been implicated in all of these processes, however no studies have investigated the role of TRPM channels specifically in TBI pathophysiology. Therefore, in the present thesis, the mRNA and protein levels of TRPM7, TRPM6, TRPM3 and TRPM2 have been quantified following experimental TBI in rats. The study was also extended to include post-mortem clinical TBI cases. Furthermore, since PD also has oxidative stress and inflammatory components, and genetic variants of TRPM7 and TRPM2 are proposed to contribute to the pathogenesis of Western Pacific PD, the present thesis characterised TRPM channel mRNA and protein levels in experimental and clinical PD cases.

1.6 Substance P

1.6.1 History

SP is an 11 amino acid peptide that belongs to the tachykinin family, a class of small peptides that are widely distributed in the central and peripheral nervous systems (Mantyh, 2002). SP was first isolated from brain and intestinal tissue in 1931 by von Euler and Gaddum, who described a hypotensive and smooth muscle stimulating agent, named substance P in reference to the powder obtained from the extraction procedure (Harrison and Geppetti, 2001). During the next half-century, SP was one of the most extensively studied bioactive substances (Severini et al., 2002). In 1971, its amino acid sequence was determined (Chang et al., 1971), which allowed the compound to be synthesised (Tregear et al., 1971) and provided a breakthrough for investigating its physiological functions (Hökfelt et al., 2001). This section reviews the current knowledge on mammalian tachykinins, with particular emphasis on SP, and its functional role in a variety of human conditions.

1.6.2 The Mammalian Tachykinins

Overview

Tachykinins were named for their ability to instigate fast contraction of smooth muscle cells (Snijdelaar et al., 2000). Other members of the mammalian tachykinin family include neurokinin A (NKA, which is also present in two elongated forms, neuropeptide K (NPK) and neuropeptide-gamma (NP-γ)), neurokinin B (NKB) (Severini et al., 2002), the more recently discovered hemokinin-1 (HK-1) (Kurtz et al., 2002; Zhang et al., 2000) and the endokinins (EKA, EKB, EKC, and

EKD) (Page, 2006; Page et al., 2003).

The mammalian tachykinins share a common C-terminal sequence, Phe-*X*-Gly-Leu-Met-NH_2, where *X* represents phenylalanine or valine (Harrison and Geppetti, 2001). The N-terminal sequences of tachykinins are divergent, and are responsible for their specific biological activities (Erspamer, 1981).

Synthesis

SP and NKA are synthesised from the preprotachykinin-A gene (TAC1, previously abbreviated to PPT-A) (Severini and Zona, 2006; Page, 2005), which is present in most human tissues (Pinto et al., 2004). Alternative splicing of TAC1 results in four messenger RNA (mRNA) isoforms: α, β, γ and δ. SP is encoded by exon 3, which is present in all four TAC1 splice transcripts. The NKA sequence is encoded by exon 6, which is present only in the β and γ isoforms of TAC1 mRNA. NKB is derived from the PPT-B (TAC3) gene (Lai et al., 1999; Harmar et al., 1990; Krause et al., 1987; Nawa et al., 1984, 1983). The PPT-C (TAC4) gene, of which there are four distinct mRNA isoforms, α, β, γ and δ, gives rise to the endokinins (Page et al., 2003) (See Figure 1.7). The biological relevance of the alternative splicing is currently unknown (Page, 2005; Severini et al., 2002), as is the case with the majority of alternative splicing events (Graveley, 2001).

Distribution

SP is widely distributed throughout the CNS and in primary afferent sensory neurons innervating a number of peripheral tissues (Pennefather et al., 2004; Harrison and Geppetti, 2001). SP immunoreactivity has been demonstrated in the mesencephalon, hypothalamus (Brownstein et al., 1976), SN (Mai et al., 1986; Brownstein et al., 1976), striatum (Brownstein et al., 1976), brainstem (Del Fiacco et al., 1983), BG, dorsal root ganglia, hippocampus, pons, amygdala and spinal cord (Ribiero-Da-Silva and Hökfelt, 2000).

Tachykinins were originally considered almost exclusively as peptides of neuronal origin (Pennefather et al., 2004). However, several immunoreactivity and mRNA quantification studies have since demonstrated the expression of tachykinins in other cell types. SP expression has been demonstrated in human immune cells, such as lymphocytes and macrophages (Lai et al., 2002b, 1999), endothelial cells (Linnik and Moskowitz, 1989) and reproductive organs (Patak et al., 2003). TAC1 and TAC3 mRNA species have been shown to be widely distributed in both neuronal and non-neuronal human tissues (Pinto et al., 2004). Furthermore, HK-1 and the EKs are primarily expressed in non-neuronal cells (Page et al., 2003; Zhang et al., 2000).

Release and Metabolism

Tachykinins are transported across biological membranes via the process of exocytosis (Snijdelaar et al., 2000). Capsaicin, the spicy component of hot peppers (Mezey et al., 2000), causes the release of tachykinins from C-fibre terminals (Franco-Penteado et al., 2006; Maggi and Meli, 1988) by activating the TRPV1 channel (Yan et al., 2006). TRPV1 is a weak Ca^{2+}-selective cation channel, which (in addition to capsaicin) is stimulated by protons, heat ($\geq 43\,^{\circ}C$) (Tominaga and Tomi-

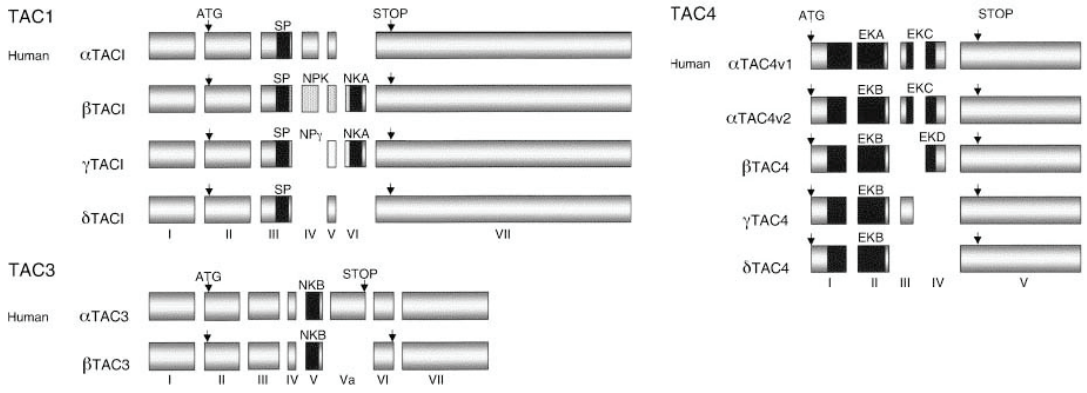

Figure 1.7: Alternative splicing of the human TAC1, TAC3 and TAC4 genes. Diagram shows exons (indicated by Roman numerals) and positions of the encoded tachykinins. ATG; methionine (start codon); STOP; stop codon. Diagram adapted from Page, 2005. NB: HK-1 (not shown) (Zhang et al., 2000) is encoded by exon 2 of the human TAC4 gene; EKA and EKB are N-terminally extended forms of HK-1 (Pennefather et al., 2004).

naga, 2005) and endogenous ligands such as anandamide (Starowicz et al., 2007).

Capsaicin-sensitive neurons transmit nociceptive information from the periphery to the CNS (Mezey et al., 2000). When administered repeatedly, capsaicin causes the depletion of neuropeptide stores from C-fibres (Vink et al., 2003), which results in an antinociceptive effect (Franco-Penteado et al., 2006). The role of SP in nociceptive transmission is discussed in Section 1.6.3.

Several enzymes are involved in the metabolism of SP, including neutral endopeptidase (NEP) (Matsas et al., 1984), and ACE (Skidgel and Erdos, 2004). NEP and ACE catalyse the hydrolysis of SP at the C-terminal region of the peptide, preventing its interaction with NK receptors (Harrison and Geppetti, 2001).

Neurokinin Receptors

The biological responses to SP, NKA and NKB are mediated by the NK receptors, NK-1R, NK-2R and NK-3R (Harrison and Geppetti, 2001). SP has the highest affinity for the NK-1R, and NKA and NKB have the highest affinities for the NK-2R and NK-3R, respectively (Saria, 1999; Maggi, 1995; Regoli et al., 1994), although each of these tachykinins is able to act upon all three receptor types (Maggi and Schwarz, 1997). SP and NKA are often co-expressed (Severini and Zona, 2006) and are known to exert their biological effects in a synergistic manner (Campos and Calixto, 2000).

The NK receptors belong to the GPCR family, and contain seven hydrophobic transmembrane segments (Strader et al., 1994). Activation of NK receptors results in PLC-mediated hydrolysis of PIP_2, which produces the second messengers DAG and IP_3, leading to an increase in intracellular concentration of Ca^{2+} (Suh and Hille, 2005; Yang et al., 2003; Harrison and Geppetti, 2001). IP_3 causes an increase in Ca^{2+} by stimulating the sarcoplasmic reticulum to release its Ca^{2+} stores. DAG allows Ca^{2+} to enter cells by activating PKC, which re-

sults in the phosphorylation and subsequent opening of voltage-gated calcium channels (Khawaja and Rogers, 1996). Activation of PLC also causes an increase in arachidonic acid mobilisation and an accumulation of cAMP (Harrison and Geppetti, 2001). However, the results of one study suggest that there may be as yet undiscovered tachykinin receptors that function independently of G-protein coupling (Yang et al., 2003), but this is yet to be confirmed.

1.6.3 Biological Effects of SP

Neurotransmission and Nociception

Studies into the functions of SP reveal its involvement in a range of physiological, pathological and behavioural processes. SP acts as a neurotransmitter and/or neuromodulator in nociceptive pathways (Zubrzycka and Janecka, 2000; Snijdelaar et al., 2000), as demonstrated by its release in response to noxious stimuli (Guo et al., 2007; Duggan et al., 1988) and the observation that NK-1R antagonists block these responses in spinal cord neurons (Radhakrishnan and Henry, 1991). However, one study has shown that SP is not involved in nociceptive transmission in very young mice and rats (King and Barr, 2003). Interestingly, SP has been shown to have memory-promoting and reinforcing effects (Hasenöhrl et al., 2000). It is also involved in regulating the vomiting reflex, and NK-1R antagonists display antiemetic activity (Rupniak and Kramer, 1999).

Inflammation

SP has been shown to induce the production of inflammatory cytokines, including TNF-α and several interleukin family members (IL-1β, IL-2 and IL-6) (Delgado et al., 2003). SP also stimulates the migration of natural killer cells (Feistritzer et al., 2003) and the release of serotonin and histamine from mast cells (Reynier-Rebuffel et al., 1994; Ebertz et al., 1987; Irman-Florjanc and Erjavec, 1983). As discussed with relevance to TBI, SP strongly evokes neurogenic inflammation, and its ability to elicit such effects as vasodilation, increases in vascular permeability and activation of immune cells indicate that SP may be involved in the pathogenesis of asthma and other airway diseases (De Swert and Joos, 2006). Furthermore, SP has been implicated in the allergic response (Ashequr Rahman et al., 2006), abdominal adhesion formation (Reed et al., 2002), and intestinal inflammation (Landau et al., 2007).

SP in CNS Disorders

Recent reports suggest a role for SP in post-traumatic stress disorder (Geracioti et al., 2006), anxiety (Hamke et al., 2006; Ebner and Singewald, 2006) and migraine (Fusayasu et al., 2006). SP is also involved in the neuropathology of depression (Geracioti et al., 2006), and NK receptor antagonists have been shown to be equally effective as traditional antidepressant drugs in treating the disease (Dableh et al., 2005). Research from our laboratory has implicated SP in the pathogenesis of TBI and PD; these studies will be discussed below.

The release of SP from C-fibres is known to cause neurogenic inflammation, a local inflammatory reaction of neurons in response to infection, toxins or trauma, which is characterised by vasodilation and oedema (Turner et al., 2006; Ro et al., 2005; Black,

2002). SP is considered to be one of the principal initiators of neurogenic inflammation, along with calcitonin gene-related peptide (CGRP) (De Swert and Joos, 2006). Our laboratory has shown that neuropeptides play an important role in neurogenic inflammation and functional deficits associated with TBI in rats (Vink et al., 2003). More recently, a study from our laboratory (Donkin et al., 2009) specifically identified SP as the primary neuropeptide involved in neurogenic inflammation, BBB disruption and cerebral oedema following experimental TBI. Notably, the administration of an NK-1R antagonist, NAT, attenuated vascular permeability and oedema formation and improved neurological outcome. Therefore, SP may represent a novel therapeutic target for TBI.

In another study from our laboratory (E. Thornton, PhD thesis), we observed increases in SP protein expression in early experimental PD in rodents. The administration of SP agonists or the ACE inhibitor, captopril, exacerbated the motor deficits resulting from PD and increased dopaminergic cell death. However, when animals were treated with NAT, these functional deficits were attenuated to levels observed in sham animals. These results suggest that SP is involved in the early pathogenesis of PD, and that NK-1R antagonists may constitute novel neuroprotective or symptomatic therapies for PD.

Upcoming studies are likely to further implicate tachykinins in the pathogenesis of human disease. Taking into consideration the results of important studies conducted by our laboratory using NK-1R antagonists, it is possible that tachykinins will be important therapeutic targets for CNS diseases in the future.

Synopsis In this section, the role of SP in a wide range of physiological and pathophysiological processes has been described. Our laboratory has demonstrated that SP plays a critical role in neurogenic inflammation, cerebral oedema and the functional deficits following experimental TBI. Furthermore, observations using a rat model of PD implicate SP in the early pathogenesis of this disease. We have studied SP at the protein level in rodent models of TBI and PD using immunohistochemistry and have shown that SP immunoreactivity increases acutely in these diseases. However, the transcriptional level of SP in these diseases has not been quantified to date. Therefore, this project aims to quantify SP mRNA levels in experimental TBI and PD using real-time RT-PCR (reviewed in Chapter 2). Furthermore, these studies will be extended to a clinical setting, in order to characterise SP mRNA and protein expression in post-mortem TBI and PD cases.

Chapter 2

Real-time RT-PCR

2.1 Introduction to PCR

The revolutionary polymerase chain reaction (PCR) was developed in the 1980s (Mullis, 1990), and allows scientists to characterise, analyse and synthesise nucleic acid sequences (Powledge, 2004). PCR can quickly and easily amplify a specific segment of nucleic acid more than a billion-fold (Vasalek and Repa, 2005), and is possible because of DNA polymerase, an enzyme whose natural function is to catalyse the synthesis of DNA (Sambrook and Russell, 2001). The specificity of PCR is achieved using sense and antisense primer molecules, sequences of 16-20 nucleotides designed to flank the DNA segment to be amplified. PCR generates double-stranded (ds) DNA sequences of interest by repetitions of a thermal cycling protocol involving denaturation, annealing and extension steps (shown in Figure 2.1).

During the annealing step, the primers hybridise to opposite strands of the target sequence and are oriented so DNA synthesis proceeds across the region between the primers (Saiki et al., 1988). In the extension step, the DNA polymerase elongates the strands by adding complementary nucleotides, thus creating a new dsDNA molecule (Vasalek and Repa, 2005). The discovery of thermostable DNA polymerase from bacteria residing in hot springs, *Thermus aquaticus* ('Taq polymerase'), has greatly increased the efficiency of PCR and facilitated its automation; early PCR required the addition of enzyme after each cycle because it was susceptible to denaturation (Sambrook and Russell, 2001; Saiki et al., 1988). Theoretically, the amount of dsDNA will double after each PCR cycle, but in reality the reaction does not proceed with perfect efficiency, due to components of the reaction being consumed, or PCR inhibitors. Efficiency of PCR amplification can be improved by optimising cycling conditions and reagent concentrations, such as Mg^{2+}, primer concentrations and annealing temperature (McPherson and Möller, 2006a).

Conventional, 'end-point' PCR uses agarose gel electrophoresis to visualise the PCR product (amplicon). Samples are loaded into the wells of an agarose gel, and a voltage applied to separate molecules according to size. In order to visualise the DNA bands in the gel, a dye (such as ethidium bromide) is used to intercalate between the bases of DNA. The gel is then exposed to ultraviolet light, causing the ethidium

NOTE:
This figure is included on page 39
of the print copy of the thesis held in
the University of Adelaide Library.

Figure 2.1: Diagram of the PCR process. A/B: Double-stranded DNA is separated into single strands by heating at $95\,°C$. C. The mixture is cooled to $55 - 65\,°C$, allowing primers to anneal to their complementary sequences. D. At $72\,°C$, DNA Polymerase adds complementary nucleotides to extend the strands. The process is repeated up to 40 times to amplify the DNA sequence of interest in an exponential fashion (Adapted from Real-Time PCR Tutorial by Dr M. Hunt, University of South Carolina, `http://pathmicro.med.sc.edu/pcr/realtime-home.htm`).

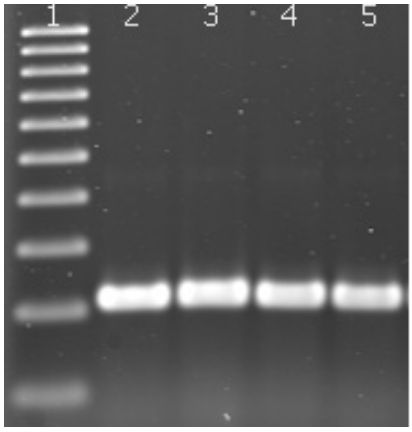

Figure 2.2: Example of an agarose gel. Following electrophoresis, the gel is stained in ethidium bromide and exposed to ultraviolet light to visualise PCR products. Lane 1: Molecular markers (top band 1000 base pairs (bp), bottom band 100bp in 100bp increments) Lanes 2-5: PCR products of approximately 200 bp size.

bromide to fluoresce. A molecular marker of known size, typically generated by restriction enzyme digestion of plasmids, is also run on the agarose gel to determine the size of the amplicon (Sambrook and Russell, 2001) (See Figure 2.2).

2.2 Reverse Transcription PCR

PCR-based assays can target DNA (the genome) or RNA (the transcriptome) (Bustin and Nolan, 2004). Using PCR to target the genome is useful for detecting polymorphisms and mutations. However, in order to quantify gene expression levels, the steady-state abundance of messenger RNA (mRNA) is measured (Farrell, 1998).

When PCR is used to characterise mRNA levels, a reverse transcription (RT) step is required to synthesise complementary DNA (cDNA) from RNA, since DNA polymerases cannot use RNA as a template for amplification (McPherson and Möller, 2006b). The RT reaction utilises reverse transcriptase, the enzyme that allows retroviruses (e.g. hepatitis C virus) to generate DNA from viral RNA. Reverse transcriptase may be derived from Moloney murine leukaemia virus (MMLV), avian myeloblastosis virus (AMV), or may be genetically engineered (Vasalek and Repa, 2005). In order to synthesise cDNA, the RT reaction must be primed; this can be achieved using random primers (random sequences of 6-15 nucleotides), oligo(dT) (deoxythymidine nucleotides designed to be complementary to the poly(A) tail of RNA), or by gene-specific primers (Ståhlberg et al., 2004). There are advantages and disadvantages associated with each priming strategy. For example, random primers may overestimate the amount of mRNA, since cDNA molecules can be generated from

multiple points along the RNA (Zhu and Altmann, 2005), including ribosomal RNA (rRNA). However, random priming generates the least bias in the resulting cDNA (Bustin and Nolan, 2004). Oligo(dT) will not reverse transcribe rRNA and is therefore more specific than random priming, but will also not prime RNA lacking a poly(A) tail (Shipley, 2006). Oligo(dT) thus requires high quality, full-length RNA and is unsuitable for fragmented RNA, such as that from formalin-fixed, paraffin-embedded (FFPE) material (Bustin and Nolan, 2004). Gene-specific priming is the most specific and sensitive cDNA synthesis strategy (Lekanne Deprez et al., 2002), but requires separate RT reactions for each target gene, which may be wasteful if limited amounts of RNA are available (Bustin and Benes, 2005).

2.3 Quantitative, Real-time RT-PCR

The combination of reverse transcription and polymerase chain reaction (RT-PCR) has facilitated the identification of specific RNA transcripts from small amounts of starting material (Shipley, 2006). It has been widely used for semi-quantitative analysis of mRNA level, and identifying mutations and polymorphisms in transcribed sequences (Sambrook and Russell, 2001). The major drawback to the end-point PCR assay is that the amplified product is measurable only when the final PCR cycle is completed (Houghton and Cockerill, 2006); it is therefore not quantitative in the sense that the final product yield is not primarily dependent upon the initial concentration of the target sequence in the sample. However, the development of the fluorescence-based, quantitative, real-time RT-PCR overcomes this limitation and has dramatically influenced the field of gene expression analysis (Wong and Medrano, 2005). In a real-time RT-PCR assay, the progress of DNA amplification is monitored within the PCR tube as it occurs; thus amplification and detection are combined into a single step (Wong and Medrano, 2005).

Real-time RT-PCR has several advantages over end-point PCR, including an extremely wide dynamic range of quantification (7-8 log decades), higher sensitivity, higher precision and reliability, and the absence of post-PCR steps, which confers a decreased risk of contamination (Wilhelm and Pingoud, 2003; Klein, 2002). It is the most sensitive method for detecting and quantifying mRNA (Bustin, 2000); in many cases it is the only method sensitive enough to measure mRNA levels of low abundant targets (Huggett et al., 2005). Real-time RT-PCR assays are 10,000 to 100,000-fold more sensitive than traditional RNase protection assays and 1000-fold more sensitive than dot blot hybridisation, and require much less starting RNA (Wong and Medrano, 2005).

2.3.1 The Real-time RT-PCR Assay

Real-time RT-PCR can be summarised into three steps: (i) the synthesis of cDNA from RNA (reverse transcription), (ii) the amplification of the cDNA using PCR, and (iii) the detection and quantification of amplification products in real time (Nolan et al., 2006). To quantify the initial amount of target nucleic acid, an amplification plot of fluorescence signal versus PCR cycle number, as well as a standard curve, are generated. Each curve in

the amplification plot (Figure 2.3a) consists of three distinct phases: the baseline, the exponential phase, and the plateau phase. During the baseline phase, PCR products are accumulating but fluorescence signals are below the minimum detection level of the instrument. The fluorescence of these PCR cycles is used to calculate the threshold, which is usually 10 times the standard deviation of the average baseline signal.

The threshold should intersect the amplification curve in the exponential phase, where the amplification is proceeding at its maximal exponential rate. A cycle threshold (Ct) value is then calculated for each sample, which reflects the cycle at which a detectable number of PCR products have accumulated above background fluorescence (Schmittgen and Livak, 2008). The Ct is also indicative of the relative amount of starting nucleic acid in each sample, such that a difference in Ct of 1 would indicate a two-fold difference in starting template between two samples. During the plateau phase, PCR products are no longer being generated at an exponential rate, due to reagent limitation or PCR inhibitors (Shipley, 2006; Wilhelm and Pingoud, 2003; Ginzinger, 2002).

The standard curve from a real-time RT-PCR assay (Figure 2.3b) is used to determine the relative abundance of nucleic acid of unknown samples based on their Ct values. The slope of the standard curve is used to calculate PCR efficiency, which would be -3.32 for an ideal assay. This correlates with 100 % PCR efficiency, where PCR products double after each cycle. PCR efficiencies below 90 % or above 110 % indicate the presence of PCR inhibitors and/or suboptimal reaction conditions and reagent concentrations. The R^2 value (coefficient of determination) describes the integrity of the data fit to the theoretical line, and is an indication of accuracy of serial dilutions and precision of pipetting.

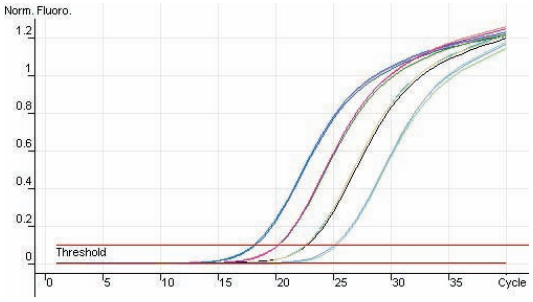

(a) Amplification Curve

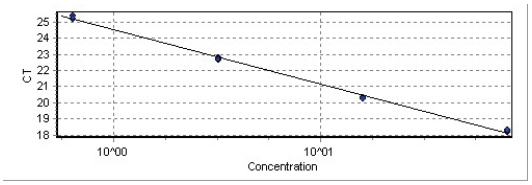

(b) Standard Curve

Figure 2.3: (a) Amplification curves from a real-time PCR assay. Normalised fluorescence signal of the dilution series on the y-axis is plotted against the PCR cycle number on the x-axis. (b)Standard curve from a real-time PCR assay. Standard curves plot Ct values versus the log starting quantity of nucleic acid of standard cDNA samples.

Detection Chemistries

'Detection chemistries' refers to the type of fluorescent chemistry employed to detect the amplified real-time PCR product, and can either be specific (probe-based) or non-specific (non-probe-based) chemistries (Bustin and Mueller, 2005).

Specific chemistries for real-time RT-PCR product detection involve the use of fluorescent oligonucleotide probes. The main advantage of using probe-based assays is that a fluorescent signal is only produced when the probe is hybridised to its complementary

target; therefore, primer-dimers and non-specific amplicons are not detected (Shipley, 2006). There are many different types of specific detection chemistries available, however, a detailed discussion is beyond the scope of this review.

Non-specific Dyes The simplest and one of the most widely used detection chemistry is the incorporation of a non-specific dye, such as SYBR Green I, which binds to the minor groove of dsDNA (Houghton and Cockerill, 2006). SYBR Green is a cyanine dye that, in solution, has a very low fluorescence and will not bind to single-stranded or denatured DNA (Shipley, 2006). However, it is able to intercalate between the two strands of dsDNA, and once bound, emits a fluorescent signal more than a thousand times greater than that of unbound dye. Therefore, during a real-time PCR assay utilising SYBR Green, an increase in fluorescent signal is observed as more dsDNA molecules are produced. The advantages of non-probe based chemistries are cost effectiveness and their relative ease of implementation (Houghton and Cockerill, 2006). One important disadvantage of using a non-specific dye is that every double-stranded molecule amplified in the reaction will be detected, including primer-dimers and non-specific products (Shipley, 2006). Therefore, when using SYBR Green, it is important to verify that the correct PCR product has been amplified, and this can be achieved by performing a melt curve analysis at the end of the PCR. This involves slowly heating the products from approximately $72\,^{\circ}C$ to $95\,^{\circ}C$ and measuring the fluorescence at $0.5 - 1.0\,^{\circ}C$ intervals: as the PCR product melts, the bound SYBR Green will be released into solution, causing the fluorescence to decrease, and this will produce a sharp slope when fluorescence is plotted against temperature (see Figure 2.4).

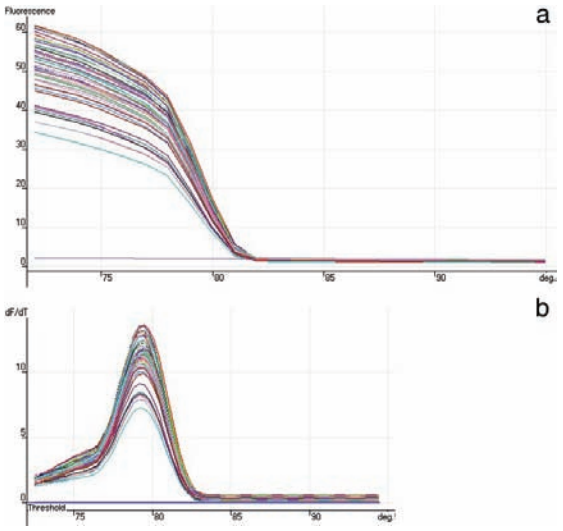

Figure 2.4: Melt curve analysis. (a) Raw data of fluorescence plotted against temperature. (b) By plotting the negative first derivative of fluorescence against temperature, a single peak is generated, which is representative of a single PCR product.

Data Analysis

The principle underlying real-time RT-PCR quantification is straightforward: the more copies of the target nucleic acid present at the beginning of the assay, the fewer cycles of amplification are required to reach the Ct (Bustin, 2005b). However, data processing can significantly affect the interpretation of real-time RT-PCR results (Larionov et al., 2005). An appropriate choice of data analysis is vital when carrying out a real-time RT-PCR assay. There are two general real-time RT-PCR quantification strategies: absolute and relative quantification.

Absolute Quantification Absolute quantification allows the precise determination of the copy number of a target sequence in a sample, and is useful in clinical diagnostics, e.g. quantifying viral or bacterial load, or monitoring responses to treatment (Bustin, 2000).

Relative Quantification Relative quantification measures the change in mRNA level of a gene relative to the levels of a co-amplified internal control (Bustin, 2005b). Controls may be endogenous, such as a reference gene; or exogenous, such as an artificial RNA template (Thellin et al., 2009). Relative quantification compares the Ct values from the gene of interest to those of one or more internal control and results are expressed as ratios of the target-specific signal to the internal reference (Bustin and Mueller, 2005). These corrected relative values of the target mRNA can then be compared between samples as a fold-difference in expression, for example, over a given time period in treated versus untreated samples (Applied-Biosystems, 2004). In many situations, it is sufficient to express changes in the relative abundance of mRNA transcripts rather than calculating the exact copy number of transcripts (Marino et al., 2003).

There are several mathematical models available for calculating the relative level of target mRNA. These include the $2^{-\Delta\Delta Ct}$ method (Schmittgen and Livak, 2008; Livak and Schmittgen, 2001), the standard curve method (Pfaffl, 2001), the linear regression model (Gentle et al., 2001) and the sigmoidal method (Liu and Saint, 2002). Nordgård et al. (2006) analysed the propagation of random error associated with relative real-time RT-PCR quantification of mRNA. Their results suggest that calculating sample-specific amplification efficiencies (as in the linear regression and sigmoidal models) severely decreases overall reproducibility. However, the use of standard curves results in random error. Therefore, the authors suggest that amplicon-specific efficiencies be determined from multiple standard curves with several replicates of each dilution, in order to minimise error.

2.3.2 Normalisation

Appropriate normalisation of gene expression data is necessary to correct for differences in the amount of amplifiable nucleic acid in individual samples as a result of different amounts of starting material, the quality of starting material (such as RNA integrity), efficiency of the reverse transcription and PCR, and experimental treatment (Radonič et al., 2004). Several normalisation strategies employed in real-time RT-PCR protocols are discussed below.

Ribosomal RNA Ribosomal RNA (rRNA) constitutes approximately 85 % of total RNA, while the mRNA fraction is between 2 - 5 % (Huggett et al., 2005). Several studies have demonstrated the consistent expression of 18S rRNA (Zhu and Altmann, 2005; Al-Bader and Al-Sarraf, 2005; Bas et al., 2004; Schmittgen and Zakrajsek, 2000) and 28S rRNA (Steele et al., 2002; Zhong and Simons, 1999) under various experimental conditions. Other studies have shown that the expression of 28S rRNA is regulated in certain situations and is therefore unsuitable as a normaliser (Maeda et al., 2005; Gutala and Reddy, 2004). The main problem with normalising to rRNA is that the rRNA:mRNA

ratio may not be consistent between samples; thus rRNA may not be representative of the overall cellular mRNA population (Zhu and Altmann, 2005; Vandesompele et al., 2002). Furthermore, RNA degradation, variability of the RT step or errors in RNA quantification will not be accounted for by normalisation to total RNA (Thellin et al., 2009).

Exogenous standards Exogenous standards represent an accurate method of normalisation because a known amount of standard can be incorporated into the RNA extraction process, which will then be affected by the same experimental error as the RNA of interest (Huggett et al., 2005). Exogenous standards can either be in vitro transcribed RNA that is homologous to the RNA of interest apart from a small insertion, deletion or mutation, or an artificial molecule with no homology to the RNA of interest (Freeman et al., 1999). Gilsbach et al. (2006) used an in vitro synthesised reference RNA from jellyfish as a normaliser for relative quantification of mRNA level. The jellyfish RNA had no homology to the RNA sequences of interest. The group found that in comparison to the standard reference genes concurrently evaluated (including GAPDH), the artificial RNA did not require validation for each experimental setting and therefore represented a more universal approach to normalisation. Several other groups have also reported reliable normalisation with exogenous reference standards (Untergasser et al., 2007; Moriya et al., 2006; Ke et al., 2000). However, exogenous RNA standards can be difficult to produce, and are subject to degradation. Also, they do not control for differences in quality of RNA template, meaning that an internal control, such as a reference gene, would still be required (Wong and Medrano, 2005). A recent article suggests that exogenous standards should be avoided in real-time RT-PCR studies (Thellin et al., 2009).

Reference genes The most popular normalisation strategy in real-time RT-PCR is the use of reference (or housekeeping) genes. Such genes should be expressed at a stable level in different tissue types and be unaffected by the experimental context under investigation (Zhu and Altmann, 2005; Stürzenbaum and Kille, 2001). However, it is well documented that most reference genes are somewhat regulated (Radonič et al., 2004; Dheda et al., 2004). For example, the mRNA level of one of the most widely used reference genes, glyceraldehyde-3-phosphate dehydrogenase (GAPDH) has been shown to vary under hypoxia (Zhong and Simons, 1999), in neoplastic cell lines (Aerts et al., 2004), in asthma (Glare et al., 2002), under stress (Derks et al., 2008) and in activated human T-lymphocytes (Bas et al., 2004). Despite these reports, GAPDH continues to be widely used as a normalising factor, in many cases without appropriate validation (Bustin, 2002). However, other groups have found the level of GAPDH to be stable (Bäckman et al., 2006; Meldgaard et al., 2006; Ullmannovà and Haškovec, 2003), thus highlighting the importance of evaluating the stability of a chosen reference gene for each new experiment in order to avoid misinterpretation of data (Meldgaard et al., 2006; Wong and Medrano, 2005; Dheda et al., 2004). While it is unlikely that a single reference gene exists that is unaffected by all biological conditions in all tissues (Gutierrez et al., 2008; Haller

et al., 2004), normalisation to the geometric mean of several reference genes (Vandesompele et al., 2002) is considered to be a reliable and conservative approach (Hellemans et al., 2007; Wong and Medrano, 2005). Indeed, recent evidence indicates that multiple reference genes are the best choice for real-time RT-PCR studies (Thellin et al., 2009). Therefore, normalisation to a panel of validated reference genes is the strategy employed in the present thesis and will be discussed in more detail in Chapter 4.

Conclusion The sensitivity and specificity of real-time RT-PCR have made it a powerful tool for quantifying mRNA levels. However, it is bound by several limitations, which are mainly due to the lack of standardised protocols from the initial RNA extraction to data analysis and interpretation of results. However, careful planning, optimisation and validation of real-time RT-PCR experiments can achieve reproducible and biologically relevant results (Bustin and Nolan, 2004). In the present thesis, the recently published 'Minimum Information for Publication of Quantitative Real-Time PCR experiments' guidelines (Bustin et al., 2009) have been followed as much as possible.

Aims and Hypotheses

The aims of the present thesis are:

1. To characterise the expression of SP at both the transcript and protein level in clinical TBI cases; and to characterise SP transcript level in a time course of experimental TBI in rodents. We hypothesised that SP expression would increase following TBI, consistent with our previous studies associating SP release with the neurological deficits in experimental TBI.

2. To quantify the mRNA level of SP in clinical cases of PD and in two rodent models of experimental PD, representing both the early and late stages of the disease. Previous studies have reported a decrease in SP expression in late-stage clinical and experimental PD, while studies from our laboratory report increased SP protein expression in early PD. Thus, we hypothesised that SP mRNA level would decrease in late-stage experimental PD and clinical PD cases, but would increase in early experimental PD.

3. To characterise the expression of TRPM channels at both the mRNA and protein level over a time course of experimental TBI in rodents and in clinical TBI cases.

4. To quantify the mRNA level of TRPM channels in clinical cases of PD and in two rodent models of experimental PD; and to characterise the protein expression of TRPM channels in the early model of experimental PD. TRPM channels have been implicated in ischaemic neuronal death and are highly expressed in the brain. We hypothesised that the expression of TRPM channels in both TBI and PD would increase, and potentially contribute to the pathophysiology of these disorders through excess Ca^{2+} influx, inflammation and oxidative stress mechanisms.

To achieve these aims, quantitative, real-time RT-PCR will be used for gene expression analysis, while immunohistochemistry will be applied to semi-quantify protein expression. A comprehensive outline of the methods used throughout this thesis is presented in the next chapter. Subsequent chapters will include a brief introduction, a summary of the methodology, a detailed results section and discussion. Chapter 4 describes our reference gene validation studies that were undertaken prior to real-time RT-PCR experiments to ensure accurate data normalisation. The following chapters characterise the expression of SP and TRPM channels in experimental and clinical TBI, and then in experimental and clinical PD. Finally, the major conclusions of the thesis will be further explored in a general discussion chapter.

Chapter 3

Materials and Methods

3.1 Materials

HPLC Grade Reagents Ethanol, isopropanol, chloroform and xylene were purchased from Ajax Finechem (Seven Hills, NSW, Australia). Methanol, hydrogen peroxide and sodium dihydrogen phosphate monohydrate (PBS powder) were purchased from Merck (Kilsyth, VIC, Australia).

Animal Surgery Adult male Sprague-Dawley rats were obtained from the Gilles Plains Animal Resource Centre (Gilles Plains, SA, Australia). Heparin sodium was obtained from Mayne Pharma (Mulgrave, VIC, Australia). Isoflurane was from Veterinary Companies of Australia (Kings Park, NSW, Australia). Lignocaine was from Troy Laboratories (Smithfield, NSW, Australia). Nine mm Autoclip wound clips were purchased from Becton Dickinson (Sparks, MD, USA). Meisinger high-speed micro drill was from Fine Science Tools (Vancouver, BC, Canada). Benchmark AngleOne rodent stereotaxic device was from Harvard Apparatus (Holliston, MA, USA). 6-hydroxydopamine-hydrobromide with 0.01 % ascorbic acid (6-OHDA) was purchased from Sigma-Aldrich (Sydney, NSW, Australia). Pentobarbitone sodium was from Virbac Australia (Milperra, NSW, Australia). PCR grade Cryotubes were from Greiner Bio-one (Frickenhausen, Germany). 10 % neutral buffered formalin was obtained from Fronine Laboratory Supplies (Riverstone, NSW, Australia).

Tissue Processing Rodent brain blockers were from David Kopf Instruments (Tujunga, CA, USA). Tissue was processed using the Sakura Tissue-Tek VIP (Torrance, CA, USA). Paraffin wax was obtained from BDH (Poole, England). Tissue was embedded in plastic cassettes using a Microm EC350-I Paraffin Embedding Center and cut with a Microm microtome (Heidelberg, Germany) fitted with Feather microtome blades (Japan). Tissue sections were placed on a Thermo Scientific tissue flotation bath (Lidcombe, NSW, Australia) and mounted onto Super-Frost Plus microscope slides (Menzel-Glaser, Braunschweig, Germany), with coverslips from Menzel-Glaser.

Immunohistochemistry reagents Abcam antibodies to TRPM channels were purchased from Sapphire Biosciences (Redfern, NSW, Australia). SP antibody was

purchased from Santa Cruz Biotechnology (Santa Cruz, CA, USA). Ethylenediaminetetraacetic acid (EDTA) (disodium salt) was purchased from Merck (Kilsyth, VIC, Australia). Lillie-Mayer's haematoxylin, eosin phloxine and histolene were from Fronine Laboratory supplies (Riverstone, NSW, Australia). Dako wax pens were from Dako (Glostrup, Denmark). Lithium carbonate and 3, 3'-diaminobenzidine tetrahydrochloride hydrate (DAB) were from Sigma-Aldrich (Sydney, NSW, Australia). Normal Horse Serum (NHS) was from SAFC Biosciences (Lenexa, KS, USA). Biotinylated anti-goat IgG was from Vector Labs (Burlingame, CA, USA). Streptavidin-peroxidase complex (SPC) was from Pierce (Rockford, IL, USA). DePeX mounting medium was from BDH (Poole, England).

Molecular Biology Reagents Platinum SYBR Green SuperMix-UDG, RNase-OUT, deoxynucleoside triphosphates (dNTPs), SuperScript III Reverse Transcriptase and TRIzol reagent were purchased from Invitrogen (Mulgrave, VIC, Australia).

Nuclease-free water, RNeasy MinElute Clean-up kit, RNeasy FFPE tissue kit, RNeasy Lipid tissue kit, RNase-free DNase set and QuantiTect Reverse Transcriptase kit were purchased from Qiagen (Doncaster, VIC, Australia).

Molecular biology grade agarose powder was from Edwards Instrument Co. (Narellan, NSW, Australia). Ethidium Bromide solution (10 mg/mL) was from Bio-Rad Laboratories (Regents Park, NSW, Australia). Molecular ladder and 6x loading dye were from Fermentas, Inc. (Quantum Scientific, QLD, Australia). Tris-borate-EDTA powder was purchased from Sigma-Aldrich (Castle Hill, NSW, Australia). RNase-*AWAY* was from Molecular BioProducts (San Diego, CA, USA). Custom oligonucleotides were synthesised by Geneworks (Adelaide, SA, Australia).

Laboratory Equipment RNA integrity was assessed with the Agilent 2100 Bioanalyzer using the RNA 6000 Nano Lab Chip Kit (Agilent, Forest Hill, VIC, Australia). Real-time PCR assays were carried out in the Corbett Rotor-Gene 3000 (Corbett Life Science, Mortlake, NSW, Australia). RNA concentration and purity were assessed using the Implen Nanophotometer (Integrated Sciences, Willoughby, NSW, Australia). Reverse transcription and end-point PCR were carried out in the Eppendorf MasterCycler (Eppendorf, North Ryde, NSW, Australia). PCR setup was conducted in an Aura PCR Workstation (Pavia, Italy). Stained tissue sections were scanned with a Nanozoomer (NDP Scan U10074-01, Hamamatsu Photonics K.K., Japan).

Human Brain Tissue Post-mortem fresh frozen human brain tissue was obtained from the Australian Brain Bank Network. More specifically, human TBI and all control brain tissues were from the Victorian Brain Bank Network, supported by The University of Melbourne, The Mental Health Research Institute of Victoria, Victorian Forensic Institute of Medicine and funded by the Neurosciences Australia and the National Health & Medical Research Council. Human PD tissue was received from the South Australian Brain Bank. Post-mortem FFPE human brain tissue was obtained from the IMVS Tissue Pathology Laboratory. All cases

selected for this study had donor or next-of-kin approval for research. The acquisition and use of human brain tissue in this study was approved by the University of Adelaide Human Ethics Committee (H-107-2007). Details of human cases are described in Appendix B.

3.2 Methods

3.2.1 Animal Ethics and Care

The experiments described herein were conducted according to National Health and Medical Research Council (NH&MRC) guidelines, and were approved by the ethics committees of the Institute of Medical and Veterinary Science (IMVS; 153a/07) and the University of Adelaide (M-016-2008).

Adult male Sprague-Dawley rats were group housed on a 12 hour night-day cycle and provided with a standard diet of rodent pellets and water *ad libitum*.

3.2.2 Rodent Model of Traumatic Brain Injury

Animals (n = 92; 400 - 450 g) were injured using the impact-acceleration model of diffuse TBI as described by Marmarou et al. (1994), which produces widespread axonal swelling, neuronal damage in the cortex and hippocampus, BBB disruption and mild subarachnoid haemorrhage in the absence of focal contusions or lesions. Behavioural and neurological deficits are also associated with this model of TBI (Morales et al., 2005; Foda and Marmarou, 1994).

To induce general anaesthesia, animals were placed inside a plastic induction chamber and anaesthetised with isoflurane at a concentration of 3 % in 1.5 L/min oxygen. When surgical depth of anaesthesia was reached, the animal was placed onto a heating pad set at $37\,^{\circ}C$ and given 1 % isoflurane in 1.5 L/min oxygen via a nose cone to maintain anaesthesia. The paw pinch reflex and eye blink reflex tests were performed to ensure surgical depth of anaesthesia prior to commencing surgery. The animal's head was shaved and 0.5 mL lignocaine was injected subcutaneously into the animal's scalp. The skull was exposed by midline incision along the dorsal surface of the head and retraction of the underlying muscle. A stainless steel disc (10 mm in diameter and 3 mm thick) was affixed to the skull with cyanoacrylate adhesive centrally between the bregma and lambda sutures and allowed to dry for several minutes. The animal was then removed from the anaesthetic, placed on a 10 cm deep foam cushion and secured with masking tape. The foam cushion was then placed underneath the injury device and TBI was administered by dropping a 450 g brass weight a distance of 2 m directly onto the stainless steel disc (See Figure 3.1). The animal was moved immediately after impact to prevent rebound impact.

Following injury, most animals experienced transient apnoea and were manually resuscitated until respiration was stable. The stainless steel disc was then removed from the skull, the midline incision was closed using surgical clips and antiseptic solution applied to the wound. Five mL saline was administered subcutaneously to prevent dehydration. Animals remained on thermal heating pads until consciousness was restored and were returned to their cages once ambulatory, where their condition was closely monitored for several more

hours. Any animal experiencing severe distress (or as advised by the Animal Care Facility) was euthanased by anaesthetic overdose (5 % isoflurane in 1.5 L/min oxygen). For comparison to injured animals, sham control animals were surgically prepared but not injured.

Figure 3.1: Induction of rodent TBI using the impact-acceleration model. Figure adapted from Marmarou et al. (1994).

Animal Sacrifice

At preselected time points following injury, animals were sacrificed either by perfusion (for immunohistochemistry analysis) or by anaesthetic overdose (for gene expression analysis). The time points chosen for the present study were: 1 hour, 3 hours, 5 hours, 1 day, 2 days, 3 days, 5 days and 7 days (5 animals per group), plus shams (n = 6). Previous studies in our laboratory have shown significant neuronal damage at 5 hours, 1 day, 3 days and 7 days following TBI (Donkin et al., 2007, 2009), however, no study to date has investigated cellular changes sooner than 5 hours after injury. Fresh frozen cerebral cortex and hippocampus tissue representing the 3 day survival time point was generated in our previous studies.

Anaesthetic Overdose Animals were anaesthetised with isoflurane (5 % in 1.5 L/min oxygen) until surgical depth of anaesthesia was confirmed by paw pinch reflex and eye blink reflex tests. Animals were immediately decapitated and brains rapidly removed. Surfaces for brain dissection and surgical tools were thoroughly cleaned with 70 % ethanol and RNase-*AWAY* immediately prior to decapitation. The left and right cerebral cortex and hippocampus regions were dissected on a sterile glass plate, transferred separately into sterile cryotubes and snap frozen in liquid nitrogen, then stored at $-80\,^{\circ}C$. Cerebral cortex and hippocampus were chosen for analysis because previous studies (Donkin et al., 2009; Gao and Chen, 2009) have demonstrated significant neuronal damage in these areas of the brain following TBI.

Perfusion Animals were anaesthetised with isoflurane (3 % in 1.5 L/min oxygen), then given 80 mg/kg pentobarbitone sodium in saline to a total volume of 1 mL, and 5000 IU heparin sodium. After surgical depth of anaesthesia was confirmed, the chest cavity was opened to expose the heart, and a blunt 19-gauge, 37 mm needle was inserted into the apex of the left ventricle and guided into position within the ascending aorta. The animal was then perfused with 10

% buffered formalin (pH 7.4). Following perfusion, brains were left to rest within the cranium for at least one hour, then intact brains were removed and fixed for at least one week in 10 % buffered formalin.

Brains were blocked and cut into consecutive 2 mm coronal sections and processed overnight. Tissue processing parameters were as follows: 20 mins each of graded ethanol baths (50 %, 70 %, 80 %, 95 %, 2 x 100 %) followed by two 1.5 hour xylene baths and finally paraffin baths of increasing time (30 mins, 2 x 60 mins, 90 mins). After processing, sections were embedded in paraffin wax.

3.2.3 Rodent Models of Parkinson's Disease

Two models of experimental PD were used in the present study, to replicate both the early and late stages of the disease. Both models utilised the compound 6-hydroxydopamine (6-OHDA), which is highly analogous to catecholaminergic neurotransmitters and is readily taken up into dopaminergic terminals by dopamine transporters (Schwarting and Huston, 1996). 6-OHDA rapidly oxidises and causes damage to neurons via the generation of free radicals. 6-OHDA can also accumulate in the mitochondria and impair the electron transport chain (Blandini et al., 2008).

The administration of 6-OHDA into the right striatum (Lee et al., 1996) results in the delayed cell death of approximately 40 % dopaminergic cells in the ipsilateral SN, representing the early stages of PD ('6-OHDA intrastriatal model'). To replicate the late stages of PD, 6-OHDA is injected into the medial forebrain bundle (MFB), at the origin of the nigrostriatal pathway (Lundblad et al., 2002), resulting in the depletion of 90 % or more dopaminergic terminals (Mela et al., 2007). The late-stage model will be referred to as the '6-OHDA SN model' in the present thesis. Dr. Emma Thornton and Mark Hassall carried out the animal surgery for the experimental PD study. Each 6-OHDA model and time point contained 5 animals per group.

To induce general anaesthesia, animals (n = 35; 250 - 300 g) were placed inside a plastic induction chamber and anaesthetised with halothane/isoflurane at a concentration of 3 % in 1.5 L/min oxygen. When surgical depth of anaesthesia was reached, the animal was placed onto a heating pad set at $37\,^{\circ}C$ and given 1 % halothane/isoflurane in 1.5 L/min oxygen via a nose cone to maintain anaesthesia. The dorsal surface of animal's head was shaved and the incision area cleaned with an alcohol swab. When withdrawal to pain reflex was absent, a midline incision was made on the dorsal surface of the head before the animal was placed onto a rodent stereotaxic device. To secure the animal to the device, the animal's upper incisor teeth were placed over the tooth bar at specific co-ordinates, and ear bars used to firmly secure the head in place. To ensure the animal was in a horizontal position, the animal was placed onto a 3.5 cm thick foam block, which also helped to maintain body temperature during the procedure. The skin and muscle was then retracted, and the skull cleaned and dried so that the midline and bregma sutures could be visualised.

For the early model of PD, two 0.7 mm burr holes were made on the surface of the skull over the right striatum using a high-speed micro drill, at the stereotaxic coordinates (1) anterior-posterior (AP): 0.5 mm,

medial-lateral (ML): 2.5 mm, and (2) AP: -0.5 mm, ML: 4.2 mm relative to bregma, with the tooth bar set at -3.9 mm. Using a 5 μL Hamilton micro syringe lowered stereotaxically 5.0 mm ventrally from the dura, 2 μL 6-OHDA (5 μg/μL in 0.9 % saline) was injected into the right striatum at a rate of 0.5 μL/min with the needle then left in place for 2 mins before being slowly retracted.

For the late model of PD, two 0.7 mm burr holes were made on the right surface of the skull above the MFB, using a high-speed micro drill, at the stereotaxic coordinates (1) AP: -4.4 mm, ML: 1.2 mm, tooth bar: -2.4 mm, and (2) AP: -4.0 mm, ML: 0.75 mm, tooth bar: 3.4 mm. Using a 5 μL Hamilton micro syringe lowered stereotaxically -8.0 mm ventrally from the dura, (1) 2.5 μL 6-OHDA and (2) 2.0 μL 6-OHDA (3 μg/μL in 0.9 % saline) was injected into the MFB at each stereotaxic co-ordinate, respectively, a rate of 0.5 μL/min with the needle then left in place for 2 mins before being slowly retracted.

Following 6-OHDA injections, the animal was removed from the stereotaxic device and anaesthetic delivery was discontinued. A small amount of Betadine antiseptic solution and lignocaine was applied to the surgical area and the incision closed using wound clips. An additional group of animals were subject to all surgical procedures except for administration of 6-OHDA (sham surgery) to serve as controls. All animals were allowed to recover on a heating pad following subcutaneous administration of 3 mL of 0.9 % saline to prevent dehydration. Animals were monitored until they were awake and mobile, and were then returned to their home cage.

Animal Sacrifice

Intrastriatal 6-OHDA animals plus shams were sacrificed 4 days after surgery by anaesthetic overdose (for gene expression analysis) or at 3 and 7 days after surgery by perfusion fixation (for immunohistochemistry), as described above for the TBI animals. These time points were chosen because previous studies from our laboratory have demonstrated cell loss replicating the early stages of clinical PD at these time points as well as significant functional and behavioural deficits (E. Thornton, PhD thesis).

Late model 6-OHDA animals plus shams were sacrificed at 1 day post-surgery by anaesthetic overdose (for gene expression analysis only). This time point was chosen to represent the cell loss of late stage clinical PD, since the lesions resulting from 6-OHDA injections into the MFB are virtually immediate (Blandini et al., 2008).

3.2.4 Immunohistochemistry

Haematoxylin and Eosin Staining

Serial 5 μm sections from paraffin blocks were cut with a microtome, floated on a water bath and mounted onto microscope slides. Sections were allowed to dry overnight before staining. On the day of staining, slides were placed in a metal rack and heated with a blow heater for 10 minutes. Sections were dewaxed with xylene (2 washes of 1 minute each) and rehydrated with 100 % ethanol (2 washes of 1 minute each) followed by a 1 minute rinse in tap water. Slides were placed into haematoxylin for 5 minutes, followed by 5 dips in acid alcohol and 10 seconds in saturated aqueous lithium carbonate, with rinses in tap water for 1 minute in between each

Table 3.1: Details of Antibodies used in Immunohistochemistry Studies

Protein	Supplier	Cat. Number	Concentration	Retrieval Solution	Origin
SP	Santa Cruz	sc9758	1/2000	EDTA	goat
TRPM2	Abcam	ab11168	1/3000	EDTA	rabbit
TRPM3	Abcam	ab56171	1/400	citrate	rabbit
TRPM6	Abcam	ab47017	1/1500	citrate	guinea pig
TRPM7	Abcam	ab729	1/150	EDTA	goat

step. Next, sections were stained in eosin for 2 minutes and dehydrated with 2 washes of 100 % ethanol for 1 minute each and 2 washes of histolene for 1 minute each. Slides were coverslipped and allowed to dry. Digital images of all sections were obtained with a Nanozoomer at a magnification of 40x.

SP and TRPM Channel Immunohistochemistry

Serial 5 μm sections from paraffin blocks were cut with a microtome, floated on a water bath and mounted onto microscope slides. Sections were allowed to dry overnight before staining. On the day of staining, slides were placed in a metal rack and heated with a blow heater for 10 minutes. Sections were dewaxed with xylene (2 washes of 1 minute each), rehydrated with 100 % ethanol (2 washes of 1 minute each) and dried briefly on blotting paper. Slides were placed in a methanol-hydrogen peroxide solution for 30 minutes to quench endogenous peroxidases (1 part hydrogen peroxide in 60 parts methanol), then washed twice in PBS for 3 minutes each. Slides were then placed into the appropriate retrieval solution (EDTA or citrate buffer, as described in Table 3.1) and were microwaved until the retrieval solution was boiling. Slides were allowed to cool, then rinsed twice in PBS for 3 minutes each. Next, each tissue section was outlined with a wax marker pen, then normal horse serum (NHS) in PBS was applied to each slide and allowed to incubate for 30 minutes. The appropriate amount of primary antibody was prepared in NHS and applied to each slide (see Table 3.1 for details) and left to incubate overnight.

The next day, slides were washed twice in PBS for 3 minutes each, then the secondary antibody was applied (1 in 250 solution of biotinylated IgG from animal of origin, see Table 3.1, in NHS) and left to incubate for 30 minutes. Slides were washed twice in PBS for 3 minutes each and then the tertiary antibody was applied (1 in 1000 solution of streptavidin-peroxidase complex in NHS) for 1 hour. After two more washes in PBS for 3 minutes each, a DAB solution was applied to each slide for 7 minutes. The DAB solution contained 0.2 M HCl, 0.2 M Tris and deionised water, which was adjusted to a pH of 7.65 - 7.70, with the addition 50 μL H_2O_2 and 1 mL DAB immediately prior to use. Slides were then washed in tap water for 10 minutes, counterstained with haematoxylin for 1 minute, followed by a rinse in tap water for 1 minute. Next, slides were dipped in acid alcohol 5 times, rinsed in tap water for 1 minute, then placed in saturated aqueous lithium carbonate for 10 seconds, followed by a final rinse in tap water. Sections were dehydrated with 2 washes of 100 % ethanol for 1 minute each and 2 washes of histolene for 1 minute each. Slides were

coverslipped and allowed to dry, then excess mounting medium removed.

Digital images of all sections were obtained with a Nanozoomer at a magnification of 40x. Slides were viewed with the Nanozoomer proprietary viewing software and the area of interest selected and exported in jpeg format. Stains were digitally separated using the colour deconvolution method of Ruifrok and Johnston (2001). The code to implement this algorithm was obtained from Landini (`http://www.dentistry.bham.ac.uk/landinig/software/software.html`) as an ImageJ macro. We used the staining vectors included with the macro. Background staining was subtracted using the 'rolling ball' method of Castle and Keller (`http://rsb.info.nih.gov/ij/plugins/rolling-ball.html`). The deconvolved DAB channel, representing the whole of the image antigen content, was semi-quantified by performing a histogram analysis and summing pixel frequency as a product of pixel intensity and then expressing this as a percentage of the total. This has the effect of weighting the histogram to make more frequent pixels 'darker' and so improve the signal to noise ratio. A resultant 'weight percent DAB' value was then obtained for each tissue section.

3.2.5 RNA Extraction

Initially, we chose fixed tissue as the source of RNA for the present study, because our laboratory has access to FFPE human and rat brain tissue, representing a wide variety of acute and chronic neurological pathologies, plus controls. Details of the methods used to extract and amplify RNA from FFPE tissue are discussed in Appendix A. After trials of several different techniques and a considerable amount of time, we were unable to obtain reproducible real-time RT-PCR results using RNA extracted from FFPE tissue. It was clear that using fresh frozen tissue would be the preferred alternative, as our pilot studies suggested that this tissue would be far more likely to generate reliable and reproducible real-time RT-PCR data. It may have been possible to characterise the FFPE tissue RNA using semi-quantitative PCR, but given that we have access to real-time RT-PCR technology, which is much more sensitive and reliable than semi-quantitative gel-based PCR (see Section 2), the RNA study using FFPE tissue was discontinued. Unfortunately, this limited the human component of the study due to the deficiency in fresh frozen human brain tissue available for research purposes.

Extraction of total RNA from frozen tissue was carried out either using TRIzol reagent (rat brain tissue) or Qiagen RNeasy Lipid Kit (human brain tissue), according to the manufacturer's instructions.

TRIzol method For rat tissue RNA extractions, approximately 50 mg tissue was homogenised in 1 mL TRIzol and allowed to incubate at room temperature for 5 minutes before being mixed with 0.2 mL chloroform and centrifuged for 15 minutes at 13,200 rpm. The aqueous phase was mixed with 0.5 mL isopropanol, incubated at room temperature for 10 minutes and centrifuged for 20 minutes at 12,000 rpm. After removal of the isopropanol, the precipitate containing the RNA was mixed with 1 mL 70 % ethanol and centrifuged for 10 minutes at 13,200 rpm. The precipitate was allowed to air dry

before resuspension in nuclease-free water. RNA samples were treated with the Qiagen RNase-free DNase set to remove any contaminating genomic DNA (gDNA), then purified and concentrated using the RNeasy MinElute clean-up kit (Qiagen) according to the manufacturer's instructions.

Qiagen method For human tissue RNA extractions, approximately 50 mg tissue was homogenised in 1 mL QIAzol reagent and allowed to incubate at room temperature for 5 minutes before being mixed with 0.2 mL chloroform and transferred into a MinElute spin column. Subsequent centrifuging and washing steps with proprietary buffers allow the RNA to bind to the column's silicon matrix, while removing impurities. An on-column DNase treatment step was included to remove residual gDNA. The RNA was eluted from the column in RNase-free water.

Working with RNA In order to minimise contamination with ribonucleases (RNases), which could compromise RNA-based experiments by degrading RNA (Sambrook and Russell, 2001), all laboratory glassware and plasticware, tissue homogenisers, benches, fumehoods, PCR machines, and microcentrifuge were subjected to a decontamination procedure prior to commencing experiments with RNA. Equipment was autoclaved where possible, then cleaned with 70 % ethanol followed by RNase-*AWAY*. Certified nuclease-free water was used in all RNA and PCR experiments. All pipette tips contained aerosol filters, and were certified sterile and nuclease-free. Pipettes dedicated for RNA and PCR work were used, and were regularly subjected to the decontamination procedure described above. Microcentrifuge tubes were pre-sterilised and certified nuclease-free.

Assessment of RNA Quantity and Quality RNA purity and integrity are critical factors influencing the accuracy of gene expression analysis (Fleige and Pfaffl, 2006). Total RNA was quantified using the Nanophotometer by measuring absorbances at 230 nm, 260 nm and 280 nm. RNA purity was assessed by the ratio of absorbances at 260 and 230 nm (A_{260}:A_{230}) and 260 and 280 nm (A_{260}:A_{280}). Pure RNA exhibits A_{260}:A_{230} and A_{260}:A_{280} ratios of $>$1.8, indicative of the absence of organic contaminants and protein, respectively, that may be carried over from the RNA extraction process (Imbeaud et al., 2005).

RNA integrity was assessed using the Agilent 2100 Bioanalyzer RNA 6000 Nano Chip (Series II) kit, according to the manufacturer's instructions. The Bioanalyzer employs automated microcapillary electrophoresis technology to separate RNA molecules according to size, and assigns each sample an RNA Integrity Number (RIN) ranging from 1 to 10, where 1 represents totally degraded RNA and 10 represents intact RNA (Schroeder et al., 2006). The Bioanalyzer is more sensitive and specific than conventional methods of RNA quality analysis such as agarose gel electrophoresis, and requires significantly less amounts of RNA (Imbeaud et al., 2005), thus making it a convenient tool for determining RNA integrity.

3.2.6 Reverse Transcription

Complementary DNA (cDNA) was synthesised using the Invitrogen SuperScript III Reverse Transcriptase kit (rat RNA) or the Qi-

agen QuantiTect Reverse Transcription kit (human RNA).

Invitrogen SuperScript III Method For rat RNA, 2 μg total RNA was added to 250 ng random hexamers, 1 mM each dNTP and nuclease-free water to 13 μL. Reactions were heated to $65\,^{\circ}C$ for 5 minutes then immediately placed on ice for 1 minute. To each tube, 4.75 μL 5x First Strand Buffer, 1 μL RNase OUT, 0.02 M dithiothreitol and 200 units SuperScript III reverse transcriptase were added. Reactions containing nuclease-free water in place of enzyme served as negative controls (No-RT controls). Reactions were incubated at $25\,^{\circ}C$ for 5 minutes, $55\,^{\circ}C$ for 60 minutes and $70\,^{\circ}C$ for 15 minutes. cDNA was diluted to 10 ng/μL with nuclease-free water, split into 2 aliquots and stored at $-20\,^{\circ}C$.

Qiagen QuantiTect Method For human RNA, 1 μg total RNA was added to 2 μL Genomic Wipeout buffer and nuclease-free water to 14 μL. The reaction was heated to $42\,^{\circ}C$ for 2 minutes then immediately placed on ice for 1 minute. To each tube, 4 μL buffer, 1 μL reverse transcriptase enzyme and 1 μL primers (a mixture of oligo(dT) and random hexamers) were added, then the reactions were incubated at $42\,^{\circ}C$ for 15 minutes followed by $70\,^{\circ}C$ for 3 minutes to inactivate the reverse transcriptase. Reactions containing nuclease-free water in place of enzyme served as negative controls (No-RT controls). cDNA was diluted to 10 ng/μL with nuclease-free water, split into 2 aliquots and stored at $-20\,^{\circ}C$.

Additional reverse transcription reactions were carried out on pooled RNA samples to generate pooled cDNA to be used for real-time PCR standard curves. Separate human and rat RNA pools were prepared from 10 representative RNA samples from each group with similar RIN values (10 μL each) and cleaned up using the RNeasy MinElute clean-up kit. cDNA was then synthesised from each RNA pool as described above, diluted to 20 ng/μL and stored at $-20\,^{\circ}C$ in single-use, 20 μL aliquots.

3.2.7 Real-time RT-PCR

Primer Design

As discussed in Section 2, careful validation of reference genes used for the normalisation of real-time RT-PCR data is necessary if accurate and biologically relevant results regarding gene expression are to be obtained. The stability of six candidate reference genes was evaluated in the human studies, with seven genes tested in the rat studies. An attempt was made to select genes from different functional classes in order to reduce the likelihood that the genes could be co-regulated (Vandesompele et al., 2002). The reference gene validation studies are described in Chapter 4. Details of genes studied, including forward and reverse primer sequences and amplicon sizes (in base pairs) are presented in Tables 3.2 and 3.3. Primers were designed using Primer3Plus software (Untergasser et al., 2007) (denoted as 'Novel'), or were obtained from the qPrimerDepot database (Cui et al., 2007), except where otherwise noted. In order to exclude amplification of gDNA, primers were designed to span exon-intron boundaries. Primers were assessed for specificity using PUNS software (Boutros and Okey, 2004) to ensure pro-

duction of a single amplicon specific to the mRNA transcript. Primer complementarity was evaluated using NetPrimer (`http://www.premierbiosoft.com/netprimer/netprlaunch/netprlaunch.html`) to minimise primer self-complementarity and primer-dimer formation, which could reduce PCR efficiency by preventing primers from binding to the target cDNA.

Real-time PCR Amplification

Optimisation Extensive optimisation was undertaken to determine appropriate PCR reaction conditions for each primer pair. This consisted initially of optimising forward and reverse primer concentrations, followed by running standard curves with a cDNA dilution series to determine optimal $MgCl_2$ concentration and annealing temperatures (T_a). With regard to the primer pairs obtained from the qPrimerDepot database, in depth optimisation was not required because primers were designed to perform efficiently at 300 nM and T_a = $60\,°C$. In order to optimise primer concentration, a series of PCR tubes were prepared containing different amounts of forward and reverse primers: 100 nM, 300 nM, 500 nM and 900 nM, with all combinations of these concentrations tested. The PCR assays were carried out as described in the PCR Assays section with a $60\,°C$ T_a and using a pooled sample of cDNA. The combination of forward and reverse primer that produced the lowest Ct value was selected. Further optimisation was then commenced using standard curves to fine tune annealing temperature and $MgCl_2$ concentration. A primer pair was considered to be optimised when the PCR reaction efficiency was between 90 % and 110 %, and the R^2 value was over 0.98 (preferably over 0.99), as determined by the Corbett Rotor-Gene 6 software. This correlates with the standard curve being linear over the entire dilution series. Reaction efficiency is calculated as a percentage according to the equation: $(10^{[-1/slope]} - 1 \times 100)$. No-RT controls were also run for each primer pair during the optimisation process to confirm specificity to the mRNA transcript, and correct amplicon size was confirmed with 2 % agarose gel electrophoresis. Optimal reaction conditions for all of the human primer pairs were: annealing temperature of $60\,°C$ and 300 nM forward and reverse primer concentrations, with the exception of TRPM2, β-actin and GAPDH, where the optimal forward and reverse primer concentrations was 400 nM. For the rat study, optimal reaction conditions were: $60\,°C$ T_a and 300 nM forward and reverse primer concentrations for all primer pairs with the exception of: GAPDH ($57\,°C$ T_a and 400 nM primer concentration) and POL2R ($56\,°C$ T_a, 400 nM primer concentration and the addition of 100 nM $MgCl_2$ to each reaction).

PCR Assays Real-time PCR reactions were carried out in a total volume of 20 μL, consisting of 10 μL 2x Platinum SYBR Green SuperMix-UDG (Invitrogen), forward and reverse primers (variable volume depending on optimal concentration), 1 μL cDNA and nuclease-free water. PCR amplification was carried out in a Corbett Rotor-Gene 3000 with an initial UDG incubation of $50\,°C$ for 2 minutes, initial denaturation of $95\,°C$ for 2 minutes, followed by 40 cycles of: $95\,°C$ for 15 sec denaturation, $x\,°C$ for 15 sec annealing, and $72\,°C$ for 15 sec extension ($x\,°C$

refers to the annealing temperatures for individual primer pairs).

Unknown cDNA samples were run in triplicate, with a set of standards (in triplicate) also included in each run, comprising five-fold serial dilutions made from aliquots of pooled cDNA. Serial dilutions comprised the following input amounts of cDNA: 50 ng, 10 ng, 2 ng, 0.4 ng. Negative controls containing water instead of cDNA were present in all runs.

Fluorescence data were collected during the extension step of each cycle. Following PCR cycling, melting curve analysis was carried out to confirm the production of a single PCR product by heating tubes from $72\,°C$ to $95\,°C$ and measuring fluorescence at $1\,°C$ increments (see Figure 2.4).

Reference Gene Stability and Data Analysis

Following PCR amplification, Ct values were calculated from the standard curve using the Corbett Rotor-Gene 6 software. The Ct of an individual sample reflects the cycle at which a detectable number of PCR products have accumulated above background fluorescence (Schmittgen and Livak, 2008). Raw values refer to uncorrected data that have not yet been normalised to the reference genes. The geNorm application (Vandesompele et al., 2002) was used to determine the most stable reference genes for the normalisation of our real-time RT-PCR data. This was carried out individually for the human and rat studies, as well as for each disease state, and is described in detail in Chapter 4. Subsequently, the most stable reference genes were applied to the normalisation of the mRNA levels of the genes of interest, using the qBasePlus program (Hellemans et al., 2007). qBasePlus utilises a modified version of the classic $2^{-\Delta\Delta Ct}$ method of relative expression analysis (Livak and Schmittgen, 2001; Schmittgen and Livak, 2008) that normalises data to multiple reference genes and takes into account gene- and run-specific amplification efficiencies. Finally, normalised sham/control mRNA levels were set to 1 to facilitate determination of mRNA fold changes in the injured groups.

Statistical Analysis

Unless otherwise specified, results graphs display mean $\pm$ SEM values. Statistical analyses were performed using GraphPad Prism version 5.00 for Windows, with $p < 0.05$ considered statistically significant. We used unpaired Student's t-tests and one-way analysis of variance (ANOVA) with Dunnett's Multiple Comparison *post hoc* test where appropriate.

Table 3.2: Details of Primer Sequences Used in Human Real-Time RT-PCR Experiments

Symbol	Accession No.	Name	Primer Sequences (5' → 3')	Amplicon Size (bp)	Reference
SP	NM_003182	Substance P	cgaccagatcaaggaggaac caaagaactgctgaggcttg	86	Novel
TRPM2	NM_001001188 NM_003307	Transient Receptor Potential Melastatin 2	cctcagttcgtggattcctg cgtgtagccacactgacaca	109	qPrimerDepot
TRPM3	BC_094699‡	Transient Receptor Potential Melastatin 3	agacccccataggtgttgct gggagaggcgactttcattt	104	Novel
TRPM7	NM_017672	Transient Receptor Potential Melastatin 7	tgggaaggctgaatatgagg agcaatatggcaggtggaac	76	Novel
GAPDH	NM_002046	Glyceraldehyde-3-phosphate dehydrogenase	ctctctgctcctcctgttcgac tgagcgatgtggctcggct	69	Carraro et al., 2005
ACTB	NM_001101	β-actin	agcctcgcctttgccga atgccggagccgttgtc	98	Novel
B2MG	NM_004048	β-2-microglobulin	ggctatccagcgtactccaa aatgtcggatggatgaaacc	109	Novel
HPRT	NM_000194	Hypoxanthine guanine phosphoribosyltransferase	tgaggatttggaaagggtgt tcccatctccttcatcacatc	88	Novel
HMBS	NM_000190	Hydroxymethyl bilane synthase	agcctactttccaagcggag gtacccacgcgaatcactct	96	qPrimerDepot
RPL13A	NM_012423	Ribosomal Protein L13a	agatggcggaggtgcag gttgatgccttcacagcgta	128	qPrimerDepot

‡TRPM3 has a large number of splice variants; primers were designed to be complementary to all of the following TRPM3 mRNA sequences: NM_020952.4, NM_024971.5, NM_206944.3, NM_206945.3, NM_206946.3, NM_206947.3, NM_206948.2, NM_001007470.1 and NM_001007471.2.

Table 3.3: Details of Primer Sequences Used in Rat Real-Time RT-PCR Experiments

Symbol	Accession No.	Name	Primer Sequences (5' → 3')	Amplicon Size (bp)	Reference
SP	NM_012666	Substance P	tggtcagatctctcacaaaagg tgcattgcgcttctttcata	99	Novel
TRPM2	NM_001011559	Transient Receptor Potential Melastatin 2	gaaggaaagaggggtgtg cattggtgatggcgttgtag	101	Yang et al., 2006
TRPM3	XM_219902 XM_001079904	Transient Receptor Potential Melastatin 3	aggcctcaaggtaattctgg cggctccttctcttggagat	124	Yang et al., 2006
TRPM6	XM_219747 XM_001078158	Transient Receptor Potential Melastatin 6	acagtcaaggcggtcattg ctggccaaactgctctgagt	120	Novel
TRPM7	AF_375874	Transient Receptor Potential Melastatin 7	ggggagttgctggtacttga aaccatgtcgcaggatgttt	96	Novel
GAPDH	NM_017008	Glyceraldehyde-3-phosphate dehydrogenase	tgcaccaccacctgcttagc ggcatggactgtggtcatgag	87	Li et al., 2004
B2MG	NM_012512	β-2-microglobulin	acatcctggctcacactgaa atgtctcggtcccaggtg	109	Novel
POL2R	XM_001079162	RNA polymerase II	tttgaggaaacggtggatgt tggcccagcataatattctca	92	Novel
HPRT	NM_012583.2	Hypoxanthine guanine phosphoribosyltransferase	ttgttggatatgcccttgact ccgctgtcttttaggctttg	105	Van Wijngaarden et al., 2007
GUSB	NM_017015	β-glucuronidase	tccttccatgtatcccaagg tggtaggggtggtgtacagg	104	Novel
TBP	NM_001004198	TATA Box Binding Protein	cagccttccaccttatgctc tgctgctgtctttgttgctc	165	Pohjanvirta et al., 2006
SDHA	AB_072907	Succinate dehydrogenase complex, subunit A	agacgtttgacaggggaatg tcatcaatccgcaccttgta	160	Pohjanvirta et al., 2006

Chapter 4

Validation of Reference Genes for Normalising Real-time RT-PCR Data

4.1 Introduction

As outlined in Chapter 2, real-time RT-PCR is the most sensitive method for detecting and quantifying mRNA transcripts (Bustin, 2000) and its development has greatly influenced the field of gene expression analysis. The real-time RT-PCR assay incorporates fluorescent molecules to measure the accumulation of PCR products during each cycle, thereby combining amplification and detection (Wong and Medrano, 2005). The transcript level of the gene of interest is normalised to one or more internal controls, which is necessary to account for differences in quantity and quality of starting material between samples (Bustin, 2005a; Radonič et al., 2004). Several strategies exist for the normalisation of real-time RT-PCR data, the most popular being the use of a reference gene (Dheda et al., 2004). Such genes should be expressed at a stable level in different tissue types and be unaffected by the experimental condition under investigation (Zhu and Altmann, 2005; Stürzenbaum and Kille, 2001). However, it is well documented that most reference genes are somewhat regulated (Jain et al., 2006; Dheda et al., 2005; Radonič et al., 2004; Tricarico et al., 2002). For example, the transcript level of one of the most commonly used reference genes, GAPDH, has been shown to vary considerably under different experimental conditions (Aerts et al., 2004; Bas et al., 2004; Glare et al., 2002; Zhong and Simons, 1999), rendering it unsuitable for normalisation in those studies. However, other groups have found the expression of GAPDH to be stable (Bäckman et al., 2006; Meldgaard et al., 2006; Ullmannovà and Haškovec, 2003), thus highlighting the importance of evaluating the stability of a chosen reference gene for each new experimental condition (Derks et al., 2008; Meldgaard et al., 2006; Wong and Medrano, 2005; Dheda et al., 2004).

It is unlikely that a single reference gene exists that is unaffected by any biological condition in all tissues (Haller et al., 2004). Vandesompele et al. (2002), however, demonstrated that normalisation to the geometric mean of the expression of multiple refer-

ence genes constitutes a more accurate approach than the use of a single reference gene. This group developed the geNorm application to determine appropriate panels of reference genes for accurate real-time RT-PCR data normalisation using pairwise variation analysis. Despite the increasing evidence that normalising real-time RT-PCR data to a single reference gene may be inappropriate, many authors continue to do so without proper validation (Bustin and Benes, 2005). Indeed, the majority of published articles regarding gene expression analysis in TBI describe the use of a single reference gene, such as GAPDH, cyclophilin, β-actin or 18S ribosomal RNA (for example, Brown et al. 2008; Yao et al. 2008; Sifringer et al. 2007; Shein et al. 2007; Pascale et al. 2006; Larner et al. 2005; Li et al. 2004), usually without including a reference gene validation protocol. Interestingly, a recent study reports acute increases in cyclophilin A protein expression following TBI (Redell et al., 2007), possibly rendering cyclophilin an inappropriate choice as a normaliser in TBI gene expression analysis studies. Since the expression of many commonly used reference genes has been shown to vary across different experimental situations, it is uncertain whether studies utilising a single gene for normalisation have measured a true change in the mRNA of interest. This point is illustrated in the present chapter. We demonstrate variable results regarding the gene expression of SP when a single, non-validated reference gene is used for normalisation (see Results).

Importantly, only a few studies have attempted to evaluate the stability of candidate reference genes for normalisation of mRNA quantification data in TBI. Our research group has previously validated reference genes at a single survival time point (3 days) in rodent TBI, using the impact-acceleration model of diffuse TBI (Cook et al., 2009a). Other studies have validated candidate reference genes in the controlled cortical impact model of TBI in mice (Thal et al., 2008), closed head injury in mice (Rhinn et al., 2008) and in the fluid percussion injury model in rats (Harris et al., 2009). However, no studies have investigated reference gene stability following clinical TBI, nor over a time course of rodent TBI using the impact-acceleration model.

In PD, even fewer studies have validated reference genes for real-time RT-PCR data normalisation. Coulson et al. (2008) evaluated candidate reference genes in three areas of the human brain in several neurodegenerative disorders, including PD. However, in the present thesis, we conducted gene expression analysis in five brain areas, only one of which was investigated in the study by Coulson et al. Furthermore, to our knowledge, no studies have evaluated reference gene stability in the 6-OHDA model of PD in rats.

With these factors in mind, identifying the most stable reference genes in each neurological condition (TBI and PD), in each species (human and rat) and in each different brain area was considered to be a vital prerequisite to gene expression analysis in the present thesis. The geNorm application (Vandesompele et al., 2002) was used to rank candidate reference genes in order of stability and to determine appropriate panels of reference genes for accurate data normalisation. This required PCR amplification of ev-

ery sample (i.e. all injured and control samples) for each reference gene that was evaluated. In the rat gene expression studies, seven candidate reference genes were evaluated: GAPDH, HPRT, B2MG, POL2R, TBP, SDHA and GUSB. In the human studies, six candidate reference genes were tested: GAPDH, HPRT, RPL13A, ACTB, B2MG and HMBS.

4.2 Materials and Methods

4.2.1 RNA Extraction and Reverse Transcription

Extraction of total RNA was carried out from the following tissue: rat TBI cerebral cortex and hippocampus with survival times of 1 hour to 7 days following injury, plus shams; rat SN and striatum from two 6-OHDA models of PD (striatal and SN 6-OHDA lesions), plus shams; human TBI and control temporoparietal cortex tissue; human PD and control tissue from 5 brain areas (SN, putamen, GP, caudate and midtemporal gyrus (MTG)). RNA concentration was determined using spectrophotometry and RNA integrity assessed using the Agilent Bioanalyzer 2100. Further details regarding animal surgery, RNA extraction and reverse transcription are described in the Materials and Methods Chapter (Section 3.2). Human case details are included in Appendix B.

4.2.2 Real-time RT-PCR

Real-time RT-PCR (including primer optimisation) for all candidate reference genes was carried out as described in Chapter 3.2. Briefly, reactions contained 10 μL 2x Invitrogen Platinum SYBR Green SuperMix-UDG, forward and reverse primers, 1 μL cDNA and nuclease-free water in a total volume of 20 μL. A set of standards was included in each run, comprising five-fold serial dilutions made from aliquots of pooled cDNA, derived from an RNA pool of all samples. Serial dilutions contained the following amounts of cDNA: 50 ng, 10 ng, 2 ng and 0.4 ng. Amplification was carried out in a Corbett Rotor-Gene 3000 with an initial UDG incubation of $50\,^{\circ}C$ for 2 minutes, initial denaturation of $95\,^{\circ}C$ for 2 minutes, followed by 40 cycles of: $95\,^{\circ}C$ for 15 sec denaturation, primer-specific annealing temperature for 15 sec and $72\,^{\circ}C$ for 15 sec extension. Fluorescence data were collected during the extension step of each cycle. Melting curve analysis was carried out after 40 cycles ($72\,^{\circ}C$ to $95\,^{\circ}C$) to verify a single PCR product. All cDNA samples were run in triplicate. Negative controls containing water instead of cDNA present in all runs, and no-RT controls were included for each gene to test for gDNA contamination.

4.2.3 PCR Data Analysis

Following PCR amplification, Ct values were calculated from the standard curve using the Corbett Rotor-Gene 6 software. The Ct of an individual sample reflects the cycle at which a detectable number of PCR products have accumulated above background fluorescence (Wilhelm and Pingoud, 2003). Triplicate Ct values for each sample were entered into the qBasePlus software (Hellemans et al., 2007) and used to generate an input file for geNorm v3.5. geNorm identified the most stable reference genes out of the candidate genes using expression stability analysis by pairwise correlations (described in detail in Vandesompele et al. 2002). An expression stability measure, *M*, was assigned to each gene,

which was used to rank candidate reference genes in order of stability. The recommended cut-off value of M is 1.5, and the lower the value of M, the more stable the expression of the candidate reference gene. Pairwise variation (V) analysis then determined the optimal number of reference genes required for accurate data normalisation in each experiment. As an example of the importance of reference gene validation, individual reference genes were used to normalise gene expression data for our gene of interest, SP, using the $2^{-\Delta\Delta Ct}$ method of relative expression analysis (Livak and Schmittgen, 2001; Schmittgen and Livak, 2008).

4.3 Results

4.3.1 RNA Quality

The concentration of extracted total RNA was quantified by measurement of the absorbance at 230 nm, 260 nm and 280 nm using a UV spectrophotometer. All samples had $A_{260:A280}$ and $A_{260:A230}$ ratios above 1.6, although most values were over 2.0, indicating relatively pure RNA. RNA integrity was assessed using automated micro-capillary electrophoresis in the Agilent Bioanalyzer. An RNA Integrity Number (RIN) was assigned to each sample by the Agilent Bioanalyzer Expert 2100 software, with a RIN of 10 representing intact RNA and a RIN of 1 representing completely degraded RNA. The mean RIN value of the rat RNA samples was 8.37 ± 0.91 (range 6.9 - 9.6), while in the human samples the mean RIN was 6.12 ± 1.04 (range 4.9 - 7.4). Representative electropherograms from rat and human RNA samples are shown in the next chapter, Figure 5.1.

4.3.2 Reference Gene Stability

geNorm determined the most stable reference genes out of the seven and six candidate genes in the rat and human TBI studies, respectively. Figure 4.1 shows geNorm results charts for the rat TBI cortex study. Since 12 different reference gene validation studies were carried out to encompass all experimental conditions, only the rat TBI results graphs have been included as examples, with the remaining studies summarised in tabular format. The most stable reference genes for each group plus recommended number of reference genes for accurate data normalisation are therefore summarised in Tables 4.1, 4.2 and 4.3. The candidate reference genes are ranked in order of stability in each table, with the most stable genes at the top of each column and the least stable genes at the bottom. The reference genes highlighted in bold represent the panels of genes required for accurate normalisation. Note that geNorm does not discriminate between the two most stable genes, since it relies on pairwise correlations. The cut-off value of V is recommended to be 0.15, below which additional reference genes are not required. The recommended threshold values of M and V were met in all rat studies, but not in all human studies. If there were no values of V below 0.15, the combination of reference genes producing the lowest value of V was chosen.

Note that in Table 4.2, the reference gene rankings and number of genes required for accurate normalisation were the same in both the early and late-stage experimental PD models.

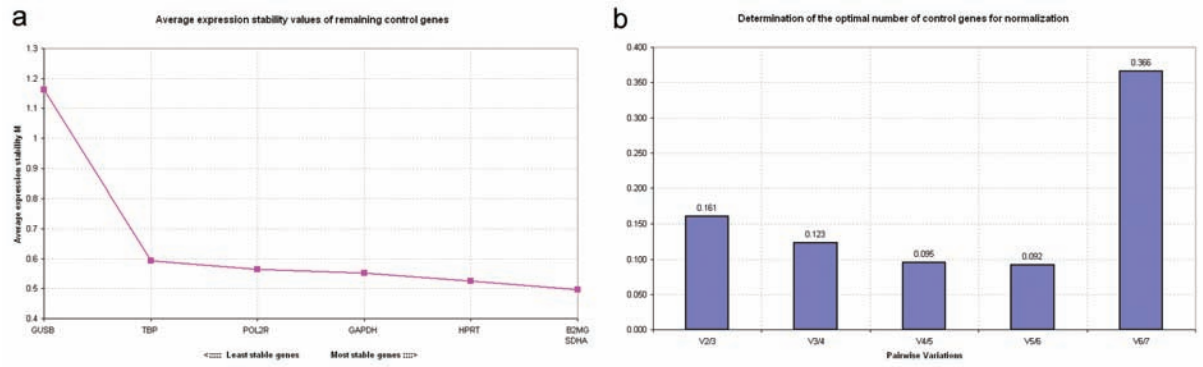

Figure 4.1: geNorm results charts for the rat TBI cortex study. (a) shows calculated M values for each reference gene and ranking of genes in order of stability, with the most stable genes at the right of the chart. In part (b), pairwise variation analysis determined that four reference genes were optimal for accurate normalisation, indicated at the V3/4 step of the chart, where the V threshold of below 0.15 is met (Vandesompele et al., 2002).

Table 4.1: geNorm Ranking of Candidate Reference Genes in TBI

Rat Cortex	Rat Hippocampus	Human Cortex
B2MG/SDHA	**HPRT/SDHA**	**GAPDH/RPL13A**
HPRT	**GAPDH**	**HPRT**
GAPDH	**TBP**	ACTB
POL2R	GUSB	HMBS
TBP	B2MG	B2MG
GUSB	POL2R	

Table 4.2: geNorm Ranking of Candidate Reference Genes in Rat PD

6-OHDA Striatum	6-OHDA SN
GUSB/SDHA	**B2MG/HPRT**
HPRT	**GAPDH**
TBP	**SDHA**
POL2R	TBP
GAPDH	GUSB
B2MG	POL2R

4.3.3 SP Normalised to Individual Reference Genes

To illustrate the importance of reference gene validation studies, SP mRNA level in the rat hippocampus following TBI was normalised to the seven candidate reference genes individually (Figure 4.2). When data were analysed this way, SP mRNA level was highly variable depending on which reference gene was used for normalisation. When normalised to POL2R or GUSB individually, SP mRNA level was significantly ($p < 0.05$) reduced in the TBI group compared to shams, as assessed by unpaired Student's t-tests. Importantly, geNorm identified POL2R as the least stable reference gene in the hippocampus out of the seven genes evaluated, and GUSB was ranked fifth. There were no significant differences ($p > 0.05$) in SP transcript levels when each of the other individual reference genes were used as normalising factors.

Also note the large error bars in Figure 4.2, demonstrating large variation between samples in each group.

Table 4.3: geNorm Ranking of Candidate Reference Genes in Human PD

SN	Caudate	GP	Putamen	MTG
B2MG/GAPDH	**B2MG/HMBS**	**ACTB/GAPDH**	**B2MG/HMBS**	**B2MG/HMBS**
HMBS	**RPL13A**	**HMBS**	**HPRT**	**RPL13A**
ACTB	**GAPDH**	**RPL13A**	**RPL13A**	GAPDH
RPL13A	**HPRT**	**B2MG**	**GAPDH**	HPRT
HPRT	ACTB	HPRT	ACTB	ACTB

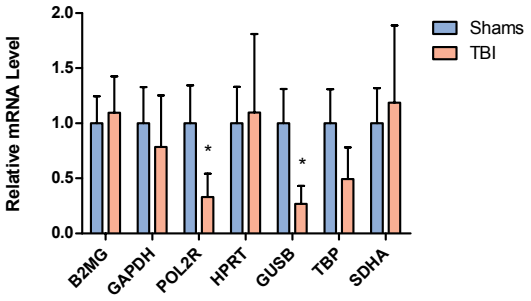

Figure 4.2: The implications of using a single, non-validated reference gene for real-time RT-PCR data analysis. SP mRNA level in rat hippocampus following TBI (3 day survival) or sham surgery is highly variable after normalisation to individual reference genes. Bars show mean ± SEM of 5 TBI animals and 6 shams. * denotes $p < 0.05$.

4.4 Discussion

Real-time RT-PCR is a robust and sensitive technique for quantifying mRNA transcripts, and constitutes a powerful tool for increasing our understanding of the genomic response to neurological disorders. It requires an appropriate normalisation strategy to control for error, the most common being the use of one or more endogenous reference genes (Nolan et al., 2006). A reference gene should be expressed at a stable level regardless of the experimental context, however, several studies have demonstrated that the expression of reference genes can vary considerably. Normalisation of real-time RT-PCR data using a single, non-validated reference gene could fail to detect small changes in the mRNA species of interest (Olsvik et al., 2005), or could lead to diverse or inaccurate biological conclusions (Dheda et al., 2005). Vandesompele et al. (2002) demonstrated that normalisation to the geometric mean of the expression of multiple reference genes represents a more accurate approach than a single gene. The geNorm application was developed by this group to identify appropriate panels of reference genes for real-time RT-PCR data normalisation, and this strategy is considered to be reliable and conservative (Hellemans et al., 2007; Wong and Medrano, 2005).

Identifying the most stable reference genes in each neurological condition (TBI and PD), in each species (human and rat) and in each different brain area was considered a vital component of the present thesis. The geNorm application was used to evaluate the stability of seven candidate reference genes in the rat studies, and six in the human studies, and to determine appropriate panels to be used for data normalisation. geNorm identified B2MG, SDHA, HPRT and GAPDH as a suitable panel of reference genes for data normalisation in the rat cerebral cortex following TBI, and HPRT, SDHA, GAPDH and TBP in the rat hippocampus. GAPDH and HPRT were also ranked among the most stable genes following TBI in the human temporoparietal cortex (Table 4.1), suggesting

that these genes may be suitable normalisers across different brain regions and species in TBI gene expression analysis studies. Interestingly, Meldgaard et al. (2006) showed that GAPDH and HPRT were suitable reference genes for data normalisation in mouse neurobiology studies, and Thal et al. (2008) found that HPRT remained stable after controlled cortical impact in mice.

In the human PD study, candidate reference genes were ranked in 5 different brain areas: SN, caudate, GP, putamen and MTG. The results (Table 4.3) indicate that B2MG and HMBS were among the most stable genes across the different brain areas. Notably, HMBS was among the most stable genes in another PD reference gene validation study in human MTG (Coulson et al., 2008). In the present study, ACTB and HPRT were generally among the least stable reference genes, except in the GP, where ACTB was one of the top two genes and B2MG was the second least stable gene. These results are particularly intriguing, as they demonstrate that stability of a candidate reference gene in one brain area does not necessarily confer stability in another. Therefore, it is likely that the use of a single reference gene would be inadequate for normalising real-time RT-PCR data when investigating gene expression in different brain areas of PD. Moreover, when comparing reference gene rankings in the human and rat SN, B2MG and GAPDH were among the most stable genes in both species (Tables 4.2 and 4.3). However, while HPRT is among the top ranked genes in the rat SN, it is the least stable gene in the human SN. Such findings highlight the importance of careful selection and validation of reference genes to be used for real-time RT-PCR normalisation, indeed for each new experimental context under investigation.

To further illustrate this point, data regarding SP mRNA level in the rat hippocampus following TBI were normalised to the seven candidate reference genes individually. When SP data were normalised to either GUSB or POL2R only, a significant ($p < 0.05$) decrease in SP transcript level was observed in TBI rats compared to shams. However, when normalised individually to the other five reference genes, there was no significant difference in SP mRNA level between TBI and uninjured rats. Furthermore, normalising to a single reference gene produced a considerable variation of relative SP transcript level between samples, which is clearly demonstrated by the large error bars in Figure 4.2. When SP mRNA levels were normalised to the panel of stable reference genes identified herein, far more consistent results were obtained (see Chapter 5).

In conclusion, the results of the present chapter demonstrate the importance of identifying and validating suitable reference genes for real-time RT-PCR normalisation, and are consistent with other studies where the choice of reference gene has influenced the biological interpretation of real-time RT-PCR data (Langnaese et al., 2008; Cappelli et al., 2008; Gutierrez et al., 2008; Aerts et al., 2004). The panels of stable reference genes identified by geNorm will be used as normalising factors for real-time RT-PCR in upcoming chapters.

Chapter 5

SP Expression Following Clinical and Experimental TBI

5.1 Introduction

TBI is the leading cause of death and disability in people under 40 years of age and represents a major public health burden (Fleminger and Ponsford, 2005). Motor vehicle accidents account for the majority of moderate-severe TBI cases (Khan et al., 2003), and survivors of TBI are often left with devastating long-term motor, cognitive and behavioural deficits. The neurological dysfunction resulting from TBI is due to direct, immediate mechanical damage to brain tissue (the primary injury) as well as indirect, delayed secondary injury mechanisms that are triggered by the primary event and may continue for days to weeks after the insult (Morales et al., 2005; Roth and Farls, 2000). Secondary injury factors include such processes as breakdown of the BBB, oedema, inflammation and excitotoxicity, all of which can be deleterious to neuronal cells (Barone and Kilgore, 2006; Golding, 2002). These processes significantly contribute to the morbidity and mortality following TBI (Cormio et al., 1997), but their molecular mechanisms require further elucidation.

Of particular significance is vasogenic oedema, which occurs in the context of BBB disruption, allowing proteins and water enter the brain (Heo et al., 2005), causing rises in intracranial pressure and promoting neuronal cell death. Research from our laboratory (Nimmo et al., 2004; Vink et al., 2003) has shown that neurogenic inflammation is central to the genesis of BBB permeability, vasogenic oedema and the functional deficits following diffuse TBI in rats. The neuropeptide, SP, is a potent initiator of neurogenic inflammation. A recent study from our laboratory (Donkin et al., 2009) has demonstrated a link between SP and the development of cerebral oedema and functional deficits following TBI, which are attenuated with the administration of an NK-1R antagonist. However, no study has quantified the mRNA level or protein expression of substance P following TBI in human clinical cases, nor over a time course of experimental TBI in rats. Therefore, in this chapter, SP expression following TBI has been characterised, specifically using real-time RT-PCR to quantify SP mRNA level and immunohistochemistry to

identify SP protein, with the hypothesis that SP mRNA level and protein expression would increase following TBI. The expression of SP was examined both in clinical TBI cases, and in a rodent model of experimental TBI with survival times from 1 hour to 1 week, however, SP immunohistochemistry was not carried out in the rat model of TBI, since this has been conducted in the aforementioned study by our laboratory (Donkin et al., 2009). A reference gene validation study was carried out prior to real-time RT-PCR quantification of SP to ensure accurate data normalisation (see Chapter 4).

5.2 Materials and Methods

5.2.1 Rodent Model of TBI

Adult male Sprague-Dawley rats (n = 46; 400 - 450 g) were group housed on a 12 h night-day cycle and provided with a standard diet of rodent pellets and water. Animals were randomly assigned into TBI (n = 40) and uninjured (n = 6) groups at the beginning of the experiment. Animals were injured using the impact acceleration model of diffuse TBI as described in detail by Marmarou et al. (1994), and outlined in Section 3.2.2 of the present thesis. Briefly, rats were anaesthetised with isoflurane and the skull exposed by midline incision. Lignocaine was applied to the incised area and a stainless steel disc (9 mm in diameter and 3 mm in depth) rigidly fixed with cyanoacrylate to the skull, placed centrally between the lambda and bregma sutures. Animals were placed in the prone position on a 10 cm foam bed and subjected to brain injury by dropping a 450 g brass weight a distance of 2 m onto the stainless steel disc. Sham control animals were surgically prepared, but not injured. A thermostatically controlled heating pad was used to maintain animals at $37\,^{\circ}C$ throughout surgery and recovery. Animals were sacrificed by anaesthetic overdose following sham surgery (n = 6) or at 1 hour, 3 hours, 5 hours, 1 day, 2 days, 3 days, 5 days or 7 days following injury (n = 5 per group). Brains were rapidly removed and the cerebral cortex and hippocampus regions dissected in total and snap frozen in liquid N_2, then stored at $-80\,^{\circ}C$. The cerebral cortex and hippocampus were chosen for analysis because previous studies (Donkin et al., 2009; Gao and Chen, 2009) have demonstrated significant neuronal damage in these brain regions following TBI.

5.2.2 Human TBI Cases

The use of post-mortem human brain tissue in this study was approved by the University of Adelaide Human Ethics Committee and all cases had written donor or next-of-kin consent for research. All human tissue used in this study was assessed by a clinical neuropathologist and given a diagnosis of either neurotrauma or normal brain. Case details regarding human tissue are described in Appendix B. For gene expression analysis, fresh frozen human brain tissue (temporoparietal cortex; coronal section 1 cm posterior to mamillary bodies) of 20 TBI and 10 age- and sex-matched control cases was obtained from the Victorian Brain Bank Network. Frozen tissue cases were subdivided into survival times of $<$ 5 hours (n = 12) and 5 - 24 hours (n = 8) based on the supplied clinical information. For immunohistochemistry analysis, post-mortem FFPE human brain tissue (parietal cortex and hip-

pocampus) from 9 TBI and 6 age- and sex-matched control cases was obtained from the tissue pathology laboratory of the IMVS. FFPE cases were subdivided into survival times of $<$ 5 hours (n = 6) and 5 - 24 hours (n = 3) based on detailed clinical information.

5.2.3 RNA Extraction and Real-time RT-PCR

Extraction of total RNA was carried out from rat TBI and sham cerebral cortex and hippocampus tissue (n = 5 TBI animals per survival time point; n = 6 shams) and human TBI (n = 20) and control (n = 10) tissue as described in detail in the Materials and Methods chapter (Section 3.2.5). Fifty mg tissue was used in each RNA extraction, and a DNase treatment was included. Total RNA was quantified by UV spectrophotometry to measure absorbance at 230 nm, 260 nm and 280 nm. RNA integrity was assessed using the Agilent Bioanalyzer RNA 6000 Nano Chip (Series II) kit. Complementary DNA was synthesised as described in Section 3.2.6, diluted to 10 ng/μL and stored at $-80\,^{\circ}C$ until PCR.

A reference gene validation study was carried out to determine the most stable reference genes for accurate real-time RT-PCR data normalisation in both the rat and human TBI studies. The reference gene validation studies have been outlined in Chapter 4.

Real-time RT-PCR was carried out as described in Section 3.2.7. Briefly, each reaction contained 10 μL 2x Invitrogen Platinum SYBR Green SuperMix-UDG, forward and reverse primers, 1 μL cDNA and nuclease-free water in a total volume of 20 μL. A set of standards was included in each run. Amplification was carried out in a Corbett Rotor-Gene 3000 and fluorescence data were collected during the extension step of each cycle.

Following PCR amplification, Ct values were calculated from the standard curve using the Corbett Rotor-Gene 6 software. Triplicate Ct values for each sample were entered into the qBasePlus software (Hellemans et al., 2007). qBasePlus calculated mRNA levels of SP, relative to multiple reference genes and taking into account run-specific amplification efficiencies. Sham/control levels were set to 1 to facilitate determination of mRNA fold changes.

5.2.4 SP Immunohistochemistry

Post-mortem human brain tissue was processed according by IMVS staff according to standard diagnostic protocols and embedded in paraffin wax. Serial 5 μM sections were cut with a microtome, mounted onto microscope slides and left to dry overnight. Sections were stained for SP as described in detail in Section 3.2.4. EDTA was used as a retrieval solution, and the resultant immunocomplex was visualised using the chromogen DAB.

Digital images of all sections were acquired using a Nanozoomer Digital Pathology Scanner at a magnification of 40x. Colour deconvolution analysis was performed to determine 'weight % DAB' values and therefore to semi-quantify SP protein content.

5.2.5 Statistical Analysis

GraphPad Prism was used to carry out one-way ANOVA with Dunnett's multiple comparison test, with $p < 0.05$ considered statistically significant.

5.3 Results

5.3.1 RNA Quality

The concentration of extracted total RNA was measured by UV spectrophotometry. All samples had $A_{260:A280}$ and $A_{260:A230}$ ratios above 1.6, although most values were over 2.0, indicating relatively pure RNA. RNA integrity was assessed using automated microcapillary electrophoresis in the Agilent Bioanalyzer. A RIN was assigned to each sample by the Agilent Bioanalyzer Expert 2100 software, with a RIN of 10 representing intact RNA and a RIN of 1 representing completely degraded RNA. The mean RIN value of the rat RNA samples was 8.37 $\pm$ 0.91 (range 6.9 - 9.6), while in the human samples the mean RIN was 6.12 $\pm$ 1.04 (range 4.9 - 7.4). Representative electropherograms from rat and human RNA samples are shown in Figure 5.1.

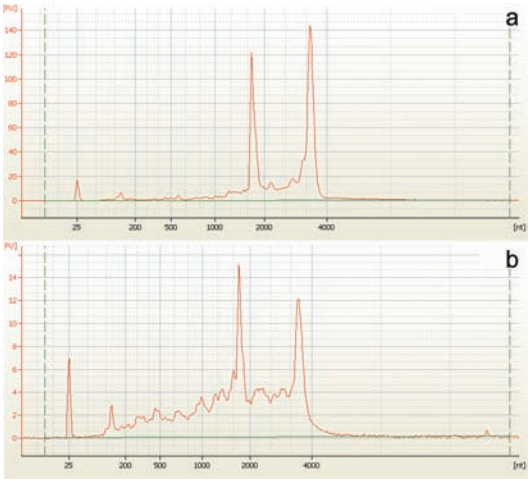

Figure 5.1: Bioanalyzer assessment of RNA Integrity. Electropherograms from (a) rat and (b) human RNA samples, with RNA Integrity Numbers (RIN) of 9.6 and 6.5, respectively.

5.3.2 SP mRNA Quantification

The qBasePlus program was used to calculate the normalised mRNA level of SP following human and rat TBI, relative to the most stable reference genes as determined by geNorm (described in Chapter 4). In the rat cerebral cortex, the most stable reference genes were B2MG, SDHA, HPRT and GAPDH, with 4 reference genes required for accurate data normalisation. In the rat hippocampus, four genes were again recommended for accurate normalisation: HPRT, SDHA, GAPDH and TBP. In the human study, GAPDH, RPL13A and HPRT were the most stable reference genes.

In the rat cerebral cortex, SP mRNA exhibited a cyclic pattern of expression (Figure 5.2a). At 3 hours post-injury there was a significant increase in SP mRNA compared to shams (8.66 $\pm$ 3.41 fold increase, $p < 0.01$). This returned to sham levels at 5 hours, but showed a trend towards increasing again in the 1 day and 2 day TBI groups (1 day: 2.56 $\pm$ 0.78 fold increase; 2 days: 5.02 $\pm$ 2.45 fold increase). At 3 days after injury, SP mRNA level had returned to sham values, but at 5 days and 7 days again showed a trend to increase (4.40 $\pm$ 1.51 and 3.83 $\pm$ 1.04 fold increases, respectively).

In the rat hippocampus (Figure 5.2b), SP mRNA level was significantly ($p < 0.05$) elevated at every time point after TBI except for the 3 day survival time.

In the human temporoparietal cortex, shown in Figure 5.2c, there was a significant ($p < 0.01$) increase in SP mRNA level in the $<$ 5 hour TBI group compared to controls, while in the 5 - 24 hour group, SP mRNA level was significantly ($p < 0.05$) decreased.

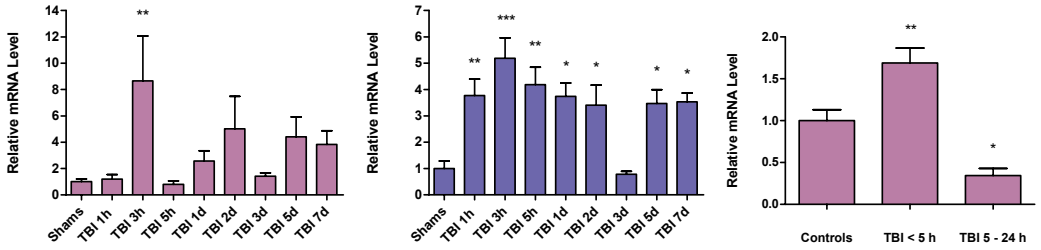

(a) Rat Cx mRNA **(b)** Rat Hipp mRNA **(c)** Human Cx mRNA

Figure 5.2: SP mRNA level following TBI, in (a) rat cortex, (b) rat hippocampus and (c) human temporoparietal cortex. Bars depict mean ± SEM of 5 animals per rat TBI group and 6 shams; 12 TBI cases (< 5 hours survival), 8 TBI cases (5 - 24 hour survival) and 10 controls in the human study, all from triplicate PCR amplifications. Cx, cortex; Hipp, hippocampus; * denotes $p < 0.05$; ** denotes $p < 0.01$; *** denotes $p < 0.001$.

5.3.3 SP Immunohistochemistry

Figure 5.3 shows representative SP immunostaining in the human parietal cortex and hippocampus of TBI and control cases. In the parietal cortex of control cases (Figure 5.3a), there is light SP immunoreactivity and some granulation in the parenchyma, within neuronal cells and in the perivascular region. In the parietal cortex of TBI cases (Figures 5.3b and c), SP immunoreactivity can still be seen within neuronal cells and in some areas of the parenchyma, but staining intensity is markedly reduced compared to the control section, and very minimal perivascular SP immunoreactivity is present.

In the control hippocampus (dentate gyrus) (Figure 5.3d), light SP immunoreactivity is visible in the parenchyma, with some slight areas of granulation. In the < 5 hour TBI hippocampus (Figure 5.3e), there is a clear reduction in SP immunoreactivity compared to the control section, with only slight areas of staining around the injured neurons. In the 5 - 24 hour TBI group (Figure 5.3f), the overall intensity of SP staining appears to be less than the control section, however, areas of granulation can be seen within the parenchyma.

Colour deconvolution analysis was used to semi-quantify SP protein expression in human TBI and control parietal cortex and hippocampus tissue sections. These results are depicted in Figure 5.4, which shows mean immunoreactivity (weight % DAB, representing the whole of the image antigen content) expressed as a percentage of control levels.

In the human parietal cortex, SP protein expression was significantly decreased in both TBI groups (< 5 hours and 5 - 24 hours; $p < 0.01$). In the human hippocampus, there was also a significant decrease in SP protein in both TBI groups ($p < 0.05$). We obtained FFPE tissue from two additional clinical TBI cases with a longer survival time of 4 days. The SP expression in the parietal cortex and hippocampus of these samples was not significantly different ($p > 0.05$) to the controls (data not shown).

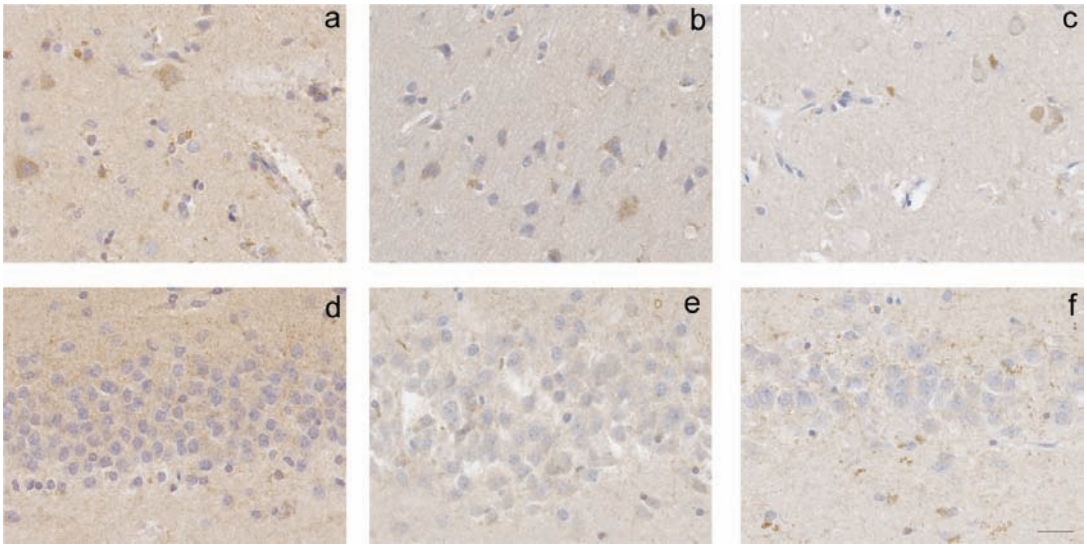

Figure 5.3: SP immunoreactivity following clinical TBI, in the parietal cortex of (a) control, (b) TBI < 5 hour survivor, (c) TBI 5 - 24 hour survivor; and the hippocampus (dentate gyrus) of (d) control, (e) TBI < 5 hour survivor, (f) TBI 5 - 24 hour survivor. Scale bar = 25 μm.

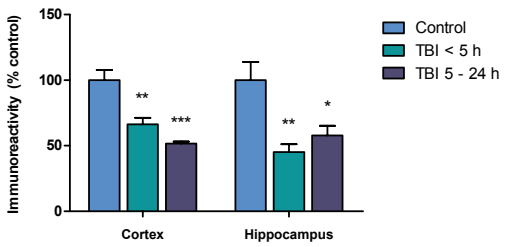

Figure 5.4: SP protein expression following clinical TBI, in parietal cortex and hippocampus (dentate gyrus). Bars depict mean immunoreactivity ± SEM of 6 human TBI cases (< 5 hours survival), 3 TBI human cases (5 - 24 hour survival) and 6 human controls, expressed as a percentage of controls. ** denotes $p < 0.01$; *** denotes $p < 0.001$.

5.4 Discussion

In response to TBI, a cascade of pathophysiological processes is initiated including inflammation, oedema, excitotoxicity and oxidative stress. These secondary injury factors are responsible for significant morbidity and mortality following TBI (Gentile and McIntosh, 1993), however, their underlying molecular mechanisms are complex, and consequently, remain incompletely elucidated. We have previously demonstrated an acute increase in the immunoreactivity of the neuropeptide, SP, following experimental TBI (Donkin et al., 2009). With the aim of furthering our understanding of the molecular and cellular processes associated with TBI pathophysiology, the present chapter has characterised the expression of SP at the transcript and protein level in clinical TBI and at the transcript level in experimental TBI. Real-time RT-PCR was used to quantify mRNA levels of SP, and included a reference gene evaluation study using geNorm. As discussed in Chapter 4, reference gene validation was considered an important component of the present study to ensure accurate normalisation of real-time RT-PCR data.

The panels of the most stable reference genes identified by geNorm were applied to

normalise SP mRNA levels in experimental and clinical TBI. In the rat cerebral cortex, SP mRNA level was variable: a significant increase was observed at the 3 hour time point, with trends to increase at 1 day, 2 days, 5 days and 7 days following injury (Figure 5.2a). In addition, SP mRNA level exhibited an almost cyclical pattern of expression over the TBI time course. In the rat hippocampus, SP mRNA level was significantly and profoundly elevated at every TBI time point except for the 3 day survival time (Figure 5.2b). These results are consistent with our hypothesis that SP mRNA levels would increase following experimental TBI, and also correlate with our studies of SP immunoreactivity, which increased acutely following experimental TBI (Donkin et al., 2009). Despite the apparent differences in expression patterns between the rat cerebral cortex and hippocampus, SP mRNA level was increased in both brain areas at 3 hours, 5 days and 7 days following injury. Of particular interest is the observation that, in both the rat cerebral cortex and hippocampus, there was a decline in SP mRNA level at 3 days post-TBI to that of sham levels. Furthermore, we have previously observed a qualitative decrease in SP immunoreactivity at this time point, where SP returned to sham levels after acute elevation (J. Donkin, PhD thesis). This could be related to the second opening of the BBB, which has been shown to occur 3 days following experimental TBI (Baskaya et al., 1997). Disruption to the BBB allows proteins, water and other molecules that would normally be excluded, to enter the brain. In TBI, this can have serious consequences, including cerebral oedema and rises in intracranial pressure. Whether the synthesis of SP is inhibited in relation to BBB disruption (for example, due to the entry of SP or other transcription-inhibiting molecules from the periphery) or via other mechanisms requires further investigation. However, given the complex nature of TBI, there are likely to be several processes that are able to modulate SP transcription and translation. A current hypothesis from our laboratory suggests that SP protein may regulate its own synthesis and release via the NK-1 autoreceptor during the acute inflammatory response to TBI. Several lines of evidence suggest that SP is able to trigger its own release by binding to the NK-1 autoreceptor (Tang et al., 2007; Malcangio and Bowery, 1999; Hu et al., 1997). The decline in SP mRNA and protein levels at the 3 day time point could therefore be a control mechanism that prevents acute inflammation from becoming chronic (F. Corrigan, Honours thesis). This could also account for the cyclical nature of SP mRNA level in the rat cerebral cortex, as negative feedback via the NK-1 autoreceptor could inhibit SP transcription when protein levels become too high.

In the human temporoparietal cortex, we measured a significant increase in SP transcript level in the $<$ 5 hour survival group, which correlates to an extent with the expression pattern observed in the rat cerebral cortex. If the rat cortex data from the first 5 hours of injury were averaged, an overall increase in SP mRNA level would be seen with similar increases to the human $<$ 5 hour group (data not shown). However, in the 5 - 24 hour TBI group of the human study, there was a significant decrease in SP mRNA level, something not observed in the rat study even if the 5 hour and 1 day data

were averaged. Nevertheless, looking qualitatively at Figures 5.2a and 5.2c, both data sets display an increase in SP mRNA level followed by a decrease. It would be desirable to obtain tissue representing additional clinical TBI time points, in order to ascertain whether SP mRNA level again increases in the human cortex in the same manner as observed in the rat cortex, particularly after the 3 day time point. However, human TBI tissue is relatively scarce and can be difficult to acquire from a comprehensive range of survival times, and the present study was limited to the first 24 hours of injury in a clinical setting.

Immunohistochemistry was used to study SP protein expression in the parietal cortex and hippocampus of clinical TBI cases. Changes in SP immunoreactivity following TBI were determined using colour deconvolution analysis, which is semi-quantitative in nature because it assesses pixel intensity of the DAB staining rather than measuring protein directly. We have previously demonstrated that SP immunoreactivity increases following experimental TBI, and this is associated with the development of cerebral oedema and neurological deficits (Donkin et al., 2009). In the present study, significant decreases in SP protein expression were observed in the cortex and hippocampus of human TBI cases, with survival times up to 24 hours, compared to controls (Figure 5.4). The decrease in SP staining intensity in the human TBI study was an unexpected result, given the results of the Donkin et al. (2009) study, where SP immunoreactivity was increased at 5 hours after injury in rats. Since our range of clinical time points was limited, the expression pattern of SP protein after 24 hours post-TBI is not clear. However, as mentioned briefly in the Results section, we were able to obtain FFPE tissue from two additional clinical TBI cases with a survival time of 4 days. SP immunoreactivity in the parietal cortex and hippocampus of these cases was not significantly different to the controls, however, this could be due to random variation, as only 2 cases with this survival time were available. However, a situation in which SP protein levels have been restored to normal levels by day 4 in clinical TBI would correlate with our experimental TBI studies. These results suggest that, in the first 24 hours following clinical TBI, SP may not be significant in the pathogenesis of TBI, at least in the CNS. However, it is possible that SP may play more of a peripheral role in clinical TBI injury processes during this time. Studies measuring concentrations of SP in the cerebrospinal fluid following TBI are ongoing in our laboratory, with future studies planning to measure plasma levels of SP in TBI patients.

Interestingly, Donkin et al. (2009) measured peripheral blood levels of SP in TBI and sham rats using enzyme-linked immunosorbent assay. At 30 mins post-TBI, there was a significant increase in plasma SP concentration to almost double the basal level measured in sham animals, which returned to sham levels at the 5 hour time point. These results indicate that, in the impact-acceleration model of experimental TBI, SP is released early after injury and enters the bloodstream, where it could initiate an inflammatory cascade that exacerbates the injury process. The ability of SP to elicit such effects as vasodilation, extravasation of plasma proteins and oedema are well docu-

mented (Campos and Calixto, 2000), in both the central (Vink et al., 2003) and peripheral (Alves et al., 1999) nervous systems. SP primes neutrophils and macrophages for oxidative burst (Lloyds and Hallett, 1993; Hartung and Toyka, 1983) and activates platelets (Gecse et al., 1996). In addition, SP has been shown to induce the production of inflammatory cytokines in immune cells, including TNF-α, IL-1β, IL-2 and IL-6 (Delgado et al., 2003). SP can also stimulate mast cells to release histamine and serotonin (Reynier-Rebuffel et al., 1994; Ebertz et al., 1987; Irman-Florjanc and Erjavec, 1983). These factors are particularly relevant to TBI because histamine, 5-HT, TNF-α, IL-1β, IL-6 and NO can all impair BBB function, many of which elicit effects from both the blood and brain tissue sides (Abbott et al., 2006). The increase in brain concentration of SP over subsequent hours in experimental TBI is likely to continue this deleterious process, promoting inflammation and oedema that may lead to neuronal cell death.

These injury mechanisms are likely to be relevant to the pathogenesis of clinical TBI, however, as discussed, more survival time points would be required in future studies. Importantly, the decrease in SP immunoreactivity observed in the human parietal cortex and hippocampus of TBI cases could be attributed to haemorrhage or ischaemia. All of the human post-mortem cases selected for immunohistochemistry had evidence of haemorrhage (subarachnoid, petechial, intraventricular or subdural haematoma), and some had hypoxic-ischaemic periods, as assessed by clinical neuropathologists. Our laboratory has shown that SP content does not increase when ischaemia is present (R. Turner, unpublished results), nor in experimental subarachnoid haemorrhage (C. Barry, unpublished results). The impact-acceleration model of rodent TBI used herein produce diffuse axonal injury in the absence of haemorrhage, hypertension, significant brainstem damage or death (Marmarou et al., 1994), while the degree of injury in the clinical cases was severe enough to result in patient death. Furthermore, experimental animals are sacrificed at specific time points, while time of death in clinical cases can often be less precise. Therefore, inherent variability between experimental models and clinical cases must be taken into account, particularly in the context of heterogeneous pathologies such as TBI.

In conclusion, the expression of the neuropeptide, SP, has been characterised at the transcript and protein level following clinical and experimental TBI. The results presented herein support a role for neuropeptides in the molecular mechanisms underlying TBI pathophysiology and may represent novel therapeutic targets. Further studies investigating changes in SP expression over a broader time course of clinical TBI are warranted.

Chapter 6

TRPM Channel Expression Following Clinical and Experimental TBI

6.1 Introduction

TBI is a leading cause of morbidity and mortality and represents a major public health burden (Vink and Nimmo, 2009). Motor vehicle incidents account for the majority of severe TBI cases, while falls, sporting accidents and assault are responsible for most mild to moderate injuries (Bruns Jr. and Hauser, 2003). Since there is no effective pharmacological treatment available for TBI, survivors are often left with long-term motor, cognitive and behavioural deficits. The neurological dysfunction resulting from TBI is due to direct, immediate mechanical damage to brain tissue (the primary injury) as well as indirect, delayed secondary injury mechanisms that are triggered by the primary event and may continue for days to weeks after the insult (Roth and Farls, 2000). Secondary injury factors include such processes as magnesium decline, oedema, oxidative stress, inflammation and excitotoxicity, all of which can be deleterious to neuronal cells (Golding, 2002; Cormio et al., 1997). However, the molecular mechanisms underlying these processes are not completely understood, and it is unlikely that targeting a single factor will result in a significant improvement in outcome (Vink and Nimmo, 2009). For example, as discussed in Section 1.2.3, therapies utilising Mg^{2+} have not been proven clinically effective, despite success in pre-clinical experimental studies.

The TRP superfamily, introduced in Section 1.5, consists of over 30 ion channels with diverse functions, properties and expression patterns (Pedersen et al., 2005). Four members of the melastatin subfamily, TRPM7, TRPM6, TRPM3 and TRPM2, are the focus of the present chapter.

The ubiquitously expressed TRPM7 consists of an ion channel fused to a protein kinase domain (Nadler et al., 2001). TRPM7 is permeable to a wide range of divalent metal ions (Monteilh-Zoller et al., 2003) and is one of only a few identified mammalian Mg^{2+} transporters. The discovery that TRPM7 was a Mg^{2+}-transporting channel generated significant interest, particularly because it regulates Mg^{2+} influx, not efflux (Wolf, 2004).

TRPM7 is involved in many cellular processes, including synaptic transmission

(Krapivinsky et al., 2006), the cell cycle (Tani et al., 2006), normal growth and development (Elizondo et al., 2005), regulation of vascular smooth muscle cells (He et al., 2005) and the proliferation of human retinoblastoma cells (Hanano et al., 2004). Strong evidence suggests that TRPM7 is necessary for cell survival and regulates Mg^{2+} homeostasis (Schmitz et al., 2003; Nadler et al., 2001), although the latter point was challenged in a recent study (Jin et al., 2008).

TRPM7 is inhibited by free intracellular Mg^{2+} and Mg.ATP complexes, and is strongly activated when intracellular Mg.ATP and Mg^{2+} concentrations are depleted (Demeuse et al., 2006; Matsushita et al., 2005; Kozak and Cahalan, 2003; Nadler et al., 2001). TRPM7 may also be regulated by GPCR, either via the cAMP and PKA pathway (Takezawa et al., 2004), or the PLC-mediated hydrolysis of PIP_2 (Runnels et al., 2002).

Considering the vital role fulfilled by TRPM7 with regard to cell viability and Mg^{2+} homeostasis, mutations in TRPM7 could be expected to result in severe pathological consequences. Indeed, the zebrafish *touchtone/nutria* phenotype, resulting from mutations in the TRPM7 gene, displayed growth retardation and serious alterations in skeletal development (Elizondo et al., 2005). Furthermore, Hermosura et al. (2005) reported a missense mutation in the TRPM7 gene, $TRPM7^{T1482I}$, in a subgroup of Western Pacific Amyotrophic Lateral Sclerosis and Parkinsonism-Dementia Complex (ALS-G and PD-G, respectively) patients, but not in matched controls. The authors propose that this mutant allele confers a functional deficit that, together with environmental factors, such as a diet low in Mg^{2+}, may predispose individuals to these neurological diseases.

TRPM7 is also involved in a number of processes relevant to TBI. For example, TRPM7 and TRPM2 have been implicated in playing direct roles in Ca^{2+}-mediated neuronal death (Aarts et al., 2003), although the exact mechanism by which this occurs requires further investigation. It has been proposed that TRPM7 mediates cell death via a positive feedback loop whereby Ca^{2+} entry into cells as a result of injury causes the production of free radicals, which activate TRPM7, leading to further Ca^{2+} influx and additional free radical production (Aarts and Tymianski, 2005b). Indeed, the activation of TRPM7 during ischaemia is proposed to be a key factor contributing to excitotoxicity and other deleterious processes (MacDonald et al., 2005). In addition, deficits in Mg^{2+} concentration, as have been demonstrated following TBI, lead to the generation of ROS (Altura et al., 2003), which could further activate TRPM7 (and TRPM2), thereby enhancing inflammation, oxidative stress and cell death. The potential role of TRPM7 in TBI pathophysiology, however, has yet to be elucidated.

TRPM6 is the closest relative of TRPM7, with which it shares 50 % homology at the amino acid level (Topala et al., 2006). TRPM6 is able to form homomeric channels, as well as heteromeric channels with TRPM7, which are biophysically and pharmacologically distinguishable (Li et al., 2006). In addition, TRPM6 is able to phosphorylate TRPM7 (Schmitz et al., 2005). TRPM6 is mainly expressed in the kidney and small intestine (Schlingmann et al., 2002), but has also been identified in the brain (Fonfria et al., 2006b). Mutations in the TRPM6 gene

have been identified as the cause of HSH (Chubanov et al., 2007; Schlingmann et al., 2002; Walder et al., 2002), an autosomal recessive disorder characterised by low serum levels of Mg^{2+} and Ca^{2+} (Schlingmann et al., 2007). The role of TRPM6 in brain function is poorly understood, and further investigation is needed to determine whether TRPM6 participates in Ca^{2+}-mediated neuronal death.

TRPM3 is the closest relative of TRPM1, and was one of the last TRP channels to be characterised (Clapham et al., 2001). TRPM3 is expressed in the human brain, kidney, testis, eye and spinal cord (Lee et al., 2003), and is proposed to be involved in renal Ca^{2+} homeostasis, and cation homeostasis in the CSF (Oberwinkler and Philipp, 2007; Grimm et al., 2003). Interestingly, high levels of TRPM3 have been detected in the brain and pituitary (Fonfria et al., 2006b), suggesting that TRPM3 may also play a significant role in brain physiology. When expressed in HEK293 cells, TRPM3 forms constitutively active channels permeable to Ca^{2+} and Mn^{2+}; currents are enhanced by a reduction in extracellular osmolarity (Grimm et al., 2003). TRPM3 is activated by D-erythro-sphingosine (Grimm et al., 2005), pregnenolone sulphate (Wagner et al., 2008) and Ca^{2+} store depletion (Lee et al., 2003). Like TRPM7 and TRPM6, TRPM3 is permeable to Mg^{2+} and is inhibited by rises in intracellular Mg^{2+} concentration (Oberwinkler, 2007; Oberwinkler et al., 2005). The exact physiological role of native TRPM3 channels, including their function in the brain, is incompletely understood, and the characterisation of transcript or protein levels of TRPM3 in neurological disorders has not previously been attempted.

TRPM2 is a non-selective cation channel that is highly permeable to Ca^{2+} and is expressed in wide range of human tissues, including immune cells and various regions of the brain (Lange et al., 2008; Heiner et al., 2006; Nagamine et al., 1998). TRPM2 can be activated in response to such factors as oxidative or nitrosative stress (Wehage et al., 2002; Hara et al., 2002), intracellular and extracellular Ca^{2+} (Starkus et al., 2007; McHugh et al., 2003) and ADP-ribose (Perraud et al., 2001). Recently, TRPM2 has been implicated in inflammation (Yamamoto et al., 2008). Several lines of evidence indicate that activation of TRPM2 by oxidative stress results in cell death via unregulated Ca^{2+} influx (Kaneko et al., 2006; Zhang et al., 2003; Hara et al., 2002). It has been proposed that the involvement of TRPM2 and TRPM7 in anoxic neuronal death may be due to the formation of functional heteromeric complexes (Aarts et al., 2003).

Considering that TRPM2 is activated by oxidative stress, mediates cell death and inflammation, and is highly expressed in the brain, this protein has been investigated in the context of CNS disorders. Transcript levels of TRPM2 were found to be elevated in a time-dependent manner following transient middle cerebral artery occlusion in the rat (Fonfria et al., 2006a). The results of another study (Fonfria et al., 2005) suggest a role for TRPM2 in H_2O_2 or Aβ peptide-induced striatal cell death. Furthermore, genetic variants of the TRPM2 gene confer a risk of developing ALS-G and PD-G (Hermosura et al., 2008) and bipolar disorder (Xu et al., 2009).

To date, no studies have investigated the potential role of TRPM channels in TBI pathophysiology. Therefore, the aims

of the present chapter were to quantify TRPM2, TRPM3, TRPM6 and TRPM7 transcript and protein levels following clinical and experimental TBI. We hypothesised that TRPM channels would be upregulated following TBI; elevated expression of TRPM2 and TRPM7 would likely contribute to Ca^{2+}-mediated neuronal cell death, while increases in the Mg^{2+}-conducting channels may also help to restore normal intracellular Mg^{2+} concentrations. Accordingly, we used real-time RT-PCR to quantify TRPM channel mRNA levels and immunohistochemistry to identify TRPM proteins, both in post-mortem clinical TBI cases, and in a rodent model of experimental TBI. A reference gene validation study utilising geNorm (Vandesompele et al., 2002) was included prior to real-time RT-PCR quantification to ensure accurate data normalisation.

6.2 Materials and Methods

6.2.1 Rodent Model of TBI

Adult male Sprague-Dawley rats (n = 92; 400 - 450 g) were group housed on a 12 h night-day cycle and provided with a standard diet of rodent pellets and water ad libitum. Animals were randomly assigned into TBI (n = 80) and uninjured (n = 12) groups at the beginning of the experiment. Animals were injured using the impact acceleration model of diffuse TBI as previously described by Marmarou et al. (1994), and as outlined in the Materials and Methods chapter (Section 3.2.2) of the present thesis. Animals were sacrificed following sham surgery (n = 6 per study) or at 1 hour, 3 hours, 5 hours, 1 day, 2 days, 3 days, 5 days and 7 days following injury (n = 5 per group per study). Animals for gene expression analysis were sacrificed by anaesthetic overdose; brains were rapidly removed and the cerebral cortex and hippocampus regions dissected in total and snap frozen in liquid N_2, then stored at $-80\,^{\circ}C$. Animals for the immunohistochemistry study were perfusion fixed with 10 % buffered formalin and left to rest for at least 1 hour before the brain was removed.

6.2.2 Human TBI Cases

The use of post-mortem human brain tissue in this study was approved by the University of Adelaide Human Ethics Committee and all cases had written donor or next-of-kin consent for research. All human tissue used in this study was assessed by a clinical neuropathologist and given a diagnosis of either neurotrauma or normal brain. Case details regarding human tissue are described in Appendix B. For gene expression analysis, fresh frozen human brain tissue (temporoparietal cortex; coronal section 1 cm posterior to mamillary bodies) of 20 TBI and 10 age- and sex-matched control cases was obtained from the Victorian Brain Bank Network. Frozen tissue cases were subdivided into survival times of $<$ 5 hours (n = 12) and 5 - 24 hours (n = 8) based on the supplied clinical information. For immunohistochemistry analysis, post-mortem FFPE human brain tissue (parietal cortex and hippocampus) from 9 TBI and 6 age- and sex-matched control cases was obtained from the tissue pathology laboratory of the IMVS. FFPE cases were subdivided into survival times of $<$ 5 hours (n = 6) and 5 - 24 hours (n = 3) based on detailed clinical information.

6.2.3 RNA Extraction and Real-time RT-PCR

Extraction of total RNA was carried out from rat TBI and sham cerebral cortex and hippocampus tissue (n = 5 TBI animals per survival time point; n = 6 shams) and human TBI (n = 20) and control (n = 10) tissue as described in detail in the Materials and Methods chapter (Section 3.2.5). Fifty mg tissue was used in each RNA extraction, and a DNase treatment was included. Total RNA was quantified by UV spectrophotometry to measure absorbance at 230 nm, 260 nm and 280 nm. RNA integrity was assessed using the Agilent Bioanalyzer RNA 6000 Nano Chip (Series II) kit. Complementary DNA was synthesised as described in Section 3.2.6, diluted to 10 ng/μL and stored at $-80\,^{\circ}C$ until PCR.

A reference gene validation study was carried out to determine the most stable reference genes for accurate real-time RT-PCR data normalisation in both the rat and human TBI studies. These studies are described in detail in Chapter 4. Primer sequences for reference genes and TRPM channels are presented in Tables 3.2 and 3.3. Real-time RT-PCR was carried out as described in Section 3.2.7. Following PCR amplification, Ct values were calculated from the standard curve using the Corbett Rotor-Gene 6 software.

Triplicate Ct values for each sample were entered into the qBasePlus software, which calculated mRNA levels of TRPM channels relative to multiple reference genes. Sham/control levels were set to 1 to facilitate determination of mRNA fold changes. TRPM6 was not characterised in clinical cases because (a number of different) primer pairs were not able to be optimised to the standard desired (see Discussion).

6.2.4 TRPM Channel Immunohistochemistry

Brains from perfusion-fixed animals were fixed for at least 1 week in formalin, and then cut into 2 mm coronal sections, processed overnight and embedded in paraffin wax. Post-mortem human brain tissue was processed according to IMVS diagnostic protocols and embedded in paraffin wax. Serial 5 μM sections were cut with a microtome, mounted onto microscope slides and left to dry overnight. TRPM channel immunohistochemistry was carried out as described in detail in Section 3.2.4, using polyclonal primary antibodies (see Table 3.1). Digital images of all sections were acquired using a Nanozoomer Digital Pathology Scanner at a magnification of 40x. Colour deconvolution analysis was performed to determine 'weight % DAB' values and therefore to semi-quantify TRPM channel protein content.

6.2.5 Statistical Analysis

Results graphs are presented as mean $\pm$ SEM. GraphPad Prism was used to carry out one-way ANOVA with Dunnett's multiple comparison test, with $p < 0.05$ considered statistically significant.

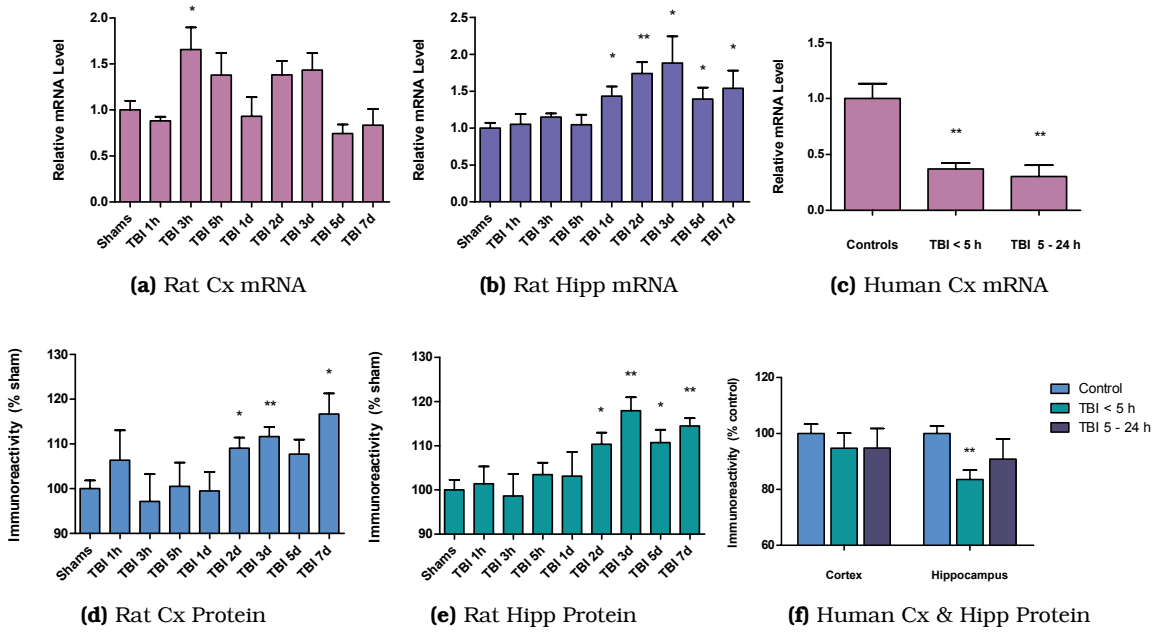

(a) Rat Cx mRNA **(b)** Rat Hipp mRNA **(c)** Human Cx mRNA

(d) Rat Cx Protein **(e)** Rat Hipp Protein **(f)** Human Cx & Hipp Protein

Figure 6.1: (a) - (c): TRPM2 mRNA level following TBI, in (a) rat cortex, (b) rat hippocampus and (c) human temporoparietal cortex. Bars depict mean ± SEM of 5 animals per rat TBI group and 6 shams; 12 TBI cases (< 5 hours survival), 8 TBI cases (5 - 24 hour survival) and 10 controls in the human study, all from triplicate PCR amplifications. (d) - (f): TRPM2 protein expression following TBI in (d) rat cerebral cortex and (e) hippocampus (dentate gyrus) and (f) clinical TBI in parietal cortex and hippocampus (dentate gyrus). Bars depict mean immunoreactivity ± SEM of 5 animals per TBI group and 6 shams, and 6 human TBI cases (< 5 hours survival), 3 TBI human cases (5 - 24 hour survival) and 6 human controls, expressed as a percentage of sham/control levels. Cx, cortex; Hipp, hippocampus; * denotes $p < 0.05$; ** denotes $p < 0.01$.

6.3 Results

6.3.1 TRPM2 Expression

TRPM2 mRNA Level

Rodent model of TBI

In the rat cerebral cortex (Figure 6.1a), TRPM2 mRNA was significantly increased at the 3 hour survival time compared to shams, with trends to increase at 2 days and 3 days post-TBI (p = 0.057 and 0.066, respectively). In the rat hippocampus (Figure 6.1b), there were significant elevations in transcript levels of TRPM2 consistently from 1 day to 7 days following TBI.

Clinical TBI cases

In the human temporoparietal cortex (Figure 6.1c), there were significant decreases in TRPM2 mRNA levels at both clinical time points (< 5 hours survival: 0.37 ± 0.05 fold decrease; 5 - 24 hours survival: 0.30 ± 0.10 fold decrease; $p < 0.01$).

TRPM2 Protein Expression

The immunohistochemistry component of the present chapter was associated with many experimental variables (i.e. experimental and clinical TBI, cortex and hippocampus, different survival time points and four TRPM channels), which resulted in a large number

of digital images of stained tissue sections. Therefore, representative TRPM channel immunohistochemistry micrographs for rat and human TBI and control sections have been included in Appendices C and D.

TRPM2 immunoreactivity was observed in neurons and microglia in the cerebral cortex and hippocampus, which have been reported to express functional TRPM2 channels (Olah et al., 2009; Fonfria et al., 2006a; Kaneko et al., 2006; Kraft et al., 2004). Colour deconvolution analysis was used to identify TRPM2 protein expression in human and rat TBI tissue sections. As discussed, this method is semi-quantitative in nature because it assesses pixel intensity of the DAB staining rather than measuring protein directly. Figures 6.1d-f show graphical results of mean immunoreactivity (i.e. weight percent DAB, representing the whole of the image antigen content) expressed as a percentage of sham/control levels.

In the rat cerebral cortex (Figure 6.1d), there was a significant increase in the expression of TRPM2 protein at 2, 3 and 7 days following TBI, with a trend to increase in the 5 day group (p = 0.09). The micrographs in Figure C.4 demonstrate these changes, where TRPM2 immunoreactivity is clearly increased within injured cortical neurons at these time points. Similarly, in the rat hippocampus (Figure 6.1e), TRPM2 was significantly elevated at all time points between 2 and 7 days post-TBI, and this is demonstrated by the increased immunoreactivity within injured hippocampal (dentate gyrus) neurons in Figure C.5. The dentate gyrus was chosen for analysis because neurons in this hippocampal region have been shown to be particularly vulnerable following TBI (Gao and Chen, 2009).

In human TBI (Figure 6.1f), TRPM2 expression was unchanged at either TBI time point compared to controls in the parietal cortex. In the human hippocampus, there was a significant ($p < 0.01$) decrease in TRPM2 immunoreactivity in the $<$ 5 hour survival TBI group compared to controls. Figure D.3 micrographs depict these trends.

6.3.2 TRPM3 Expression

TRPM3 mRNA Level

Rodent model of TBI

In the rat cerebral cortex (Figure 6.2a), there were no significant differences in TRPM3 mRNA level in TBI rats compared to shams. In the rat hippocampus (Figure 6.2b), TRPM3 mRNA level was significantly elevated at every time point following TBI, except for 3 hours and 5 hours post-TBI, where there were trends to increase (3 hours: 1.47 $\pm$ 0.30 fold increase, p = 0.14; 5 hours: 1.79 $\pm$ 0.42 fold increase, p = 0.07).

Clinical TBI cases

In the human temporoparietal cortex (Figure 6.2c), there was no significant difference in TRPM3 mRNA level between controls and the $<$ 5 hour TBI survival group. There was a trend to increase in the 5 - 24 hours survival group (1.63 $\pm$ 0.42 fold increase, p = 0.12).

TRPM3 Protein Expression

In the present study, TRPM3 immunoreactivity was observed in neurons of the cerebral cortex and hippocampus. These results are consistent with recent studies which detected TRPM3 protein in primary hippocampal neurons (Crispino et al., 2008) and

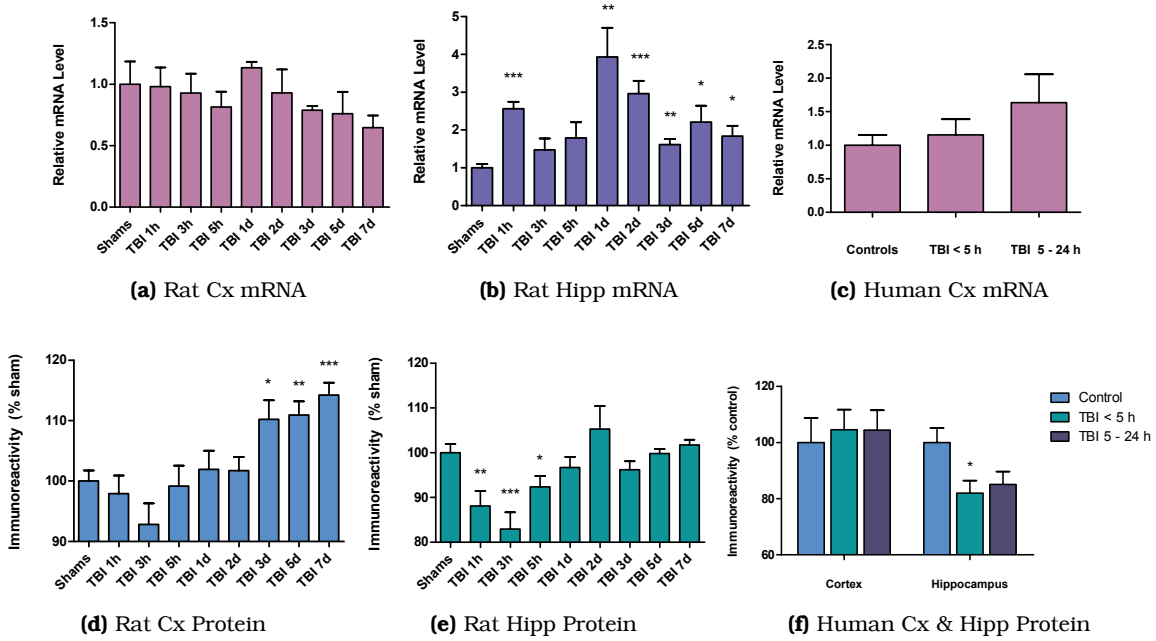

(a) Rat Cx mRNA **(b)** Rat Hipp mRNA **(c)** Human Cx mRNA

(d) Rat Cx Protein **(e)** Rat Hipp Protein **(f)** Human Cx & Hipp Protein

Figure 6.2: (a) - (c): TRPM3 mRNA level following TBI, in (a) rat cortex, (b) rat hippocampus and (c) human temporoparietal cortex. Bars depict mean ± SEM of 5 animals per rat TBI group and 6 shams; 12 TBI cases (< 5 hours survival), 8 TBI cases (5 - 24 hour survival) and 10 controls in the human study, all from triplicate PCR amplifications. (d) - (f): TRPM3 protein expression following TBI in (d) rat cerebral cortex and (e) hippocampus (dentate gyrus) and (f) clinical TBI in parietal cortex and hippocampus (dentate gyrus). Bars depict mean immunoreactivity ± SEM of 5 animals per TBI group and 6 shams, and 6 human TBI cases (< 5 hours survival), 3 TBI human cases (5 - 24 hour survival) and 6 human controls, expressed as a percentage of sham/control levels. Cx, cortex; Hipp, hippocampus; * denotes $p < 0.05$; ** denotes $p < 0.01$; *** denotes $p < 0.001$.

TRPM3 transcripts in cultured cortical neurons (Aarts et al., 2003). Figures 6.2d-f show graphical results of mean immunoreactivity expressed as a percentage of sham/control levels.

In the rat cerebral cortex (Figure 6.2d), there was a significant increase in the expression of TRPM3 protein at 3, 5 and 7 days following TBI compared to shams. In the rat hippocampus (dentate gyrus), TRPM3 protein expression was significantly decreased between 1 hour and 5 hours post-TBI (Figure 6.2e). The changes in TRPM3 immunoreactivity within injured cortical and hippocampal neurons at these time points are shown by the micrographs in Figure C.6 and C.7.

In the human parietal cortex, TRPM3 expression was unchanged at either TBI time point compared to controls, while in the human hippocampus, there was a significant ($p < 0.05$) decrease in TRPM3 immunoreactivity in dentate gyrus neurons in the < 5 hour TBI group compared to controls, and a trend to decrease in the 5 - 24 hour survival group ($p = 0.069$) (Figure 6.2f). The micrographs in Figure D.4 demonstrate these changes.

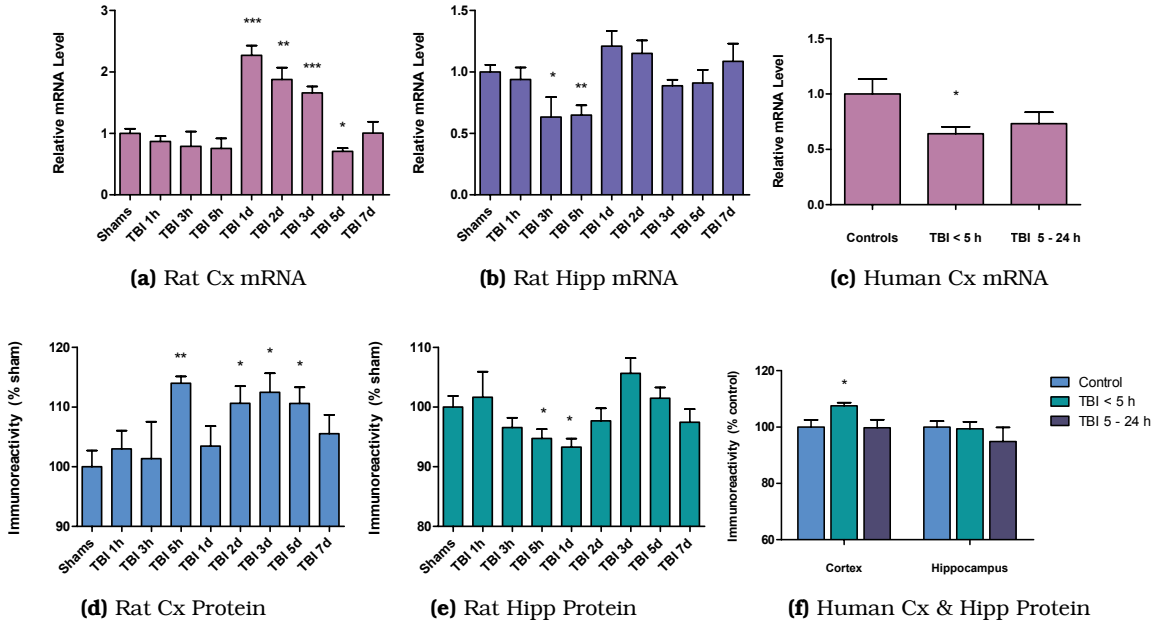

(a) Rat Cx mRNA **(b)** Rat Hipp mRNA **(c)** Human Cx mRNA

(d) Rat Cx Protein **(e)** Rat Hipp Protein **(f)** Human Cx & Hipp Protein

Figure 6.3: (a) - (c): TRPM7 mRNA level following TBI, in (a) rat cortex, (b) rat hippocampus and (c) human temporoparietal cortex. Bars depict mean ± SEM of 5 animals per rat TBI group and 6 shams; 12 TBI cases (< 5 hours survival), 8 TBI cases (5 - 24 hour survival) and 10 controls in the human study, all from triplicate PCR amplifications. (d) - (f): TRPM7 protein expression following TBI in (d) rat cerebral cortex and (e) hippocampus (dentate gyrus) and (f) clinical TBI in parietal cortex and hippocampus (dentate gyrus). Bars depict mean immunoreactivity ± SEM of 5 animals per TBI group and 6 shams, and 6 human TBI cases (< 5 hours survival), 3 TBI human cases (5 - 24 hour survival) and 6 human controls, expressed as a percentage of sham/control levels. Cx, cortex; Hipp, hippocampus; * denotes $p < 0.05$; ** denotes $p < 0.01$; *** denotes $p < 0.001$.

6.3.3 TRPM7 Expression

TRPM7 mRNA Level

Rodent model of TBI

There was a significant increase ($p < 0.01$) in TRPM7 transcript level in the rat cerebral cortex between 1 day and 3 days post-TBI compared to shams (Figure 6.3a). In the 5 day group, TRPM7 mRNA level was significantly reduced compared to shams (0.71 ± 0.05 fold decrease). In the rat hippocampus (Figure 6.3b), TRPM7 mRNA level was significantly decreased at 3 hours and 5 hours following TBI, with a trend to increase at 1 day post-TBI ($p = 0.13$).

Clinical TBI cases

In the human temporoparietal cortex (Figure 6.3c), there was a significant ($p < 0.05$) decrease in TRPM7 mRNA level in the < 5 hour survival group (0.64 ± 0.06 fold decrease). In the 5 - 24 hour TBI group, TRPM7 showed a trend to decrease (p = 0.16).

TRPM7 Protein Expression

TRPM7 immunoreactivity was observed within neurons and microglia in the cerebral cortex and hippocampus, which have previously been reported to express functional TRPM7 channels (Wei et al., 2007; Aarts et al., 2003; Jiang et al., 2003). Figures

6.3d-f show graphical results of mean immunoreactivity expressed as a percentage of sham/control levels. In the rat cerebral cortex (Figure 6.3d), TRPM7 protein was significantly elevated in the 5 hour, 2 day, 3 day and 5 day TBI groups compared to shams. In the rat dentate gyrus (Figure 6.3e), TRPM7 expression was significantly decreased at 5 hours and 1 day post-TBI, which is demonstrated by the micrographs in Figures C.8 and C.9.

In the clinical TBI study (Figure 6.3f), TRPM7 expression was increased in the parietal cortex of the $<$ 5 hour survival TBI group compared to controls and unchanged in the 5 - 24 hour survival group. In the human hippocampus, there were no changes in TRPM7 immunoreactivity in either TBI group compared to controls. The micrographs in Figure D.5 depict these trends.

6.3.4 TRPM6 Expression

TRPM6 mRNA Level

In the rat cerebral cortex, there was a significant increase ($p < 0.01$) in TRPM6 transcript level at the 1 day TBI survival time point (Figure 6.4a). In the 7 day TBI group, TRPM6 mRNA levels showed a trend to decrease compared to shams (0.54 ± 0.07 fold decrease, $p = 0.10$).

TRPM6 mRNA levels in the rat hippocampus were significantly elevated at every TBI time point compared to shams ($p < 0.01$), with the most profound increases seen at 1 hour, 3 hours, 1 day and 2 days following TBI, where TRPM6 transcript levels were increased more than 10-fold of sham levels (Figure 6.4b).

As mentioned, TRPM6 was not characterised in clinical TBI cases in the present study. We initially attempted to quantify TRPM6 mRNA levels in clinical TBI, however, PCR primer pairs were not able to be optimised to an acceptable standard. Similarly, TRPM6 immunohistochemistry was not attempted in human TBI cases in the current thesis.

TRPM6 Protein Expression

Previous reports have detected TRPM6 transcripts in cultured cortical (Aarts et al., 2003) and hippocampal neurons (Wei et al., 2007). In the present study, we observed TRPM6 immunoreactivity in neurons of the rat cerebral cortex and hippocampus. Figure 6.4 shows graphical results of mean immunoreactivity expressed as a percentage of sham levels.

In the rat cerebral cortex (Figure 6.4c), there was a significant increase in the expression of TRPM6 protein at the 5 day time points compared to shams, with trends to increase at the 1 hour, 1 day and 3 day time points ($p = 0.06$, 0.08 and 0.08, respectively).

In the rat hippocampus (dentate gyrus), TRPM6 protein expression was significantly elevated in the 5 hours, 1 day and 7 day TBI groups (Figure 6.4d). These increases in TRPM6 immunoreactivity within injured cortical and hippocampal neurons at these time points are shown by the micrographs in Figure C.10 and C.11.

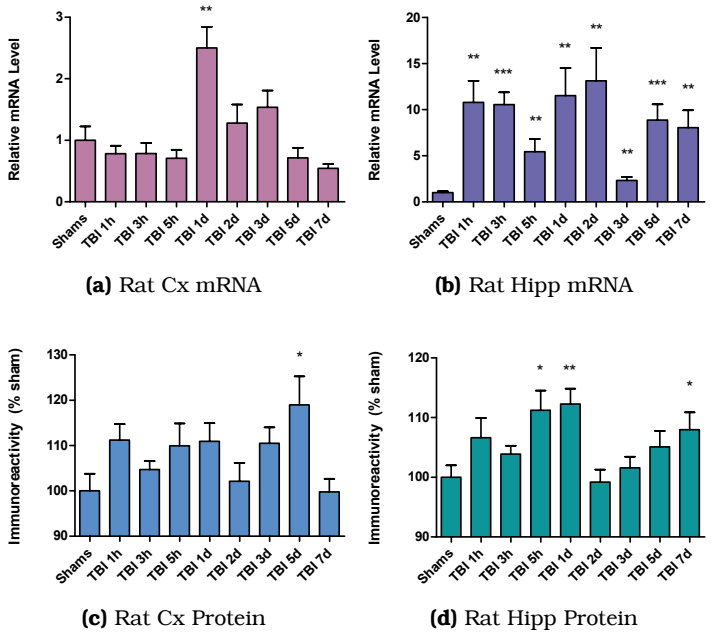

(a) Rat Cx mRNA **(b)** Rat Hipp mRNA

(c) Rat Cx Protein **(d)** Rat Hipp Protein

Figure 6.4: (a) - (b): TRPM6 mRNA level following TBI, in (a) rat cortex and (b) rat hippocampus. Bars depict mean ± SEM of 5 animals per TBI group and 6 shams from triplicate PCR amplifications. (c) - (d): TRPM6 protein expression following TBI in (c) rat cerebral cortex and (d) hippocampus (dentate gyrus). Bars depict mean immunoreactivity ± SEM of 5 animals per TBI group and 6 shams, expressed as a percentage of sham levels. Cx, cortex; Hipp, hippocampus; * denotes $p < 0.05$; ** denotes $p < 0.01$; *** denotes $p < 0.001$.

6.4 Discussion

6.4.1 TRPM2

The present chapter provides the first demonstration of changes in transcript and protein expression levels of TRPM2 following clinical and experimental TBI, suggesting that TRPM2 may play a role in TBI pathophysiology. In the human temporoparietal cortex, there were significant decreases in TRPM2 mRNA level at both the $<$ 5 hours and 5 - 24 hours survival times, trends which were not observed in the rat cerebral cortex at corresponding time points. As discussed in the previous chapter, the impact acceleration model of rodent TBI used herein produces diffuse axonal injury in the absence of haemorrhage, hypertension, significant brainstem damage or death (Marmarou et al., 1994). Conversely, almost all of the clinical cases had evidence of haemorrhage and other neuropathologies (see case notes in Appendix B, Table B.1), and injuries were severe enough to result in patient death. Of further significance, experimental animals are sacrificed at specific time points after injury, while time of death in clinical cases can often be less precise. Therefore, some degree of variability between experimental models and clinical cases must be taken into account, particularly in the context of heterogeneous pathologies such as TBI.

TRPM2 mRNA levels showed slightly different expression patterns between the differ-

ent brain areas of the rat, with hippocampal TRPM2 transcript levels increasing over time from 1 day to 7 days following TBI, and cortical levels increasing very acutely at 3 hours post-TBI and showing trends to increase at 2 days and 3 days.

Regarding protein expression of TRPM2, in the rat cerebral cortex, TRPM2 immunoreactivity was significantly elevated within injured neurons at 2 days, 3 days and 7 days following TBI, with a trend towards an increase in the 5 day group. These results correlate to an extent with the TRPM2 mRNA levels in the rat cerebral cortex, where a tendency to increase in the 2 day and 3 day groups was observed. In the human parietal cortex, there were no changes in TRPM2 protein expression at either TBI time point compared to controls, which is consistent with the transcript levels, and mirrors the rat cerebral cortex results at the equivalent survival times.

In the rat hippocampus, TRPM2 protein content within injured neurons was significantly elevated between 2 days and 7 days following TBI, which corresponds to the increases in TRPM2 transcript levels at these time points, and showed virtually the same expression pattern as in the rat cerebral cortex. In the human hippocampus, we found a significant decrease in TRPM2 immunoreactivity in the < 5 hour survival TBI group. Immunoreactivity of TRPM2 in the hippocampus was comparable between rat and human TBI cases at the clinical time points.

TRPM2 is associated with several cellular processes relevant to TBI pathophysiology. The biochemical changes elicited by TBI include inflammation and oxidative stress, both of which have been associated with TRPM2 activation. Inflammation is a critical factor in TBI that promotes neurotoxicity. Disruption to the BBB in response to brain insult is associated with the transmigration of leukocytes to the area of damage, activation of glial cells, and accumulation of cytokines, chemokines and oxidants (Morganti-Kossmann et al., 2007). TRPM2 is expressed in immune cells such as neutrophils and macrophages (Perraud et al., 2004; Sano et al., 2001), and could therefore participate in neuroinflammation following TBI. Indeed, TRPM2 has been identified as a key participant in monocyte chemokine production induced by H_2O_2 (Yamamoto et al., 2008). The activation of TRPM2 in response to oxidative stress causes rises in intracellular Ca^{2+} levels and increased susceptibility to cell death (Kaneko et al., 2006; Fonfria et al., 2005; Zhang et al., 2003; Hara et al., 2002). Oxidants such as H_2O_2 have been reported to gate TRPM2 channels directly (Kraft et al., 2004; Wehage et al., 2002), and TRPM2 is also activated by ADPR (Perraud et al., 2001), which may be produced in the cytosol, nucleus or mitochondria at elevated levels in response to oxidative stress (for review, see Kühn et al., 2005). Interestingly, Ca^{2+} enhances current through TRPM2; therefore a positive feedback mechanism has been proposed, whereby activation of TRPM2 leads to Ca^{2+} entry into cells, which can further stimulate the channels and promote cell death (McHugh et al., 2003).

The results of the rodent TBI component revealed an upregulation of TRPM2 protein expression in injured cortical and hippocampal neurons, something not observed in the clinical cases. Importantly, these increases did not occur until 2 days after experimen-

tal TBI. Due to the relative shortage of fresh frozen human neurotrauma tissue our clinical TBI cases were limited to very acute survival times of less than 24 hours. The exact role of TRPM2 following TBI and how it could contribute to TBI pathophysiology requires further investigation. However, taken together, the results of the present study suggest that the role of TRPM2 in TBI-induced oxidative stress, inflammation and neuronal cell death may not be relevant in the first 24 hours of injury. TRPM2 may, however, participate in these events from day 2 until at least day 7 post-TBI.

6.4.2 TRPM3

To our knowledge, this is the first study to characterise the expression of TRPM3 in relation to a CNS disorder. In clinical TBI, there were no changes in the mRNA level or protein expression of TRPM3 in the parietal cortex at either survival time point. Similarly, in the rat cerebral cortex, there were no changes in TRPM3 mRNA level throughout the TBI time course. However, TRPM3 protein was significantly increased within injured neurons in the rat cerebral cortex between 3 days and 7 days post-TBI, but was unchanged in the first 24 hours following injury, which is consistent with the cortical TRPM3 protein results in clinical TBI. More clinical TBI time points would be desirable in order to assess whether TRPM3 protein expression increases after 24 hours post-TBI.

In the rat hippocampus, TRPM3 protein expression was significantly decreased during the acute stages of TBI (1 hour to 5 hours). These results correlate with the clinical TRPM3 protein results in the hippocampus, in which TRPM3 protein was significantly decreased in the < 5 hour survival group, with a trend to decrease in the 5 - 24 hour survival group. Interestingly, TRPM3 mRNA level was significantly increased at nearly every TBI time point in the rat hippocampus, yet there were no increases in TRPM3 protein in this brain region.

A number of possibilities could account for increases in TRPM3 mRNA level not extending to increases in TRPM3 protein content. For example, acute changes in mRNA translation factors have been demonstrated following TBI (Chen et al., 2007), and mRNA levels do not always correlate with protein expression (Gygi et al., 1999). In addition, protein synthesis has shown to be inhibited following cerebral reperfusion (DeGracia, 2004), which could also be applicable to TBI, as well as in conditions of oxidative stress (Shenton et al., 2006). Furthermore, metabolic depression in the injured brain may reduce cells' capacity to package proteins into vesicles for release.

However, an additional explanation for the differences between TRPM3 mRNA levels and protein expression could be due to alternative splicing of TRPM3 transcripts, which leads to a large number of splice variants, for which the physiological relevance is poorly understood (Oberwinkler and Philipp, 2007). The TRPM3 primer pairs used in the present study were designed to amplify all known splice variants of TRPM3, in order to encompass all possible functional TRPM3 channels. However, it is unclear from which amino acid region the TRPM3 primary antibody (Abcam; cat no. ab56171) was derived, because the exact sequence is proprietary. It is therefore possible that only a proportion of all possible variants were targeted by the TRPM3 primary antibody, which could account for the lack of

correlation between TRPM3 mRNA levels and protein expression observed herein.

As discussed, the exact physiological role of native TRPM3 channels, including their function in the brain, is incompletely understood. Despite this, TRPM3 was chosen as a gene and protein of interest in the present thesis due to its relatively high expression in the brain, its chromosomal location, its permeability to Ca^{2+} and Mg^{2+} and the observation that, like TRPM7 and TRPM6, TRPM3 is inhibited by rises in intracellular Mg^{2+} concentration. Given that TBI results in intracellular Mg^{2+} depletion, we therefore hypothesised that TRPM3 expression may increase following TBI as a possible means by which to compensate for the loss of Mg^{2+}. Indeed, in the rat cerebral cortex, there was an increase in TRPM3 protein levels from day 3 to day 7 post-TBI. However, the acute decreases in hippocampal TRPM3 protein levels, in both experimental and clinical TBI cases, were somewhat unexpected. In either case, the implications of the changes in TRPM3 expression following TBI requires further investigation to elucidate the exact role that TRPM3 may play in TBI pathophysiology. The currently unresolved function of TRPM3 channels in the brain thereby limits the present discussion.

A recent report by Wagner et al. (2008) has demonstrated that TRPM3 is directly activated by the steroid hormone, pregnenolone (in its water-soluble form, pregnenolone sulphate, PS). In this report, the authors link the activation of TRPM3 by PS to insulin secretion in pancreatic β-cells. The activation of TRPM3 by PS is an important and interesting finding that may also have relevance to TBI. Pregnenolone is derived from cholesterol and is the precursor to other steroids, including progesterone and oestrogen (Nilius and Voets, 2008). It is well established that both progesterone and oestrogen have neuroprotective effects following TBI (Stein, 2008; O'Connor et al., 2005). In addition, levels of the protein that delivers cholesterol to the inner mitochondrial membrane for conversion to pregnenolone are elevated following excitotoxic brain injury, which is suggested to be a protective mechanism against neurodegeneration (Sierra et al., 2003). Indeed, another study (Shirakawa et al., 2005) showed that PS was able to attenuate α-amino-3-hydroxy-5-methylisoxazole-4-propionic acid (AMPA) cytotoxicity in cultured rat cortical neurons. However, Weaver Jr et al. (1998) demonstrated that PS could potentiate NMDA-induced cell death in hippocampal neurons. Whether TRPM3 could participate in such pathophysiological or neuroprotective processes following TBI requires further investigation. Importantly, it is also not clear whether PS is a physiologically relevant activator of TRPM3 (Nilius and Voets, 2008), or whether other steroid hormones, such as progesterone, are able to activate TRPM3.

6.4.3 TRPM7

In the present chapter, we have demonstrated significant changes in TRPM7 expression following TBI, which indicate that TRPM7 may be relevant to TBI pathophysiology. In a previous study, TRPM7 expression was acutely increased following experimental stroke (Jiang et al., 2008), however, the present study is the first to investigate the potential role of TRPM7 in TBI. In the rat cerebral cortex, there were significant elevations in TRPM7 mRNA level between 1 day

and 3 days after TBI, followed by a significant decrease at 5 days. These results correlate with levels of TRPM7 protein, which were significantly increased within injured neurons in the 5 hour, 2 day, 3 day and 5 day TBI groups compared to shams. In the human temporoparietal cortex, TRPM7 transcript level was significantly reduced in the < 5 hour survival group, with protein expression of TRPM7 significantly increased at this time point. Similar trends in TRPM7 protein expression were observed in clinical and experimental TBI up to the 5 hour time point.

As mentioned, TRPM7 has been implicated in playing a direct role in Ca^{2+}-mediated neuronal death (Aarts et al., 2003), thus, increases in TRPM7 channels following TBI could exacerbate this process (see Figure 6.5). Furthermore, oxidative stress and the production of free radicals have been demonstrated to be key secondary injury factors in TBI (Barone and Kilgore, 2006; Cormio et al., 1997). Since TRPM7 is activated by ROS and RNS, oxidative stress could lead to the production of positive feedback loops, whereby unregulated Ca^{2+} influx via TRPM7 channels stimulate secondary signalling pathways that further enhances oxidative stress, leading to tissue damage and cell death. Deficits in Mg^{2+} concentration can also lead to the generation of ROS and RNS (Altura et al., 2003), which further activate TRPM7 (and potentially TRPM2), thereby enhancing inflammation, oxidative stress and cell death. Moreover, ATP is depleted as a result of severe brain injury (Cormio et al., 1997). As discussed, low intracellular Mg^{2+} and Mg.ATP levels strongly activate TRPM7 (Monteilh-Zoller et al., 2003; Hermosura et al., 2002; Nadler et al., 2001). Given that Mg^{2+} levels remain suppressed for several days following injury (Heath and Vink, 1996), this is potentially a critical and persistent pathway leading to cell death after TBI.

Free radicals also increase microvascular permeability, and have been shown to cause BBB disruption and oedema following ischaemia (Heo et al., 2005). Indeed, oedema is one of the most important secondary injury factors in TBI with respect to patient outcome (Marmarou et al., 2000). Changes in extracellular Ca^{2+} concentrations as a result of injury also activate TRPM7 (Aarts and Tymianski, 2005a) and TRPM2 (Starkus et al., 2007). All of these factors could potentiate the cell death process by the generation of free radicals and causing the sustained activation of TRPM7, TRPM2 and TRPM2/TRPM7 multimers.

TBI results in massive influxes of Zn^{2+} ions to neurons, which is a major factor in neuronal cell toxicity and death (Hellmich et al., 2007; Suh et al., 2000). While voltage-gated calcium channels have been proposed to carry this current, Zn^{2+} could also enter cells through TRPM7 channels, which is permeable to a wide range of divalent cations including Zn^{2+}. Although trace metal ions are necessary for the catalytic function of enzymes and normal cellular function, their accumulation above trace levels is highly toxic (Monteilh-Zoller et al., 2003). Precise regulation of ion channels such as TRPM7 is vital to maintain normal physiological conditions and their overstimulation in pathological processes like TBI may lead to cell death. TRPM7 has a low, constitutive activity in resting cells that is likely to provide a constant flow of Mg^{2+} and Ca^{2+} into the

Figure 6.5: Potential mechanisms of TRPM channel-mediated cell death in TBI. Following TBI, the entry of Ca^{2+} into cells via NMDAR stimulates neuronal nitric oxide synthase (nNOS) leading to the production of nitric oxide (NO). Rises in intracellular Ca^{2+} concentration $[Ca^{2+}]_i$ promote $0_2{}^-$ release from mitochondria, which reacts with NO to produce highly reactive peroxynitrite radicals ($ONOO^-$). Free radicals damage cellular macromolecules and further activate TRPM2 and TRPM7 channels, allowing the influx of even more Ca^{2+}. Mitochondria also produce ADPR which stimulates TRPM2. TBI causes $[Mg^{2+}]_i$ depletion and decreases in cellular pH, which activates TRPM7 and TRPM6 (and TRPM7/TRPM6 dimers). The kinase (K) domains of TRPM7 and TRPM6 may also influence signalling processes and inflammation. Disruption to the BBB allows water, proteins and metal ions to enter the brain (not shown); toxic trace metals (such as Zn^{2+}) may enter cells through TRPM7, while inflammatory mediators (such as TNF-α) further activate TRPM2. Prolonged depletion of Mg^{2+} and excess production of ROS and RNS could exacerbate this positive feedback loop and overactivate TRPM2 and TRPM7 (and potentially TRPM2/TRPM7 dimers). The resultant unregulated Ca^{2+} influx leads to excitotoxicity, enhances oxidative stress and inflammatory processes, and eventually activates pro-apoptotic signalling cascades resulting in cell death. Figure also appears in Cook et al., 2009b.

cell (Fleig and Penner, 2004). TRPM7 channel activity is strongly enhanced when intracellular Mg^{2+} is depleted. Therefore, the reduction in Mg^{2+} concentration following TBI combined with increases in ROS and RNS, which further stimulate TRPM7 in a positive feedback loop, may result in impaired inhibition of TRPM7 activity. The resultant overactivation of TRPM7 could therefore result in extensive entry of cations other than Mg^{2+} into the cell, potentially causing significant cell death.

TRPM7 has also been implicated in the pathological response to vessel wall injury, which may be relevant to both the primary and secondary injury processes of TBI. At the time of insult, shearing of nerve fibres results in massive ion fluxes across cell membranes, loss of membrane potential and rapid release of neurotransmitters from damaged neurons. This results in excitotoxicity and evokes an inflammatory response, which stimulates further pathological processes, eventually leading to apopto-

sis and necrosis (Vink and Van Den Heuvel, 2004). In response to shear stress, which results in an increase in fluid flow, a significant number of TRPM7 channels accumulated at the plasma membrane in less than 2 minutes, and an increase in TRPM7 current was detected in vascular smooth muscle cells (Oancea et al., 2005). This rapid response by TRPM7 most likely makes it one of the first molecules to react to shear stress. TRPM7 was also identified as the stretch-activated channel that is activated by osmotic swelling in epithelial cells, and is involved in cellular volume regulation by providing a Ca^{2+}-influx pathway (Numata et al., 2007), which may be relevant to cerebral oedema following TBI.

Finally, TRPM7 might participate in cell death after TBI by responding to changes in extracellular pH (Jiang et al., 2005; Kozak et al., 2005). High concentrations of protons may be generated in pathological processes like TBI, leading to an acidic ($pH < 6.0$) state and thus enhancing TRPM7 activity.

In the rat hippocampus, significant decreases in TRPM7 mRNA level were observed at 3 hours and 5 hours post-TBI, compared to shams. These results correspond to the TRPM7 protein expression in this region of the brain, which were decreased at 5 hours and 1 day following injury. There were no changes in hippocampal levels of TRPM7 protein in the clinical TBI cases at either time point, but there were similar expression patterns in both clinical and experimental TBI over the first 5 hours of injury. The results obtained regarding TRPM7 expression in the hippocampus were somewhat unexpected. As mentioned, based on the known functions of TRPM7, particularly in relation to regulating Mg^{2+} homeostasis and in mediating neuronal cell death, we hypothesised that the expression of TRPM7 would increase after TBI. It is possible that the decrease in TRPM7 expression observed in the rat hippocampus following TBI could be a protective mechanism to prevent TRPM7-induced cell death, something not observed in the cerebral cortex. These differences in TRPM7 mRNA and protein expression between the cortex and hippocampal regions suggest that distinct pathophysiological mechanisms are occurring in the different brain regions. In any case, the role of TRPM7 channels in Mg^{2+} transport following TBI seems less important than their facilitation of other cation fluxes, as well as the potential role of the kinase domain in inflammatory processes.

6.4.4 TRPM6

In the present study, TRPM6 mRNA level and protein expression were investigated following experimental TBI. The TRPM6 study was discontinued in clinical TBI because, after four attempts to optimise human TRPM6 primer pairs, we were unable to attain PCR efficiency or R^2 values of sufficiently high standard for accurate or reproducible PCR results. In addition, at the beginning of the experiment, it was unknown whether significant changes in transcript or protein levels of TRPM6 following TBI would even be observed. Although TRPM7 and TRPM2 have been demonstrated as mediating ischaemic neuronal cell death, the role in TRPM6 in these processes is unclear. Due to the high cost of PCR reagents, after extensive testing of four sets of TRPM6 primers, it was decided that TRPM6 characterisation in clinical TBI would not be pursued in the present study. However, given that the current experimen-

tal TBI study has yielded interesting results with TRPM6, it would certainly be worthwhile for a future study to characterise TRPM6 expression in clinical TBI.

In the cerebral cortex, TRPM6 mRNA level was significantly increased in the 1 day TBI group compared to shams, and TRPM6 protein expression was significantly increased in the 5 day TBI group, with a trend to increase at the 1 day time point.

In the rat hippocampus, TRPM6 mRNA levels were elevated at every TBI time point, and displayed the largest changes in transcript levels of the entire TRPM channel study, with 10-fold increases at several TBI time points. This, however, did not translate to such profound increases in TRPM6 protein, with only the 5 hour, 1 day and 7 day time points showing significant elevations in TRPM6 protein expression compared to shams. As discussed above for TRPM3, there are several reasons why protein and mRNA levels may not match, especially following TBI.

As mentioned, it is currently unclear whether TRPM6 participates in neuronal cell death along with TRPM7 and TRPM2 (Aarts et al., 2003). However, considering its localisation in the brain, its permeability to Mg^{2+}, ability to form functional heteromers with, and to phosphorylate, TRPM7, TRPM6 too may be relevant in processes leading to cell death. The increased expression of TRPM6 following TBI in the present study suggests that TRPM6 channels may indeed be involved in TBI pathophysiology.

6.4.5 Conclusions

The present chapter has demonstrated, for the first time, changes in the expression of TRPM2, TRPM3 and TRPM7 at both the protein and transcript level following experimental and clinical TBI. Changes in the mRNA and protein expression of TRPM6 were also observed in experimental TBI. The results presented herein suggest that TRPM channels may participate in TBI secondary injury factors. However, it is unlikely that targeting a single factor of the TBI secondary injury process will result in a significant improvement in patient outcome. TRPM channels, therefore, may represent novel therapeutic targets as part of a multifactorial treatment strategy for TBI. Further investigations of the potential role of TRPM channels in TBI pathophysiology are warranted.

Chapter 7

SP Gene Expression in Clinical and Experimental Parkinson's Disease

7.1 Introduction

PD is a progressive movement disorder that affects approximately 1 % of the population over 60 years of age (De Lau and Breteler, 2006). The strongest PD risk factor is age (Driver et al., 2009), with up to 4 % of people over 80 years affected by the disease (Yao and Wood, 2009). PD is characterised by the degeneration of dopaminergic neurons in the SNpc, leading to a reduction of DA levels in the striatum (Hald and Lotharius, 2005). Without adequate levels of DA, motor neurons are unable to execute smooth, coordinated movements, resulting in the classic motor symptoms of PD: resting tremor, rigidity, bradykinesia and postural instability (Braak and Del Tredici, 2008). Another major neuropathological feature of PD is the presence of eosinophilic, intracytoplasmic protein aggregates known as Lewy bodies and Lewy neurites, which contain α-synuclein (Thomas and Beal, 2007).

The aetiology of PD is incompletely understood, but is likely to involve a number of interacting pathophysiological mechanisms, including inflammation, oxidative stress, mitochondrial dysfunction, abnormal protein handling and Ca^{2+} dysregulation (Thomas, 2009), which are influenced by candidate susceptibility genes and environmental exposures (Huang et al., 2004). While the majority of PD cases ($>$ 90 %) are sporadic in nature, recent studies have identified mutations in several genes that cause familial forms of the disease (Schapira, 2009; Ross and Smith, 2007).

Current treatment strategies aimed at restoring levels of DA are effective in controlling PD motor symptoms. However, over time DA replacement therapy is associated with 'wearing off' effects and motor fluctuations and, importantly, it do not slow disease progression (Schapira and Olanow, 2004; Lang and Lozano, 1998b). Therefore, a neuroprotective agent that inhibits or prevents dopaminergic neuronal death is urgently required.

Neuropeptides, in particular, SP, have gained attention as potential therapeutic targets for PD. SP is widely distributed in the CNS and functions as a neurotransmitter and/or neuromodulator (Snijdelaar et al.,

2000). SP is highly expressed in brain regions relevant to PD, including the SN, GP, caudate nucleus, putamen and cerebral cortex (Raffa, 1998). In several studies of clinical and experimental PD, decreases in SP expression have been demonstrated at both the protein and transcript level (Winkler et al., 2003; Wade and Schneider, 2001; Morissette et al., 1999; Gresch and Walker, 1999; Herrero et al., 1995; Sivam, 1991; Gerfen et al., 1990; Lindefors et al., 1989; Voorn et al., 1987; Tenovuo et al., 1984; Mauborgne et al., 1983). This led to the suggestion that depletion of SP may be a key pathophysiological event in PD and it was hypothesised that restoring SP levels may improve outcome. Indeed, the administration of high doses of SP to 6-OHDA lesioned rats increased levels of DA in the striatum, nucleus accumbens and frontal cortex (Krasnova et al., 1999), thus reversing the neurotoxic effects of 6-OHDA. In other studies, treatment with SP alleviated the functional and behavioural deficits induced by unilateral 6-OHDA lesion (Nikolaus et al., 1997; Mattioli et al., 1992).

However, findings from our laboratory (E. Thornton, PhD thesis) indicate that SP could actually exacerbate dopaminergic cell loss in PD. SP protein expression was significantly increased in 6-OHDA rats compared to shams, and this was associated with a poor functional outcome. Treatment with SP agonists or the ACE inhibitor, captopril, which prevents the degradation of SP, exacerbated the motor deficits resulting from PD and increased dopaminergic cell death. However, when animals were treated with the SP receptor antagonist, NAT (Cascieri et al., 1994; MacLeod et al., 1993), functional deficits were reduced to levels observed in sham animals, suggesting that SP may contribute to dopaminergic cell death in the early stages of PD. These results are in contrast to previous reports, where decreases in SP expression were generally observed. Importantly, the studies from our laboratory investigated SP expression in the early stages of PD, while the reports mentioned above used late-stage animal models of PD or post-mortem clinical cases, where the majority of dopaminergic cell loss has already occurred. Therefore, SP may play an active role in the degeneration of dopaminergic cells in early PD, while the depletion of SP in late-stage PD could be secondary to neuronal cell loss.

Previous reports of SP gene expression in PD have generally used *in situ* hybridisation (ISH) to detect preprotachykinin (PPT, the gene encoding SP) mRNA. However, no studies have used quantitative, real-time RT-PCR to characterise the gene expression of SP in PD. As discussed in Chapter 2, real-time RT-PCR is the most sensitive and accurate method of quantifying mRNA levels. Thus, the aims of this chapter were to use real-time RT-PCR to quantify SP gene expression in 5 brain areas of clinical PD cases, as well as in early and late-stage 6-OHDA models of experimental PD in rats. We hypothesised that SP mRNA level would decrease in the clinical PD cases and in the late-stage 6-OHDA model, and that increases would be observed in the early 6-OHDA model to coincide with the elevated expression of SP previously observed by our laboratory.

7.2 Materials and Methods

7.2.1 Rodent Models of PD

As mentioned, two models of experimental PD were used in the present study, to replicate both the early and late stages of the disease. Both models utilised the neurotoxin 6-OHDA to induce dopaminergic cell loss (Schwarting and Huston, 1996). For early experimental PD, 6-OHDA was administered into the right striatum ('6-OHDA intrastriatal model'), while the late stages of PD were replicated by injecting 6-OHDA into the medial forebrain bundle (MFB), at the origin of the nigrostriatal pathway ('6-OHDA SN model'). Additional animals were subject to all surgical procedures except for administration of 6-OHDA (sham surgery) to serve as controls for each model.

Animal surgery was carried out as described in the Materials and Methods chapter (Section 3.2.3). Briefly, animals (n = 20; 250 - 300 g) were anaesthetised with halothane/isoflurane. A midline incision was made on the dorsal surface of the head and the animal was placed onto a rodent stereotaxic device. The animal's upper incisor teeth were placed over the tooth bar at specific coordinates, and ear bars used to firmly secure the head in place. The skin and muscle was then retracted, and the skull cleaned and dried so that the midline and bregma sutures could be visualised.

For the intrastriatal (early) model of PD, two 0.7 mm burr holes were made over the right striatum using a high-speed micro drill at the stereotaxic coordinates (1) AP: 0.5 mm, ML: 2.5 mm, and (2) AP: -0.5 mm, ML: 4.2 mm relative to bregma, with the tooth bar set at -3.9 mm. Using a 5 μL Hamilton micro syringe lowered stereotaxically 5.0 mm ventrally from the dura, 2 μL 6-OHDA (5 μg/μL in 0.9 % saline) was injected into the right striatum at a rate of 0.5 μL/min with the needle then left in place for 2 mins before being slowly retracted.

For the SN (late) model of PD, two 0.7 mm burr holes were made over the right MFB using a high-speed micro drill at the stereotaxic coordinates (1) AP: -4.4 mm, ML: 1.2 mm, tooth bar: -2.4 mm, and (2) AP: -4.0 mm, ML: 0.75 mm, tooth bar: 3.4 mm. Using a 5 μL Hamilton micro syringe lowered stereotaxically -8.0 mm ventrally from the dura, (1) 2.5 μL 6-OHDA and (2) 2.0 μL 6-OHDA (3 μg/μL in 0.9 % saline) was injected into the MFB at each stereotaxic co-ordinate, respectively, a rate of 0.5 μL/min with the needle then left in place for 2 mins before being slowly retracted.

Animals were sacrificed by anaesthetic overdose; brains were rapidly removed and the striatum and SN dissected out in total and immediately snap frozen in liquid N_2. Intrastriatal 6-OHDA animals plus shams were sacrificed 4 days after surgery; previous studies from our laboratory have demonstrated cell loss replicating the early stages of clinical PD at these time points as well as significant functional deficits (E. Thornton, PhD thesis). Late model 6-OHDA animals plus shams were sacrificed at 1 day post-surgery; this time point was chosen to represent the cell loss of late stage clinical PD, since the lesions resulting from 6-OHDA injections into the MFB are virtually immediate (Blandini et al., 2008).

7.2.2 Human PD Cases

The use of post-mortem human brain tissue in this study was approved by the University of Adelaide Human Ethics Committee and all cases had written donor or next-of-kin consent for research. All human tissue used in this study was assessed by a clinical neuropathologist and given a diagnosis of either idiopathic PD or normal brain. Case details regarding human tissue are described in Appendix B. Fresh frozen human brain tissue from PD and control cases was received from the South Australian Brain Bank and the Victorian Brain Bank Network, respectively. For each case, we obtained tissue from the SN plus surrounding areas of the BG: GP, caudate nucleus and putamen, plus a region of the temporal cortex, the midtemporal gyrus (MTG) (see Figure 7.1), totalling 5 brain regions. We were interested to determine whether any changes in gene expression were restricted to the SN, or whether PD would have more global effects on the BG. The MTG was chosen because late-stage clinical PD can also affect the cerebral cortex (Schapira, 2008).

Figure 7.1: Human brain regions studied in the present chapter, showing globus pallidus, caudate nucleus, putamen, substantia nigra and cortex. Within the cortex, the midtemporal gyrus (MTG) was the region of interest. Figure adapted from `thejsms.com/85/`.

7.2.3 RNA Extraction and Real-time RT-PCR

Extraction of total RNA was carried out from rat PD and sham ipsilateral striatum and SN tissue (for each model: n = 5 PD animals; n = 5 shams) and human PD (n = 6 from each brain region) and control tissue (n = 7 from each brain region) as described in detail in the Materials and Methods chapter (Section 3.2.5). Fifty mg tissue was used in each RNA extraction, and a DNase treatment was included. Total RNA was quantified by UV spectrophotometry to measure absorbance at 230 nm, 260 nm and 280 nm. RNA integrity was assessed using the Agilent Bioanalyzer RNA 6000 Nano Chip (Series II) kit. Complementary DNA was synthesised as described in Section 3.2.6, diluted to 10 ng/μL and stored at $-80\,^{\circ}C$ until PCR.

A reference gene validation study was carried out to determine the most stable reference genes for accurate real-time RT-PCR data normalisation in both the rat and human PD studies. The reference gene validation studies are described in detail in Chapter 4. Real-time RT-PCR was carried out as described in Section 3.2.7. Following PCR amplification, Ct values were calculated from the standard curve using the Corbett Rotor-Gene 6 software. Triplicate Ct values for each sample were entered into the qBasePlus software, which calculated mRNA levels of SP relative to multiple reference genes.

7.2.4 Statistical Analysis

Unpaired Student's t-tests were carried out, with $p < 0.05$ considered statistically significant.

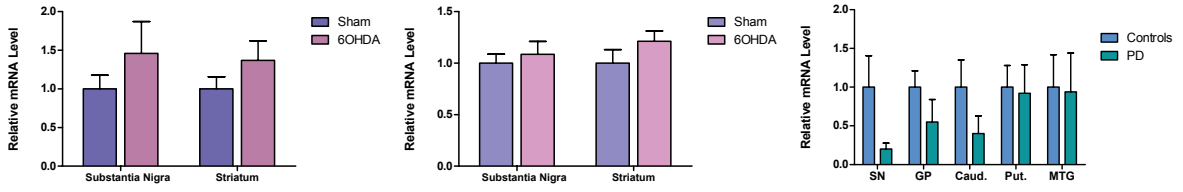

(a) Intrastriatal Model **(b)** SN Model **(c)** Clinical PD

Figure 7.2: (a) - (b): SP mRNA level in experimental PD, in the SN and striatum of (a) 6-OHDA intrastriatal model of early PD, and (b) 6-OHDA SN model of late-stage PD. Bars depict mean ± SEM of 5 PD animals and 5 shams per model, from triplicate PCR amplifications. (c): SP mRNA level in clinical PD. Bars depict mean ± SEM of 6 PD cases and 7 controls, in 5 brain areas, from triplicate PCR amplifications. SN, substantia nigra; GP, globus pallidus; Caud, caudate nucleus; Put, putamen; MTG, midtemporal gyrus

7.3 Results

7.3.1 Experimental PD

Intrastriatal Model

In the early model of experimental PD, (Figure 7.2a) there were slight trends to increases in SP mRNA level in the 6-OHDA lesioned rats compared to shams. These trends were observed in both the SN and striatum, but did not reach statistical significance.

SN Model

In the late model of experimental PD, there were no changes in SP mRNA level between 6-OHDA rats and shams in either brain area (Figure 7.2b).

7.3.2 Clinical PD

Graphical results of SP mRNA levels across the 5 brain areas of clinical PD are shown in Figure 7.2c. In the SN, there was a trend to decrease in SP transcript level in PD cases compared to controls (0.20 ± 0.07 fold decrease, p = 0.15). The transcript level of SP in the GP and caudate was reduced by approximately half in the PD cases compared to controls, but did not reach statistical significance ($p > 0.05$). There was no change in SP mRNA level in the putamen or MTG.

7.4 Discussion

The present chapter is the first to characterise SP mRNA levels in clinical and 6-OHDA-induced experimental PD using quantitative, real-time RT-PCR with validated reference genes as normalising factors. To our knowledge, there is only one other study (Colebrooke et al., 2007) that has used real-time RT-PCR to measure SP mRNA levels in PD; this study was carried out in a novel mouse model of PD with a modification to the vesicular monoamine transporter-2 gene. Previous studies investigating SP transcript levels in PD have primarily used ISH to identify PPT mRNA (Nisbet et al., 1995; Gresch and Walker, 1999). ISH is an effective method to detect and anatomically localise nucleic acids, but is qualitative with regard to gene expression analysis (Kadkol et al., 1999). The recent development of quantitative, real-time RT-PCR has revolutionised gene expression analysis, surpassing semi-quantitative techniques with its simplicity

and high-throughput capabilities combined with far greater accuracy, sensitivity and reproducibility (Bustin et al., 2009; Wilhelm and Pingoud, 2003). Real-time RT-PCR is thus the method of choice for quantifying nucleic acids (Bustin, 2000).

Chapter 4 evaluated reference gene stability in clinical and experimental PD and determined appropriate panels of reference genes for accurate normalisation of gene expression data. It was interesting to note that the most stable reference genes in clinical PD differed among the five 5 brain areas studied (see Table 4.3 in Chapter 4), consistent with the recommendation that reference genes should be validated whenever an experimental variable is changed (Dheda et al., 2004).

In the intrastriatal 6-OHDA (early) model of experimental PD, SP mRNA level showed a trend to increase in the SN and striatum of the 6-OHDA treated animals (4 days survival) compared to shams. In our previous study (E. Thornton, PhD thesis), enzyme-linked immunosorbent assay detected a significant increase in SP protein in the ipsilateral striatum of 6-OHDA lesioned animals with 3 days survival, and in the contralateral SN at 7 days post-6-OHDA treatment. Furthermore, semi-quantitative immunohistochemistry revealed increased SP immunoreactivity throughout the entire ipsilateral striatum in PD animals at day 3 and day 7 following 6-OHDA lesion. In the SN, cytoplasmic SP immunoreactivity was greater in dopaminergic neurons of 6-OHDA treated animals at day 7 compared to shams. These increases in SP protein expression corresponded to neuroinflammatory changes (reactive astrocytes and microglia), disruption to the BBB and degeneration of dopaminergic neurons. SP is a potent initiator of neurogenic inflammation (Donkin et al., 2009; Nimmo et al., 2004) and induces cytokine release from microglia and astrocytes (Chauhan et al., 2008). Given that our previous study also showed that a SP receptor antagonist reduced dopaminergic cell loss and improved functional deficits in 6-OHDA lesioned animals, it is possible that SP plays a pathophysiological role in the early stages of PD by promoting dopaminergic cell death, exacerbating neuroinflammation and disrupting the BBB. This hypothesis is supported by the results of the present chapter, which suggest that transcriptional regulation of SP may be an important factor in this process. However, statistical significance was not reached in the present study, which may be attributed to the high variability in SP mRNA data, particularly in the sham group in the SN.

In the late (SN) model of experimental PD, there were no changes in SP mRNA level between 6-OHDA lesioned animals and shams. This was somewhat unexpected, because previous studies using this model report significant reductions in PPT mRNA level in the striatum of 6-OHDA lesioned rats compared to controls (Winkler et al., 2003; Gresch and Walker, 1999; Gerfen et al., 1990). Significant decreases in SP mRNA levels have been reported within 1 day of 6-OHDA lesions, with rapid decreases occurring as striatal DA levels are depleted (Contreras-Vidal et al., 1998; Nisenbaum et al., 1994). In the present study, only one survival time point (1 day) was investigated, and we did not see the reduction in SP mRNA level reported in other studies. However, as mentioned, previous studies have used ISH to detect SP

mRNA, while the current study used quantitative, real-time RT-PCR. This probably accounts for the differences in results. In the present study, RNA was extracted from a homogenate of approximately 50 mg tissue from each brain area. Consequently, cells other than dopaminergic neurons were included in the analysis. Recent studies have overcome this potentially confounding issue using laser capture microdissection (LCM) to isolate single dopaminergic neurons for analysis (Simunovic et al., 2009; Gründermann et al., 2008). In future studies it would be useful to use LCM to ensure specificity to dopaminergic neurons, however, this technique was not available for the present study.

Considering that cell loss in the late model of PD is likely to occur virtually immediately (Blandini et al., 2008), very acute increases in SP mRNA level (within hours) would be expected to occur, if elevated SP expression does in fact contribute to early cell loss in PD as hypothesised in our previous study (E. Thornton, PhD thesis). This would theoretically be followed by a decrease in SP mRNA level as the disease progresses. Although we were not able to demonstrate this in the present study, a very recent study from our laboratory showed that SP protein expression decreased specifically in the SNpc, but not across the entire SN, in late-stage 6-OHDA treated animals compared to shams (M. Hassall, Honours thesis). Interestingly, when the 6-OHDA lesioned animals were treated with L-DOPA, SP expression was restored to sham levels; this has also been demonstrated for PPT mRNA levels (Zeng et al., 1994) and suggests a positive feedback loop whereby SP promotes the release of DA and vice versa (Humpel et al., 1991; Bannon et al., 1987). In future studies, it would be worthwhile to analyse SP gene expression at additional time points following 6-OHDA lesions and with more animals per group to clarify the exact nature of SP mRNA level in early and late experimental PD.

In clinical PD, SP mRNA level showed a tendency to decrease in the SN of PD cases compared to controls (0.20 ± 0.07 fold decrease, $p = 0.15$). These results correspond to the decreases in SP immunoreactivity in the SN of PD patients reported in previous studies (Tenovuo et al., 1984; Mauborgne et al., 1983), and support the suggestion that depletion of SP in the SN may be important in PD pathogenesis (Chen et al., 2004; Barker, 1991). It is likely that these decreases in SP are a result of decreased DA levels in the striatum (Gerfen et al., 1990). However, due to variability in the control group, data in the present study did not reach statistical significance. Variability in the sham (control) group was also observed in the early experimental PD study, suggesting that SP mRNA levels may fluctuate between individuals even in normal situations. It is also possible that some of the control data were influenced by the 'scant plaques' identified by clinical neuropathologists upon microscopic examination of the brain (see case notes in Appendix B, Table B.3), or even by patient medications. Unfortunately, more detailed clinical information was not available for the control cases, so these explanations remain speculative. In future studies, more PD cases would be required to clarify these results and increase their statistical power.

In addition, there were non-significant reductions in SP mRNA level in the GP and caudate nucleus of clinical PD cases, and

no changes in the putamen. These results are fairly consistent with a previous study (Nisbet et al., 1995), which demonstrated decreases in PPT mRNA levels in the GP and SN of PD patients, but not in the caudate or putamen. Furthermore, Mauborgne et al. (1983) found a reduction in SP immunoreactivity in the SN and external GP of PD patients, but not in the caudate, putamen or internal segment of the GP. Sivam (1991), however, showed that PPT mRNA was reduced in the putamen of PD patients only when DA loss was greater than 80 %. While the exact role of SP in PD requires further investigation, it is interesting that the changes in SP expression are more pronounced in specific areas of the BG than others. This may be an important factor in determining how SP may contribute to the progression of the disease. Mauborgne et al. (1983) suggest that the loss of SP immunoreactivity in the SN could be a metabolic consequence of SN dopaminergic cell degeneration; indeed, it is likely that striatal DA innervation is required to maintain basal SP levels (Cruz and Beckstead, 1989).

Finally, SP mRNA level was unchanged between PD cases and controls in the cortical region of interest, the MTG. To our knowledge, this is the first study to quantify SP mRNA level in the MTG region of PD brains. However, a previous study (Sivam, 1991) found no changes in PPT mRNA level in the frontal cortex of PD patients, and Tenovuo et al. (1984) reported no difference in SP immunoreactivity in the cerebral cortex in PD and control brains.

It is also interesting to note that the potential role of SP in PD pathogenesis may vary depending on the stage of the disease. In the early stages of PD, excess SP may exacerbate dopaminergic cell death by promoting inflammation and BBB disruption (E. Thornton, PhD thesis). These results are in contrast to several late-stage PD studies of both clinical and experimental PD (including several different animal models), where deficits in SP have been proposed to be a key event in PD cell death (reviewed in Raffa, 1998). Whether SP depletion is a primary pathology, a consequence of the DA denervation leading to a reduction in the capacity to produce tachykinins, or as a result of prolonged L-DOPA treatment is uncertain (De Ceballos et al., 1993; Sivam, 1991). However, considering that DA and SP potentially promote each other's release in a positive feedback loop (Bannon et al., 1987), it is likely that reduced SP levels are a direct loss of DA input to the striatum. Clearly, more studies are required to elucidate the precise role of SP throughout the entire course of PD.

In conclusion, the results of the present chapter build on those of previous studies, and will contribute to elucidating the molecular mechanisms underlying PD pathogenesis.

Chapter 8

TRPM Channel Expression in Clinical and Experimental Parkinson's Disease

8.1 Introduction

PD is the second most common neurodegenerative disorder after AD and affects approximately 1 % of the population over 60 years of age (De Lau and Breteler, 2006). The neuropathological hallmarks of PD include the loss of dopaminergic neurons in the SNpc and intracytoplasmic protein aggregates known as Lewy bodies (Thomas and Beal, 2007). The degeneration of dopaminergic neurons in the SNpc results in a reduction of DA levels in the striatum (Hald and Lotharius, 2005). DA is required for motor neurons to co-ordinate movement and its depletion leads to the classic motor symptoms of PD: resting tremor, rigidity, bradykinesia and postural instability (Braak and Del Tredici, 2008).

Although the aetiology of PD is not completely understood, environmental exposures and genetic predisposition are likely to influence an individual's susceptibility to develop the disease. Several environmental risk factors for PD have been identified, such as pesticides and exposure to metals, whereas smoking and caffeine consumption have been reported to reduce the risk of PD (Elbaz and Tranchant, 2007; Lai et al., 2002a). There are a number of candidate susceptibility genes that may be associated with PD; variants of certain genes may be positively or inversely associated with PD risk (reviewed in Huang et al., 2004). Recent studies have identified mutations in several genes that cause the autosomal dominant and recessive (familial) forms of PD (Schapira, 2009; Ross and Smith, 2007). However, the majority of PD cases are sporadic in nature, and research into the genetic mutations of familial PD have provided insight into the pathogenesis of the sporadic form. These studies have identified a number of processes that may be associated with the pathophysiology of PD, including inflammation, oxidative stress, mitochondrial dysfunction, abnormal protein handling and Ca^{2+} dysregulation (Thomas, 2009).

The currently available treatments for PD are symptomatic and mainly consist of DA replacement therapies (reviewed in Stacy, 2009). Thus, a neuroprotective agent that slows or prevents the progression of PD is

urgently required. Recently, members of the TRP family of ion channels have gained attention in PD research and may represent potential therapeutic targets. The TRP superfamily consists of over 30 ion channels with diverse functions, properties and expression patterns (Pedersen et al., 2005). The present chapter focuses on three members of the melastatin subfamily, TRPM7, TRPM3 and TRPM2.

The ubiquitously expressed TRPM7 consists of an ion channel fused to a protein kinase domain (Nadler et al., 2001). TRPM7 is permeable to a wide range of divalent metal ions (Monteilh-Zoller et al., 2003) and is one of only a few identified mammalian Mg^{2+} transporters. The functions of TRPM7 are diverse, and include synaptic transmission (Krapivinsky et al., 2006), normal growth and development (Jin et al., 2008; Elizondo et al., 2005), and regulating vascular smooth muscle cells (He et al., 2005). Strong evidence suggests that TRPM7 is necessary for cell survival and is important in Mg^{2+} homeostasis (Schmitz et al., 2003; Nadler et al., 2001), although the latter point is currently contentious (Jin et al., 2008).

TRPM2 is a non-selective cation channel that is highly permeable to Ca^{2+} and is expressed in wide range of human tissues, such as immune cells and various regions of the brain (Lange et al., 2008; Heiner et al., 2006; Nagamine et al., 1998), including the striatum (Uemura et al., 2005). TRPM2 can be activated in response to such factors as oxidative or nitrosative stress (Wehage et al., 2002; Hara et al., 2002), intracellular and extracellular Ca^{2+} (Starkus et al., 2007; McHugh et al., 2003) and ADP-ribose (Perraud et al., 2001).

TRPM7 and TRPM2 are likely to play significant roles in CNS pathophysiology. Several lines of evidence indicate that the activation of TRPM2 by oxidative stress results in cell death via unregulated Ca^{2+} influx (Kaneko et al., 2006; Zhang et al., 2003; Hara et al., 2002). TRPM7 has also been implicated in playing a direct role in Ca^{2+}-mediated neuronal death (Aarts et al., 2003). It has been proposed that Ca^{2+} entry into cells as a result of injury causes the production of free radicals, which activate TRPM7 and TRPM2, leading to further Ca^{2+} influx and additional free radical production in a positive feedback loop (Aarts and Tymianski, 2005b).

Furthermore, TRPM channels have been identified as potential susceptibility genes in ALS-G and PD-G. These disorders are found with a relatively high incidence on islands of the Western Pacific, and the following have been suggested as candidate environmental factors associated with these diseases: toxins from the cycad plant, deficiencies in Ca^{2+} and Mg^{2+}, and high exposure to aluminium, manganese and other toxic metals (Plato et al., 2003; Cox and Sacks, 2002). Recent studies by Hermosura et al. (2008, 2005) have reported mutations in the TRPM7 and TRPM2 genes in ALS-G and PD-G patients, but not in matched controls, suggesting that TRPM channels may be important in the pathogenesis of neurodegenerative disorders.

Mg^{2+} also appears to be associated with the onset and progression of PD. Epidemiological studies have revealed that PD patients have slightly reduced Mg^{2+} levels in hair (Forte et al., 2005) and significantly decreased Mg^{2+} concentrations in the CSF (Bocca et al., 2006). In the study by Bocca

et al. (2006), CSF Mg^{2+} concentrations were negatively associated with the severity and duration of the disease. In another study (Yasui et al., 1992), levels of Mg^{2+} were significantly decreased in several areas of the brain, including the BG.

Other recent studies provide further evidence that Mg^{2+} may be significant in PD. Hashimoto et al. (2008) found that Mg^{2+} was able to inhibit MPP^{+}-induced toxicity to rat dopaminergic neurons *in vitro*. In a very recent report, Muroyama et al. (2009) showed that mice fed a Mg^{2+}-deficient diet exhibited depression and anxiety-related behaviour, and these mice were more susceptible to reduced striatal DA levels following administration of MPTP compared to control mice.

Aside from a role in disease onset, Mg^{2+} administration has been shown to reduce levodopa-induced dyskinesia in MPTP-treated monkeys (Chassain et al., 2003), suggesting an interaction between neurotransmitter release and Mg^{2+} (Vink et al., 2009). In another study (Golts et al., 2002), Mg^{2+} inhibited the aggregation of α-synuclein, the principal component of Lewy bodies.

TRPM3 is expressed in the human brain, kidney, testis, eye and spinal cord (Lee et al., 2003), and is proposed to be involved in renal Ca^{2+} homeostasis, and cation homeostasis in the CSF (Oberwinkler and Philipp, 2007; Grimm et al., 2003). High levels of TRPM3 have been detected in the brain and pituitary (Fonfria et al., 2006b), including the BG (Kunert-Keil et al., 2006), suggesting that this protein may play a significant role in brain physiology.

TRPM3 is permeable to Ca^{2+} and Mg^{2+} (Oberwinkler and Philipp, 2007), and channel activity is enhanced by a reduction in extracellular osmolarity (Grimm et al., 2003) and inhibited by rises in intracellular Mg^{2+} concentration (Oberwinkler, 2007; Oberwinkler et al., 2005). TRPM3 is activated by D-erythro-sphingosine (Grimm et al., 2005), pregnenolone sulphate (Wagner et al., 2008) and Ca^{2+} store depletion (Lee et al., 2003). The exact physiological role of native TRPM3 channels, including their function in the brain, is incompletely understood. To date, no studies have characterised the transcript or protein levels of TRPM3 in neurological disorders.

The aims of the present chapter were to characterise the gene expression of TRPM2, TRPM3 and TRPM7 in the striatum and SN of two 6-OHDA rodent models of PD, representing both the early and late stages of the disease, and in clinical PD cases across 5 brain areas relevant to PD. Real-time RT-PCR was carried out to quantify transcript levels of TRPM channels normalised to multiple reference genes. In addition, we aimed to semi-quantify TRPM channel protein expression in the early-stage rodent model of PD using immunohistochemistry and colour deconvolution analysis. The expression of TRPM2 and TRPM7 was hypothesised to increase in PD, where they may contribute to oxidative stress and pathways leading to dopaminergic cell death. Although the functions of TRPM3 remain to be established, we hypothesised an increase in TRPM3 expression given its permeability to Mg^{2+} and Ca^{2+} and considering that it is inhibited by intracellular Mg^{2+}.

Table 8.1: Summary of Brain Regions Studied in the Present Chapter

Type of PD	mRNA Study‡	Protein Study*
Intrastriatal 6-OHDA (early experimental PD)	ST and SN (4 day survival)	ST and SN (3 day and 7 day survival)
SN 6-OHDA (late experimental PD)	ST and SN (1 day survival)	–
Clinical PD	SN, GP, Caud, Put, MTG	–

‡ST, striatum; SN, substantia nigra; GP, globus pallidus; Caud, caudate nucleus; Put, putamen; MTG, midtemporal gyrus.
∗ – denotes that FFPE tissue was not available for the present study.

8.2 Materials and Methods

A summary of the experimental design for the current chapter is shown in Table 8.1.

8.2.1 Rodent Models of PD

Two models of experimental PD were used in the present study, to replicate both the early and late stages of the disease. For early-stage PD, 6-OHDA was administered into the right striatum, while the late stages of PD were replicated by injecting 6-OHDA into the MFB. Additional animals were subject to all surgical procedures except for administration of 6-OHDA (sham surgery) to serve as controls for each model.

Animal surgery was carried out as described in the Materials and Methods chapter (Section 3.2.3). Briefly, animals (n = 20; 250 - 300 g) were anaesthetised with halothane/isoflurane. A midline incision was made on the dorsal surface of the head and the animal was placed onto a rodent stereotaxic device. The animal's upper incisor teeth were placed over the tooth bar at specific coordinates, and ear bars used to firmly secure the head in place. The skin and muscle was then retracted, and the skull cleaned and dried so that the midline and bregma sutures could be visualised.

For the intrastriatal (early) model of PD, two 0.7 mm burr holes were made over the right striatum using a high-speed micro drill at the stereotaxic coordinates (1) AP: 0.5 mm, ML: 2.5 mm, and (2) AP: -0.5 mm, ML: 4.2 mm relative to bregma, with the tooth bar set at -3.9 mm. Using a 5 μL Hamilton micro syringe lowered stereotaxically 5.0 mm ventrally from the dura, 2 μL 6-OHDA (5 μg/μL in 0.9 % saline) was injected into the right striatum at a rate of 0.5 μL/min with the needle then left in place for 2 mins before being slowly retracted.

A similar procedure was applied in the SN (late) model of PD, with burr holes made at the following stereotaxic coordinates: (1) AP: -4.4 mm, ML: 1.2 mm, tooth bar: -2.4 mm, and (2) AP: -4.0 mm, ML: 0.75 mm, tooth bar: 3.4 mm. Using a micro syringe lowered stereotaxically -8.0 mm ventrally from the dura, (1) 2.5 μL 6-OHDA and (2) 2.0 μL 6-OHDA (3 μg/μL in 0.9 % saline) was injected into the MFB at each stereotaxic co-ordinate.

Animals were sacrificed by anaesthetic overdose; brains were rapidly removed and the striatum and SN dissected out and immediately snap frozen in liquid N_2. Intrastriatal 6-OHDA animals plus shams for gene expression analysis were sacrificed 4 days af-

ter surgery, while animals for immunohistochemistry were sacrificed at 3 and 7 days following surgery. Previous studies from our laboratory have demonstrated cell loss replicating the early stages of clinical PD at these time points as well as significant functional deficits (E. Thornton, PhD thesis). Late model 6-OHDA animals plus shams were sacrificed at 1 day post-surgery; this time point was chosen to represent the cell loss of late stage clinical PD, since the lesions resulting from 6-OHDA injections into the MFB are virtually immediate (Blandini et al., 2008). In the late model of PD, gene expression analysis only was carried out; at the time of writing, experiments generating late-stage 6-OHDA FFPE tissue are ongoing.

8.2.2 Human PD Cases

The use of post-mortem human brain tissue in this study was approved by the University of Adelaide Human Ethics Committee and all cases had written donor or next-of-kin consent for research. All human tissue used in this study was assessed by a clinical neuropathologist and given a diagnosis of either idiopathic PD or normal brain. Case details regarding human tissue are described in Appendix B. Fresh frozen human brain tissue from PD and control cases was received from the South Australian Brain Bank and the Victorian Brain Bank Network, respectively. For each case, we obtained tissue from five brain regions: SN, GP, caudate nucleus, putamen and MTG (see Figure 7.1 in the previous chapter). We were interested to determine whether any changes in gene expression were restricted to the SN, or whether PD would have more global effects on the BG.

8.2.3 RNA Extraction and Real-time RT-PCR

Extraction of total RNA was carried out from rat PD and sham ipsilateral striatum and SN tissue (for each model: n = 5 PD animals; n = 5 shams) and human PD (n = 6 from each brain region) and control tissue (n = 7 from each brain region) as described in detail in the Materials and Methods chapter (Section 3.2.5). Fifty mg tissue was used in each RNA extraction, and a DNase treatment was included. Total RNA was quantified by UV spectrophotometry to measure absorbance at 230 nm, 260 nm and 280 nm. RNA integrity was assessed using the Agilent Bioanalyzer RNA 6000 Nano Chip (Series II) kit. Complementary DNA was synthesised as described in Section 3.2.6, diluted to 10 ng/μL and stored at $-80\,^{\circ}C$ until PCR.

A reference gene validation study was carried out to determine the most stable reference genes for accurate real-time RT-PCR data normalisation in both the rat and human PD studies; these studies are described in detail in Chapter 4. Real-time RT-PCR was carried out as described in Section 3.2.7. Following PCR amplification, qBasePlus was used to calculate mRNA levels of TRPM channels, relative to multiple reference genes.

8.2.4 TRPM Channel Immunohistochemistry

Brains from perfusion-fixed animals were fixed for at least 1 week in formalin, and then cut into 2 mm coronal sections, processed overnight and embedded in paraffin wax. Serial 5 μM sections were cut with a microtome, mounted onto microscope slides and left to dry overnight. TRPM channel immunohis-

tochemistry was carried out as described in detail in Section 3.2.4, using polyclonal primary antibodies (see Table 3.1). Digital images of all sections were acquired using a Nanozoomer Digital Pathology Scanner at a magnification of 40x. Colour deconvolution analysis was performed to determine 'weight % DAB' values and therefore to semi-quantify TRPM channel protein content.

8.2.5 Statistical Analysis

Unpaired Student's t-tests and one-way ANOVA with Dunnett's multiple comparison test were performed using GraphPad Prism, with $p < 0.05$ considered statistically significant.

8.3 Results

8.3.1 Rodent Models of PD

TRPM2 Expression

Figure 8.1 shows graphical results of TRPM2 mRNA level in the early and late models of experimental PD, plus semi-quantitative immunohistochemistry results in the early PD model.

In the intrastriatal 6-OHDA model of early PD, there were no changes in TRPM2 mRNA level (Figure 8.1a) between PD animals and shams in either the striatum or SN.

TRPM2 immunoreactivity was detected in neurons and microglia in the striatum and SN of sham and 6-OHDA lesioned animals. These brain regions have previously been shown to express TRPM2 (Fonfria et al., 2006a; Uemura et al., 2005; Nagamine et al., 1998). Representative staining is shown in the micrographs in Figures 8.5 and 8.6. Colour deconvolution analysis revealed no change in TRPM2 protein expression between PD animals and shams in the SN (Figure 8.1b). However, TRPM2 was significantly increased in the striatum of 7 day PD animals compared to shams (p = 0.05), and a trend to increase in the 3 day group.

In the late model of experimental PD, shown in Figure 8.1c, TRPM2 mRNA level demonstrated a trend to increase in both the striatum and SN of 6-OHDA treated animals versus shams (p = 0.14 in both brain areas; striatum: 2.61 $\pm$ 0.71 fold increase, SN: 1.75 $\pm$ 0.44 fold increase).

TRPM3 Expression

Graphical results of TRPM3 mRNA level in the early and late models of experimental PD, plus semi-quantitative immunohistochemistry results for the early PD model are shown in Figure 8.2.

In the intrastriatal 6-OHDA model of early PD (Figure 8.2a), TRPM3 mRNA level was significantly decreased in both the striatum and SN of 6-OHDA lesioned animals compared to shams (striatum: 0.48 $\pm$ 0.14 fold decrease; SN: 0.51 $\pm$ 0.05 fold decrease).

TRPM3 immunoreactivity was detected within neurons in the striatum and SN in sham and 6-OHDA lesioned animals. TRPM3 expression has previously been demonstrated in the BG (Kunert-Keil et al., 2006). TRPM3 protein expression was significantly ($p < 0.01$) decreased in both brain areas at 7 days following 6-OHDA treatment compared to shams (Figure 8.2b), but not in the 3 day PD group. The micrographs in Figures 8.5 and 8.6 depict these changes.

In the late model of PD, TRPM3 mRNA level was significantly increased in the SN of 6-OHDA animals compared to shams (5.76 $\pm$ 1.33 fold increase, Figure 8.2c).

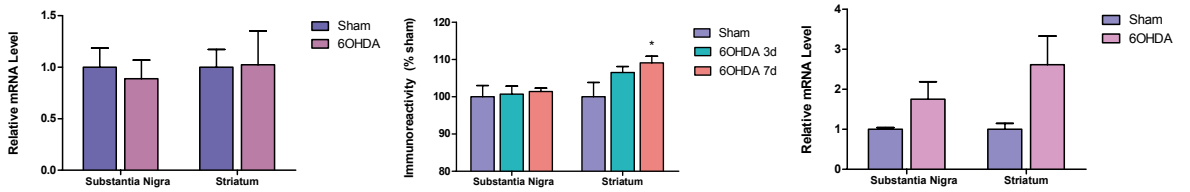

(a) ST Model mRNA **(b)** ST Model Protein **(c)** SN Model mRNA

Figure 8.1: (a) TRPM2 mRNA level and (b) TRPM2 protein expression in the 6-OHDA intrastriatal model of early PD. (c) TRPM2 mRNA level in the 6-OHDA SN model of late-stage PD. Bars depict mean ± SEM of 5 PD animals and 5 shams per model per time point. ST, striatum. * denotes $p < 0.05$.

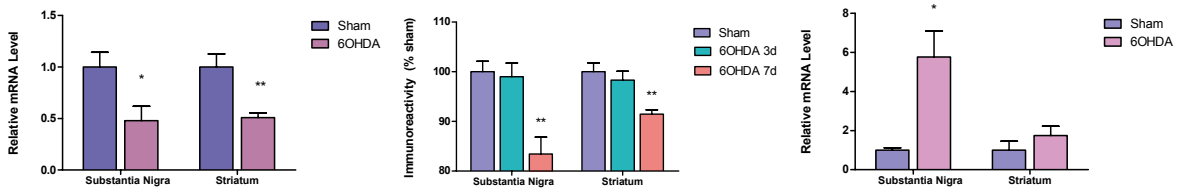

(a) ST Model mRNA **(b)** ST Model Protein **(c)** SN Model mRNA

Figure 8.2: (a) TRPM3 mRNA level and (b) TRPM3 protein expression in the 6-OHDA intrastriatal model of early PD. (c) TRPM3 mRNA level in the 6-OHDA SN model of late-stage PD. Bars depict mean ± SEM of 5 PD animals and 5 shams per model per time point. ST, striatum; * denotes $p < 0.05$; ** denotes $p < 0.01$.

TRPM7 Expression

Figure 8.3 shows graphical results of TRPM7 mRNA level in the early and late models of experimental PD, as well as semi-quantitative immunohistochemistry results in the early PD model.

In the intrastriatal 6-OHDA model of early PD, TRPM7 mRNA level was unchanged in either brain area of PD animals compared to shams (Figure 8.3a).

TRPM7 immunoreactivity was identified in neurons of the striatum and SN in sham and 6-OHDA lesioned animals. Colour deconvolution analysis revealed a significant ($p < 0.01$) increase in TRPM7 protein expression in the striatum at 3 days and 7 days after 6-OHDA lesion, but not in the SN. This is demonstrated by the micrographs in Figures 8.5 and 8.6, which show strong immunoreactivity in striatal neurons of the PD animals compared to shams, but no significant differences in the SN.

Figure 8.3c depicts TRPM7 transcript levels in the 6-OHDA SN model of late PD. In both the striatum and SN of PD animals, TRPM7 mRNA level was significantly increased compared to shams (striatum: 1.64 ± 0.15 fold increase; SN: 1.74 ± 0.16 fold increase; $p < 0.05$).

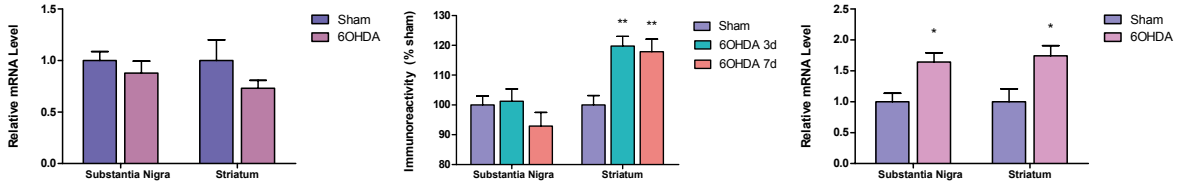

(a) ST Model mRNA **(b)** ST Model Protein **(c)** SN Model mRNA

Figure 8.3: (a) TRPM7 mRNA level and (b) TRPM7 protein expression in the 6-OHDA intrastriatal model of early PD. (c) TRPM7 mRNA level in the 6-OHDA SN model of late-stage PD. Bars depict mean ± SEM of 5 PD animals and 5 shams per model per time point. ST, striatum; * denotes $p < 0.05$; ** denotes $p < 0.01$.

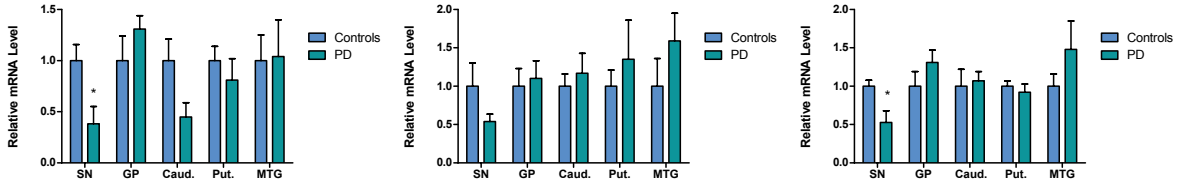

(a) TRPM2 **(b)** TRPM3 **(c)** TRPM7

Figure 8.4: TRPM Channel mRNA levels in clinical PD and control cases. (a) TRPM2, (b) TRPM3, (c) TRPM7. Bars depict mean ± SEM of 6 PD cases and 7 controls, from triplicate PCR amplifications. SN, substantia nigra; GP, globus pallidus; Caud, caudate nucleus; Put, putamen; MTG, midtemporal gyrus; * denotes $p < 0.05$.

8.3.2 Clinical PD

TRPM2 mRNA Level

Figure 8.4a shows graphed TRPM2 gene expression data across the five brain regions in clinical PD. In the SN, TRPM2 mRNA level was significantly decreased in the PD group compared to controls (0.38 ± 0.17 fold decrease, $p < 0.05$). There was a trend to decrease in the caudate (0.45 ± 0.14 fold decrease; $p = 0.06$) and no changes in the putamen, GP or MTG.

TRPM3 mRNA Level

Graphical results of TRPM3 gene expression data in clinical PD are shown in Figure 8.4b. TRPM3 mRNA level demonstrated a trend to decrease in the SN of PD patients compared to controls (0.54 ± 0.09 fold decrease; $p = 0.15$). There were no significant changes in TRPM3 gene expression in the other brain regions.

TRPM7 mRNA Level

TRPM7 mRNA data for the five brain regions in PD and control cases are shown in Figure 8.4c. In the SN of PD patients, TRPM7 transcript level was significantly decreased compared to controls (0.53 ± 0.15 fold decrease; $p < 0.05$). No significant changes were observed in the putamen, caudate, GP or MTG.

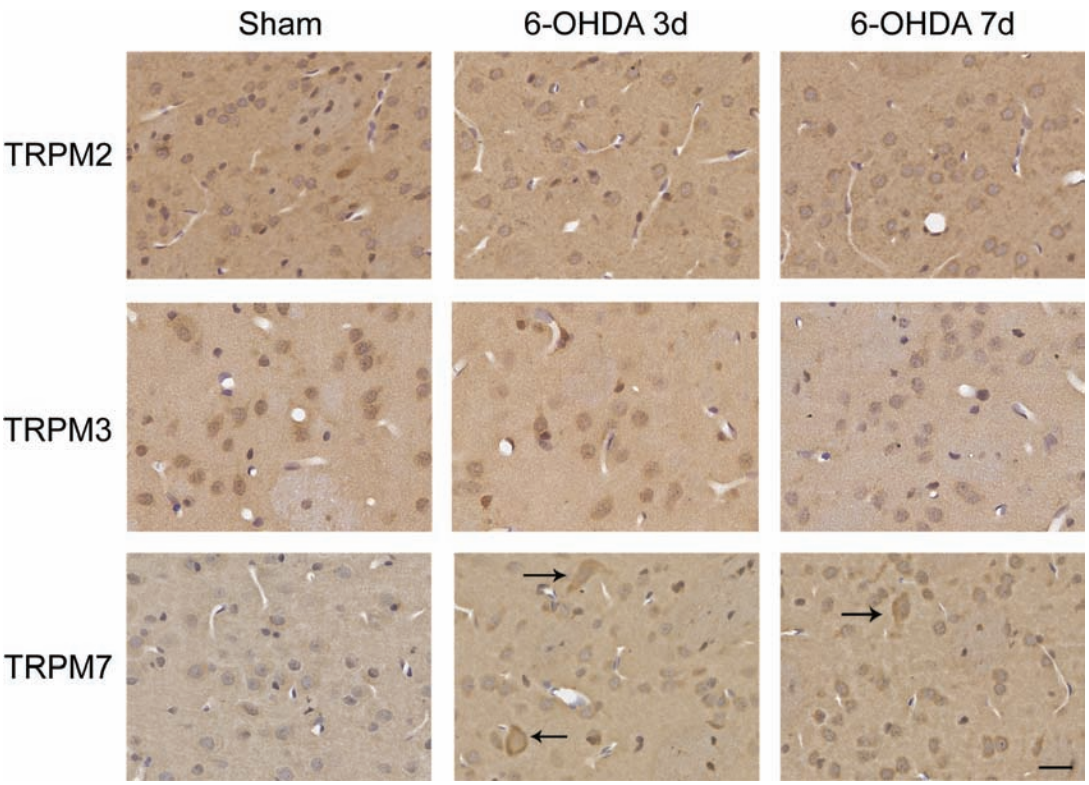

Figure 8.5: TRPM channel immunoreactivity in the striatum of sham and 6-OHDA treated animals. Top row: TRPM2 staining; middle row: TRPM3 staining; bottom row: TRPM7 staining. Colour deconvolution analysis revealed a significant decrease in TRPM3 protein in the 7 day 6-OHDA group compared to shams. A decrease in TRPM3 immunoreactivity can be seen within striatal neurons at this time point. TRPM7 protein was significantly elevated in both 6-OHDA groups compared to shams; this increase in TRPM7 immunoreactivity within striatal neurons is indicated by arrows. Scale bar = 25 μm.

8.4 Discussion

The present study is the first to demonstrate changes in the expression of TRPM channels in relation to PD, indicating that TRPM channels may be important in the pathophysiology of this neurodegenerative disorder.

8.4.1 TRPM2

While the aetiology of PD remains unknown, it is likely to involve such processes as oxidative stress, inflammation, dysregulated Ca^{2+} homeostasis and mitochondrial dysfunction (Thomas, 2009). Considering that TRPM2 has been implicated as a participant in these cellular events, this protein may be significant to PD. For example, TRPM2 is activated in response to oxidative and nitrosative stress (Hara et al., 2002; Wehage et al., 2002), may aggravate inflammation (Yamamoto et al., 2008) and mediates neuronal cell death via unregulated Ca^{2+} influx (Aarts et al., 2003). Moreover, TRPM2 contains an enzymatic domain homologous to a mitochondrial ADPR pyrophosphatase (Perraud et al., 2001) and is activated by ADPR (Perraud et al., 2005). During states of oxidative stress, mitochondria produce ADPR, which may stimulate TRPM2 and lead to rises in intracellular Ca^{2+} and Na^{+} levels

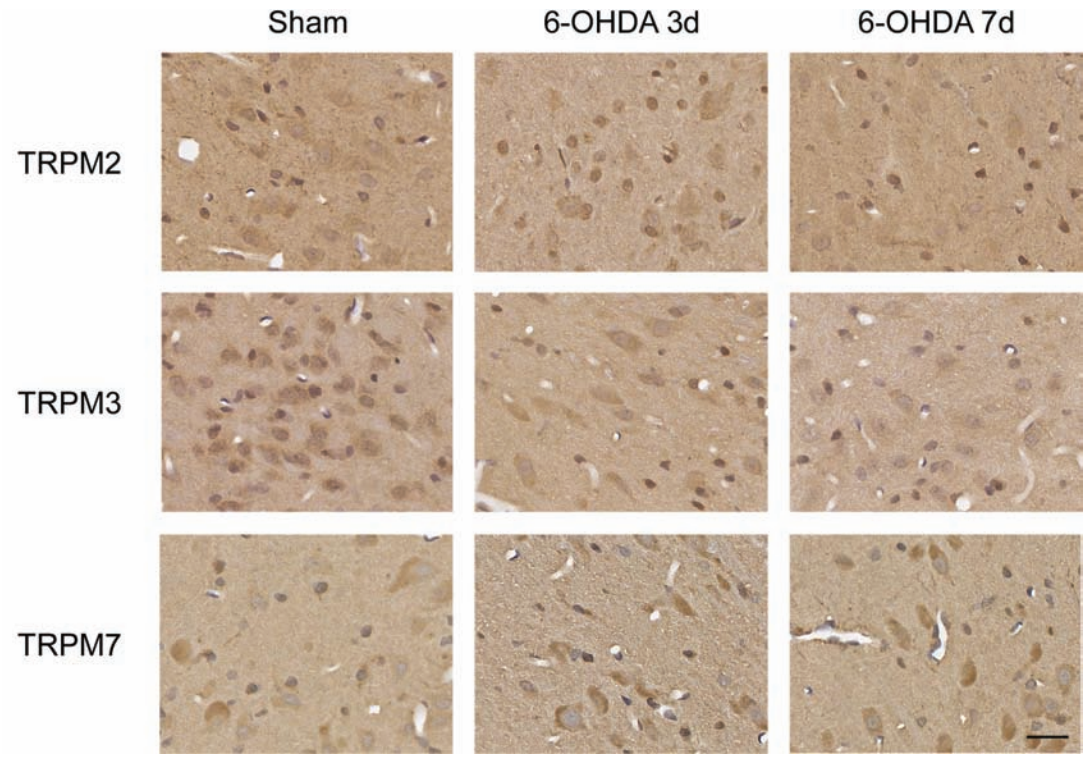

Figure 8.6: TRPM channel immunoreactivity in the SN of sham and 6-OHDA treated animals. Top row: TRPM2 staining; middle row: TRPM3 staining; bottom row: TRPM7 staining. Colour deconvolution analysis showed a significant decrease in TRPM3 protein in the 6-OHDA 7 day group compared to shams. A decrease in TRPM3 immunoreactivity can be seen within striatal neurons at this time point. There were no changes observed in TRPM2 or TRPM7 immunoreactivity. Scale bar = 25 μm.

that could compromise mitochondrial function (Hermosura and Garruto, 2007). A very recent report showed that TRPM2 channels were activated by mitochondrial ROS in SNpc neurons exposed to rotenone, resulting in Ca^{2+} influx (Freestone et al., 2009). Of further significance, the expression of TRPM2 channels was upregulated in astroglia in response to oxidative stress, which was accompanied by an inhibition of protein synthesis (Bond and Greenfield, 2007). Finally, Fonfria et al. (2005) found that H_2O_2 and Aβ peptide caused significant Ca^{2+} influx and cell death in striatal neurons endogenously expressing TRPM2.

Hermosura et al. (2008) have identified a genetic variant of TRPM2 in patients with ALS-G and PD-G. The *TRPM2*^{P1018L} mutation produced TRPM2 channels that were not able to maintain sustained ion influx, resulting in the attenuation of intracellular Ca^{2+} rises in response to H_2O_2. This mutation could contribute to the pathophysiology of neurodegenerative disorders by interfering with Ca^{2+}-dependent downstream signalling pathways, which may have particular significance to the normal function of cells such as microglia (Kraft et al., 2004).

Therefore, strong evidence indicates that TRPM2 may be associated with many processes relevant to PD pathophysiology. How-

ever, the present study is the first to characterise TRPM2 mRNA and protein levels in PD. Based on the findings from previous studies of TRPM2 in CNS disorders, we hypothesised that TRPM2 expression would increase in PD, particularly in the early stages of the disease, where it could contribute to dopaminergic cell death by enhancing oxidative stress and inflammation and providing a pathway for unregulated Ca^{2+} influx.

In contrast to our hypothesis, in the early experimental model of PD (intrastriatal 6-OHDA lesion), there were no changes in TRPM2 mRNA level between PD and sham animals in either the SN or striatum. Immunohistochemistry was also carried out in this experimental model to semi-quantify TRPM2 protein expression in the early stages of PD. In the striatum, there was a trend to increase in TRPM2 protein expression in the 3 day 6-OHDA groups, and a significant elevation in the 7 day group.

Our previous study (E. Thornton, PhD thesis) found significant dopaminergic cell loss in animals with intrastriatal 6-OHDA lesions compared to shams at 10 days following surgery, continuing throughout the assessment period of 21 days. At 7 days post-lesion, a non-significant increase in cell loss was observed. However, lesioned animals displayed significant functional deficits as early as 3 days following 6-OHDA treatment, corresponding to the loss of striatal DA terminals. For the gene expression analysis component of the present study, the number of animals available was limited, and we therefore chose a survival time of 4 days post-6-OHDA administration. This time point was hypothesised to correspond to the early molecular changes in PD preceding severe dopaminergic cell loss. For the immunohistochemistry component, we were interested in studying protein levels at similar time points to the gene expression study, therefore, survival time points of 3 days and 7 days were chosen. In future studies it would be desirable to include additional survival time points to enable a more comprehensive assessment of the molecular changes of early experimental PD.

The results of the present chapter suggest that the role of TRPM2 in PD pathogenesis does not appear to be significant in the very early stages of the disease. This is consistent with other studies of TRPM2 in CNS disorders. In ischaemic stroke (Fonfria et al., 2006a), TRPM2 mRNA level increased, but only after 7 days post-injury. Unpublished results from our laboratory (N. Cook, T. Kleinig, C. Van Den Heuvel and R. Vink) showed that TRPM2 mRNA level did not increase in the first 24 hours following intracerebral haemorrhage. Finally, in the present thesis, TRPM2 expression was elevated between 2 days and 7 days after TBI, but not at the very acute time points (1 hour to 1 day).

In the SN 6-OHDA (late) model of experimental PD, TRPM2 mRNA level showed trends to increase in both the striatum and SN, but due to variability in the 6-OHDA treated groups, these results did not reach statistical significance.

In clinical PD, TRPM2 mRNA level was significantly reduced in the SN in PD patients compared to controls, with a trend to decrease in the caudate nucleus, which almost reached statistical significance (p = 0.06). We cannot discount the possibility that the decreases observed were due to the loss of dopaminergic neurons in these

brain regions. However, given that TRPM2 is also expressed in microglia (Kraft et al., 2004), which become activated and increase in number in PD (Schapira, 2009), the loss of TRPM2 may contribute to PD pathophysiology in an alternative way. The genetic variant of TRPM2, described by Hermosura et al. (2008) in PD-G patients, $TRPM2^{P1018L}$, produced ion channels that could not maintain sustained ion influx. The authors propose that in cells such as microglia, where TRPM2 may be required for normal function (Kraft et al., 2004), the loss-of-function variant could have deleterious consequences and may contribute to neurodegeneration (Hermosura et al., 2008). Whether the decrease in TRPM2 mRNA level in the present study elicits a similar effect remains to be established.

Clearly, more research is required to clarify the role of TRPM2 in PD pathophysiology. However, considering the functions of TRPM2, particularly with regard to its activation by oxidative stress and as a mediator of neuronal cell death, it would be interesting to pursue further studies to determine whether TRPM2 participates in dopaminergic cell death and the processes leading to PD.

8.4.2 TRPM3

To our knowledge, the present thesis is the first to characterise TRPM3 mRNA level and protein expression in relation to any CNS disorder. In Chapter 6, we demonstrated changes in TRPM3 expression following clinical and experimental TBI, while in the present chapter, changes in TRPM3 expression were observed in both models of experimental PD. These novel findings are significant and provide insight into the molecular mechanisms underlying the pathogenesis of these neurological disorders.

As previously discussed, the exact physiological role of native TRPM3 channels, including their function in the brain, is incompletely understood. Despite this, TRPM3 was chosen as a gene and protein of interest in the present thesis due to its relatively high expression in the brain, its chromosomal location and its permeability to Ca^{2+} and Mg^{2+}. Furthermore, like TRPM7, TRPM3 is inhibited by rises in intracellular Mg^{2+} concentration. This is relevant to PD because Mg^{2+} is likely to be associated with the pathogenesis of this disease.

As mentioned, PD patients have reduced Mg^{2+} levels in hair (Forte et al., 2005) and CSF (Bocca et al., 2006) and significantly decreased concentrations of Mg^{2+} in several areas of the brain, including the BG (Yasui et al., 1992). Furthermore, studies in animal models of PD associate a low Mg^{2+} diet with increased vulnerability of dopaminergic neurons to environmental toxins (Muroyama et al., 2009; Oyanagi et al., 2006). Given that TRPM3 is permeable to Mg^{2+}, we hypothesised that TRPM3 expression, along with TRPM7, may increase in PD in an attempt to restore Mg^{2+} homeostasis.

However, contrary to our hypothesis, in the intrastriatal 6-OHDA (early) model of PD, TRPM3 mRNA level was significantly decreased in the striatum and SN in 6-OHDA animals compared to shams (4 day survival). Consistent with these results, TRPM3 protein expression was significantly reduced in both brain areas in the 7 day intrastriatal 6-OHDA group compared to shams, but not in the 3 day group. These results indicate that within 4 days of 6-OHDA lesion to the

striatum, TRPM3 becomes transcriptionally downregulated, resulting in significant reductions in TRPM3 protein levels by day 7. While the exact role of TRPM3 in Mg^{2+} homeostasis in the brain is unclear, the decrease in TRPM3 expression observed herein could contribute to the reduction in Mg^{2+}, or other cations, in dopaminergic neurons, and possibly influence downstream signalling pathways. As mentioned, the function of native TRPM3 channels in the brain is currently unresolved, thus restricting the present discussion to speculation.

Intriguingly, we did find a significant increase in TRPM3 mRNA levels in the SN 6-OHDA late model of PD, supporting our original hypothesis. There was a profound increase in the SN of 6-OHDA lesioned animals to almost 6 times sham levels, something not observed in the striatum. We did not conduct immunohistochemistry studies on late-stage experimental PD tissue, however, this would be interesting to pursue in future studies.

In the clinical PD study, there were no changes in TRPM3 mRNA level in any of the five brain regions studied, however, in the SN, there was a trend to decrease in TRPM3 mRNA levels (p = 0.15). The implications of the trends and changes in TRPM3 expression observed in relation to PD requires further research to establish the exact role that TRPM3 may play in the pathophysiology of this disease. It is not known whether the changes in TRPM3 expression demonstrated in the present chapter contribute to, or are a consequence of, the processes leading to dopaminergic cell death in PD.

A recent report (Wagner et al., 2008) has demonstrated that TRPM3 is directly activated by PS, which was associated with insulin secretion in pancreatic β-cells. This is an interesting finding that supports the suggestion that steroid hormones elicit rapid biological effects via interaction with ion channels, in addition to classic genomic mechanisms (reviewed in Shulman, 2002). The activation of TRPM3 by PS may also be relevance to brain function and, potentially, to the pathogenesis of PD. Although a controversial issue, steroid hormones may play a neuroprotective role in PD, with a higher incidence of PD reported in men than women (Van Den Eeden et al., 2003), which may be attributed to female steroid hormones. A number of studies have been conducted to investigate sex differences in PD (reviewed in Gillies and McArthurs, 2009 and Bourque et al., 2009). A detailed discussion of these findings is beyond the scope of the present thesis, however, it appears that oestrogen and progesterone may exert a neuroprotective effect on striatal dopaminergic neurons. It is interesting to speculate that TRPM3 may participate in these processes. However, it is not clear whether progesterone and oestrogen are able to activate TRPM3 in addition to PS, or if PS is a physiologically relevant activator of TRPM3 (Nilius and Voets, 2008).

8.4.3 TRPM7

The ubiquitously expressed TRPM7 is an intriguing protein with a number of cellular functions. Of particular importance is the observation that TRPM7 is required for cell viability (Nadler et al., 2001) and is likely to regulate Mg^{2+} homeostasis in vertebrate cells (Schmitz et al., 2003). TRPM7 channel activity is inhibited by intracellular Mg^{2+} and is strongly activated when Mg^{2+} is depleted (Kozak and Cahalan, 2003; Nadler et al.,

2001).

Hermosura et al. (2005) reported a missense mutation in the TRPM7 gene, *TRPM7*^{T1482I}, in a subgroup of ALS-G and PD-G patients but not in matched controls. The protein encoded by this variant (where threonine is replaced by isoleucine at position 1482) displays a higher sensitivity to inhibition by levels of intracellular Mg^{2+}. Thr1482, which lies between the channel and kinase domains of TRPM7, is evolutionarily conserved between many species, and phosphorylation of threonine in this position is likely to be important for channel function. Isoleucine cannot be phosphorylated, therefore, the mutant allele found in ALS-G and PD-G patients could potentially confer a functional deficit. Given that TRPM7 is likely significant in maintaining homeostasis of Mg^{2+} and Ca^{2+}, the authors propose that the higher sensitivity to Mg^{2+} of the TRPM7 variant, combined with the Mg^{2+}- and Ca^{2+}-deficient environment, could result in severe cellular deficiencies of these metal ions, which may contribute to the aetiology of neurodegenerative diseases (Nilius et al., 2007; Hermosura et al., 2005).

Of further significance, Oyanagi et al. (2006) investigated the effects of a low Mg^{2+} and/or low Ca^{2+} diet in rats over two generations, in order to simulate the actual conditions of human life on Guam, where several generations live in the same environment. The authors report that, over generations, a continuous Mg^{2+} deficiency (one-fifth of the normal level) led to a significant loss of dopaminergic neurons of the SN. These effects were only observed in rats exposed to a low Mg^{2+} diet constantly from the foetal and newborn stages to the prime of life, and were more pronounced in the Mg^{2+}-deficient group than the Mg^{2+}- and Ca^{2+}-deficient group. These findings support a role for low Mg^{2+} intake in the pathogenesis of PD-G.

Considering that low Mg^{2+} may also be involved in the pathophysiology of sporadic PD, we sought to investigate whether changes in TRPM7 expression would occur in clinical and experimental PD cases. The present study is the first to characterise TRPM7 mRNA and protein levels in relation to PD. We hypothesised that TRPM7 expression would increase in PD as a possible means in which to compensate for reductions in Mg^{2+}, particularly in the early stages of the disease.

In the early experimental model of PD, there were no changes in TRPM7 mRNA level between intrastriatal 6-OHDA treated animals and shams (4 day survival). However, increases in TRPM7 protein expression were observed in the striatum of 6-OHDA animals at both 3 days and 7 days following surgery. There were no changes in TRPM7 protein levels in the SN. The increases in TRPM7 protein in the striatum is an interesting result, particularly because transcript levels were not similarly elevated. This does not necessarily indicate a lack of correlation between mRNA and protein levels, because the time point examined in the gene expression study (4 days) lies between the two time points of the protein study (3 and 7 days). It is possible that TRPM7 mRNA level was upregulated at some point prior to the 4 day time point, as well as afterwards, resulting in the increases in TRPM7 protein seen at 3 and 7 days. These results also suggest that sometime between 3 days and 7 days following 6-OHDA administration, TRPM7 protein expression may have

decreased, given that the mRNA level was not elevated at 4 days. We can only speculate about the expression pattern of TRPM7 but it would be interesting for future studies to further investigate this issue.

In the late model of PD, there were significant increases in TRPM7 mRNA level in both the SN and striatum of 6-OHDA treated animals compared to shams (1 day survival). At the time of writing, late-stage 6-OHDA FFPE tissue was just being generated in our laboratory; therefore, a future study could carry out TRPM7 immunohistochemistry using this tissue to determine whether TRPM7 protein is also elevated in this model.

These increases in TRPM7 expression observed in PD could be related to Mg^{2+} homeostasis. Mg^{2+} is essential to many cellular processes and, consequently, dysregulated Mg^{2+} handling is associated with a number of pathophysiological states (Konrad et al., 2004). For example, low Mg^{2+} concentrations may exacerbate oxidative stress and promote inflammatory changes (Mazur et al., 2006; Blache et al., 2006; Altura et al., 2003), factors which are likely to be relevant to dopaminergic cell death in PD. As discussed, several groups have identified reductions in Mg^{2+} levels in PD patients (Bocca et al., 2006; Forte et al., 2005; Yasui et al., 1992), and studies in animal models have associated low dietary Mg^{2+} with increased vulnerability of dopaminergic neurons to environmental toxins (Muroyama et al., 2009; Oyanagi et al., 2006). Notably, Mg^{2+} administration was able to inhibit MPP^{+}-induced toxicity in cultured rat dopaminergic neurons (Hashimoto et al., 2008).

Given that TRPM7 has been proposed to regulate Mg^{2+} homeostasis via Mg^{2+} influx (Wolf, 2004) and is strongly activated by low levels of intracellular Mg^{2+} (Nadler et al., 2001), it is possible that the increases in TRPM7 expression observed in PD are an attempt to restore intracellular Mg^{2+} concentrations. However, these increases in TRPM7 could be deleterious to dopaminergic neurons, because TRPM7 also provides a pathway for Ca^{2+} and toxic trace metals, including Fe^{2+}, to enter cells (Monteilh-Zoller et al., 2003). Fe^{2+} influx through TRPM7 may be particularly relevant to neurodegeneration considering its association with α-synuclein deposition and oxidative stress in PD (Kozlowski et al., 2009; Molina-Holgado et al., 2007). Of further significance, TRPM7 may be involved in the pathophysiology of another neurodegenerative disorder, AD. AD is likely to include an oxidative stress component, in which Aβ plays a critical role (Barnham et al., 2004). The production of ROS by Aβ may activate TRPM7 (and TRPM2), resulting in excess Ca^{2+} influx that may damage neurons (Yamamoto et al., 2007; Fonfria et al., 2005). In addition, TRPM7 is permeable to Zn^{2+} (Monteilh-Zoller et al., 2003), which is associated with AD and can be highly toxic to neurons (Bush, 2006).

TRPM7 has also been implicated as a mediator of anoxic neuronal death (Aarts et al., 2003). The exact mechanism by which this occurs remains to be clarified, but appears to involve a positive feedback loop whereby Ca^{2+} entry into cells as a result of ischaemic injury causes the production of free radicals, which activate TRPM7, leading to further Ca^{2+} influx and additional free radical production (Aarts and Tymianski, 2005b). Although these processes were described in relation to ischaemia, it is possible that TRPM7

may also promote dopaminergic cell death in PD in a similar manner. Initially, low Mg^{2+} concentrations would activate TRPM7 channels and enhance Ca^{2+} entry through NMDAR, TRPM7 and possibly TRPM2. This could lead to the positive feedback loop described by Aarts and Tymianski (2005b), resulting in cell death (see also Figure 6.5 in Chapter 6). Furthermore, ROS production as a result of low Mg^{2+} concentration could further activate TRPM7, thereby enhancing inflammation, oxidative stress and cell death (Altura et al., 2003).

In the clinical component of the present study, TRPM7 mRNA level was significantly reduced in the SN of PD patients, with no changes observed in the GP, caudate nucleus, putamen or MTG. It is possible that the decrease observed in the SN is a consequence of the degeneration of dopaminergic neurons in PD patients. However, TRPM7 is ubiquitously expressed (Nadler et al., 2001); therefore, it is also be present in glial cells (Jiang et al., 2003). A decrease in TRPM7 expression in PD may have detrimental effects to cells dependent on cation influx through this channel, as well as second messenger pathways induced by the TRPM7 kinase domain.

Finally, it should be noted that RNA was extracted from a homogenate of approximately 50 mg tissue from each brain area, and thus, cells other than dopaminergic neurons were included in the analysis. Recent studies have used laser capture microdissection to isolate single dopaminergic neurons for analysis (Simunovic et al., 2009; Gründermann et al., 2008). This technique was not available for the present study, however, would be useful to pursue in future studies in order to target the molecular processes occurring specifically within dopaminergic neurons in PD.

8.4.4 Conclusions

The present chapter is the first study to demonstrate changes in the expression of TRPM2, TRPM3 and TRPM7 at both the protein and transcript level following experimental and clinical PD. These results indicate that TRPM channels may be involved in the pathophysiology of PD, and it is possible that these proteins may represent novel therapeutic targets for PD. However, whether TRPM channels directly participate in pathological processes leading to dopaminergic cell death, or whether changes in their expression are a consequence of neuronal degeneration, requires further investigation. Thus, additional studies of the potential role of TRPM channels in PD pathogenesis are warranted.

Chapter 9

General Discussion

The pathophysiological mechanisms underlying TBI and PD remain incompletely understood. One approach to increase our understanding of these complex neurological disorders is to investigate changes at the molecular level, including gene and protein expression analyses. Accordingly, the present thesis has addressed the aims of characterising the gene and protein expression of the neuropeptide, SP, and members of the TRPM channel family in TBI and PD. We demonstrate changes in the expression of SP and TRPM channels that may be significant to the pathogenesis of these neurological disorders. The results presented herein will contribute to unravelling the molecular mechanisms underlying TBI and PD and ultimately to the development of novel treatment strategies.

TBI and PD confer a significant socioeconomic burden and effective neuroprotective therapies are urgently required. TBI is a leading cause of death and disability and particularly impacts individuals under 40 years of age. The neurological dysfunction resulting from TBI is due to both direct, immediate mechanical damage to brain tissue and delayed, secondary injury processes (Morales et al., 2005). Secondary injury involves a series of complex biochemical changes that are triggered by the primary event and may continue for days to weeks after the insult (Roth and Farls, 2000). These changes include disruption to the BBB, oedema, ischaemia, inflammation, excitotoxicity, oxidative stress, Mg^{2+} decline and mitochondrial dysfunction, all of which can be deleterious to neuronal cells (Barone and Kilgore, 2006; Golding, 2002; Cormio et al., 1997; Gentile and McIntosh, 1993). Secondary injury factors are associated with significant morbidity and mortality following TBI (Gentile and McIntosh, 1993), however, since they manifest over time, these processes may be amenable to pharmacological intervention (Werner and Engelhard, 2007).

PD is the second most common neurodegenerative disorder, affecting approximately 1 % of people aged over 60 years, and is increasing in prevalence as the population ages (Yamawaki et al., 2009; De Lau and Breteler, 2006). The neuropathological features of PD include the loss of dopaminergic neurons in the SNpc and intracytoplasmic protein aggregates known as Lewy bodies, of which α-synuclein is the main component (Thomas and Beal, 2007). The degeneration of dopaminergic neurons in the SNpc results

in a reduction of DA levels in the striatum (Hald and Lotharius, 2005). DA is required for motor neurons to co-ordinate movement and its depletion leads to the classic motor symptoms of PD: resting tremor, rigidity, bradykinesia and postural instability (Braak and Del Tredici, 2008). Research over recent decades has identified a number of pathophysiological processes that may be associated with the degeneration of dopaminergic neurons and the onset of PD, including inflammation, oxidative stress, mitochondrial dysfunction, abnormal protein handling and Ca^{2+} dysregulation (Thomas, 2009). These processes are likely to be influenced by genetic susceptibility and environmental factors (Huang et al., 2004).

Although TBI and PD represent distinct aetiologies and pathogeneses, several processes appear to be relevant to neuronal cell death in both disorders, such as inflammation, oxidative stress, excitotoxicity, mitochondrial dysfunction, BBB dysfunction, and Mg^{2+} decline. Moreover, recent studies from our laboratory have implicated the release of SP in the development of neurological deficits in both TBI and PD. In rodent TBI, SP immunoreactivity was elevated following injury and was associated with BBB dysfunction, oedema formation and functional deficits (Donkin et al., 2009). In our studies of early experimental PD, SP release was increased in 6-OHDA lesioned animals and exacerbated dopaminergic cell death, thereby promoting disease progression (E. Thornton, PhD thesis). In both studies, a SP receptor antagonist attenuated the neurological deficits and improved outcome.

To date, no studies have investigated whether SP is transcriptionally regulated in experimental or clinical TBI, nor have SP protein levels been examined in clinical TBI cases; these constituted some of the aims of the present thesis. Furthermore, no studies have measured SP mRNA levels in PD using quantitative, real-time RT-PCR. We therefore aimed to achieve this in clinical PD cases as well as in two rodent models of experimental PD (representing early and late-stage PD).

Reference Gene Validation

Real-time RT-PCR was used to characterise mRNA levels of SP in clinical and experimental TBI and PD. As reviewed in Chapter 2, real-time RT-PCR is the method of choice for quantifying mRNA transcripts, due to its wider dynamic range of quantification, higher sensitivity and precision, and a decreased risk of contamination compared to gel-based PCR (Klein, 2002; Bustin, 2000). It requires an appropriate normalisation strategy to control for error, the most common being the use of one or more endogenous reference genes (Nolan et al., 2006). A reference gene should be expressed at a stable level regardless of the experimental context under investigation (Stürzenbaum and Kille, 2001), however, the expression of reference genes may vary considerably. Indeed, some commonly used reference genes may be unsuitable for normalising real-time RT-PCR data in certain situations (Gubern et al., 2009; Olsvik et al., 2005; Bas et al., 2004). Previous studies have highlighted the need to validate reference genes for each new experimental condition (Derks et al., 2008; Gutierrez et al., 2008; Dheda et al., 2005). Normalisation of real-time RT-PCR data using a single, non-validated reference gene may lead to incorrect data interpretation (Bustin et al.,

2009). In contrast, normalisation to the geometric mean of the expression of multiple reference genes (Vandesompele et al., 2002) is considered to be a reliable and conservative approach (Wong and Medrano, 2005).

Recent studies employing quantitative real-time RT-PCR in TBI and PD have generally used a single reference gene for normalisation, usually without including a reference gene validation protocol (for example, Simunovic et al., 2009; Brown et al., 2008; Yao et al., 2008; Shehadeh et al., 2008; Shein et al., 2007). In Chapter 4, the implications of using a single reference gene for data normalisation in experimental TBI were demonstrated (see also Cook et al., 2009a). Data regarding SP gene expression were initially normalised to each of seven candidate reference genes individually. Using this approach, SP mRNA level was highly variable depending on which reference gene was utilised as a normalising factor. Thus, reference gene validation was considered a vital prerequisite to gene expression analysis in the present thesis.

Accordingly, the stability of our candidate reference genes was evaluated using geNorm (Vandesompele et al., 2002), which allowed us to identify appropriate panels of reference genes for data normalisation in each distinct experimental condition of the study. The variables taken into account included the different neurological conditions (TBI and PD), species (human and rat) and the diverse brain regions of interest in each study. As discussed in Chapter 4, we found that the stability of a candidate reference gene in one brain area did not necessarily confer stability in another, even within the same disease and species. For example, in the human PD study, where five different brain areas were investigated, B2MG was one of the two most stable reference genes in every brain area except the GP, where it ranked fifth. In addition, the panel of stable genes identified in the rat cerebral cortex following TBI were different to those in the rat hippocampus. Therefore, it is likely that the use of a single reference gene would be inadequate for normalising real-time RT-PCR data when investigating gene expression in TBI and PD. Such findings highlight the importance of careful selection and validation of reference genes to be used for real-time RT-PCR normalisation. Consequently, reference gene validation has now become standard practice in our laboratory.

SP in Acute and Chronic Neurological Disorders

Once we had established suitable panels of reference genes that would allow us to accurately normalise our gene expression data, we proceeded with real-time RT-PCR assays for our genes of interest.

In Chapter 5, SP mRNA level was quantified in clinical TBI cases and over a time course of experimental TBI in rats. As expected, SP mRNA level was elevated in the cerebral cortex and hippocampus of TBI rats compared to shams, correlating with our previous study (Donkin et al., 2009) that identified an increase in SP immunoreactivity following experimental TBI. These results suggest that SP may be involved in TBI pathophysiology. Indeed, SP exerts a number of biological effects relevant to TBI, particularly with regard to inflammatory processes and cerebral oedema. SP is able to elicit vasodilation, extravasation of plasma proteins

and oedema (neurogenic inflammation), in both the CNS and PNS (Vink et al., 2003; Black, 2002; Alves et al., 1999). SP primes neutrophils and macrophages for oxidative burst (Lloyds and Hallett, 1993; Hartung and Toyka, 1983) and activates platelets (Gecse et al., 1996). In addition, SP has been shown to induce the production of inflammatory cytokines in immune cells, including TNF-α, IL-1β, IL-2 and IL-6 (Delgado et al., 2003). SP can also stimulate mast cells to release histamine and serotonin (Reynier-Rebuffel et al., 1994; Ebertz et al., 1987; Irman-Florjanc and Erjavec, 1983). These factors are likely to be highly relevant to TBI because histamine, serotonin, TNF-α, IL-1β, IL-6 and NO can all impair BBB function, many of which elicit effects from both the blood and brain tissue sides (Abbott et al., 2006). Our previous study (Donkin et al., 2009) also measured a significant increase in plasma SP concentration in TBI rats 30 mins after injury. These results indicate that SP is released early after TBI and enters the bloodstream, where it could initiate an inflammatory cascade that exacerbates the injury process. The increase in brain concentration of SP over subsequent hours in experimental TBI is likely to continue this deleterious process, promoting neurogenic inflammation and oedema that may lead to neuronal cell death.

In the human TBI study, there were significant decreases in SP immunoreactivity in the cortex and hippocampus of human TBI cases in both survival groups (up to 24 hours), in contrast to our hypothesis that SP expression would increase after injury. It is possible that the decreases in SP immunoreactivity observed in clinical TBI could be attributed to haemorrhage or ischaemia, at least one of which was present in every clinical TBI case selected for the present study. Our laboratory has shown that SP content does not increase during ischaemia (R. Turner, unpublished results), nor in experimental subarachnoid haemorrhage (C. Barry, unpublished results). The exact reason for this is unknown. However, the findings of the present thesis may indicate that in the first 24 hours following TBI in human cases, SP does not play a significant role in the deleterious secondary injury processes. Importantly, the results presented herein also underscore the inherent differences between experimental and clinical TBI. The impact-acceleration model of rodent TBI used in the present study produces diffuse axonal injury in the absence of haemorrhage, hypertension, significant brainstem damage or death (Marmarou et al., 1994), while the degree of injury in the clinical cases was severe enough to result in patient death. As mentioned, clinical assessments carried out by neuropathologists reported haemorrhage and/or ischaemia in all clinical TBI cases. Furthermore, experimental animals are sacrificed at specific time points, while time of death in clinical cases can often be less precise. Therefore, experimental models may not always correlate completely with clinical observations, particularly when heterogeneous pathologies such as TBI are being investigated.

In Chapter 7, transcript levels of SP were quantified in both experimental and clinical PD. In the intrastriatal 6-OHDA (early) model of experimental PD, SP mRNA level showed a trend to increase in the SN and striatum of 6-OHDA lesioned animals com-

pared to shams. These results are consistent with our previous study demonstrating an increase in SP expression in the early stages of PD (E. Thornton, PhD thesis), which was associated with neuroinflammatory changes (reactive astrocytes and microglia), BBB dysfunction and degeneration of dopaminergic neurons and terminals. SP may therefore be significant to the pathophysiology of early PD by contributing to disease progression. The role of SP in initiating neurogenic inflammation and stimulating an inflammatory cascade, as discussed above in relation to TBI, is also highly relevant to PD. Furthermore, SP may promote the release of glutamate (Marti et al., 2005), leading to excitotoxicity. SP may also enhance oxidative stress by stimulating the excess release of DA (Humpel et al., 1991), which could then undergo autooxidation. All of these processes could contribute to the loss of dopaminergic neurons in early PD.

In clinical PD, we observed a trend to decrease in SP mRNA level in the SN of PD cases compared to controls. These results correspond to the decreases in PPT mRNA levels and SP immunoreactivity in the SN of PD patients reported in previous studies (Nisbet et al., 1995; Tenovuo et al., 1984; Mauborgne et al., 1983), and support the hypothesis that depletion of SP in the SN may be important in PD pathogenesis (Chen et al., 2004; Barker, 1991). In late-stage experimental PD, although the present study found no changes in SP mRNA level between SN 6-OHDA lesioned animals and shams, another recent study from our laboratory showed a decrease in SP immunoreactivity specifically in the SNpc, but not across the entire SN (M. Hassall, Honours thesis). Considering that the gene expression component of the present thesis analysed a homogenate of tissue representing the entire SN and part of the surrounding BG, whereas immunohistochemistry enabled the differentiation of specific brain regions, this is likely to account for the difference in results. While the exact role of SP in PD requires further investigation, it is interesting that the changes in SP expression are more pronounced in specific areas of the BG than others, and may vary depending on the stage of the disease. This could be an important factor in determining how SP may contribute to the progression of PD. Mauborgne et al. (1983) suggest that the loss of SP immunoreactivity in the SN could be a metabolic consequence of SN dopaminergic cell degeneration; indeed, it is likely that striatal DA innervation is required to maintain basal SP levels (Cruz and Beckstead, 1989).

The results of the present thesis thus support a role for SP in both TBI and PD. Taken together with the findings of our previous studies (Donkin et al., 2009; E. Thornton, PhD thesis; R. Turner, PhD thesis), we provide strong evidence implicating SP release in the pathogenesis of both acute and chronic neurological disorders.

TRPM Channels in Acute and Chronic Neurological Disorders

The present thesis also focused upon characterising the expression of members of the TRPM family of ion channels in relation to acute and chronic neurological disorders.

In Chapter 6, we characterised TRPM channel expression, specifically, TRPM2, TRPM3, TRPM6 and TRPM7, at the transcript and protein level in clinical and experimental TBI. We provide the first evidence of changes

in TRPM channel mRNA and protein expression following TBI and propose that these proteins may be important in the secondary injury processes associated with TBI.

In previous studies of acute brain injury, TRPM7 and TRPM2 have been implicated in playing direct roles in ischaemic neuronal death (Aarts et al., 2003). TRPM7 has been suggested to mediate cell death via a positive feedback loop whereby Ca^{2+} entry into cells as a result of injury causes the production of free radicals, which activate TRPM7, leading to further Ca^{2+} influx and additional free radical production (Aarts and Tymianski, 2005b). Several lines of evidence indicate that the activation of TRPM2 by oxidative stress results in cell death via unregulated Ca^{2+} influx (Kaneko et al., 2006; Zhang et al., 2003; Hara et al., 2002), and TRPM2 has also been implicated in inflammation (Yamamoto et al., 2008). Importantly, a decline in intracellular Mg^{2+} concentration, a well established phenomenon following TBI, can lead to the generation of ROS (Altura et al., 2003), which could further activate TRPM7 (as well as TRPM2), thereby exacerbating inflammation, oxidative stress and cell death pathways.

Of further significance, transcript levels of TRPM2 were elevated (Fonfria et al., 2006a) and the expression of TRPM7 was shown to increase (Jiang et al., 2008) following experimental stroke. However, the present study is the first to characterise TRPM channel expression in TBI.

In Chapter 6, TRPM7 expression was shown to be significantly elevated in the cerebral cortex of TBI animals as well as in clinical TBI. These increases suggest that TRPM7 may be involved in neuronal death following TBI, possibly by participating in the Ca^{2+}- and ROS-mediated positive feedback loops proposed by Aarts and Tymianski (2005b). Alternatively, increases in TRPM7 expression could be an attempt to restore TBI-induced depletions of intracellular Mg^{2+}. As discussed, changes in TRPM7 expression could have serious deleterious consequences to neurons; a downregulation in TRPM7 expression could be detrimental to cells by contributing to Mg^{2+} dysregulation, while an increases in TRPM7 channels could lead to Ca^{2+}-mediated neuronal cell death as well as the entry of toxic trace metals such as Zn^{2+}.

TRPM2 expression was similarly elevated at both the protein and transcript level in experimental TBI. Interestingly, the upregulation of TRPM2 protein did not occur until 2 days post-TBI, and was not observed in clinical TBI cases (up to 24 hour survival). These findings suggest that the role of TRPM2 in TBI pathophysiology may not be significant in the first 24 hours of injury. However, from day 2 until at least day 7 following experimental TBI, TRPM2 may also contribute to neuronal cell death in a similar manner to TRPM7 by enhancing oxidative stress and inflammation.

We observed increases in the expression of TRPM6 following experimental TBI, and changes in TRPM3 were also detected. At the present moment, the role of these proteins in brain function is not well understood, and further investigation is needed to determine how TRPM6 and TRPM3 could contribute to TBI pathophysiology.

In Chapter 8, transcript levels of TRPM channels were characterised in clinical and experimental PD, and immunohistochemistry was used to semi-quantify TRPM chan-

nel expression in the rodent model of early PD. We examined TRPM2, TRPM3 and TRPM7 in this chapter, as it has yet to be determined whether TRPM6 is localised in brain regions relevant to PD.

TRPM channels were of interest in the present study because recent studies have identified TRPM7 and TRPM2 as potential susceptibility genes for ALS-G and PD-G. Hermosura et al. (2005) reported a missense mutation in the TRPM7 gene, *TRPM7*^{T1482I}, in ALS-G and PD-G patients but not in matched controls. The protein encoded by this variant displays a higher sensitivity to inhibition by levels of intracellular Mg^{2+}. Given that TRPM7 is likely a significant regulator of Mg^{2+} homeostasis, and possibly Ca^{2+}, this genetic variant could result in severe cellular deficiencies of these metal ions and may contribute to the aetiology of neurodegenerative disorders (Nilius et al., 2007; Hermosura et al., 2005). The same group (Hermosura et al., 2008) subsequently identified a missense mutation in the TRPM2 gene, *TRPM2*^{P1018L}, in ALS-G and PD-G patients. The channels of these TRPM2 variants do not maintain sustained ion influx, resulting in the inhibition of intracellular Ca^{2+} rises. The genetic variant of TRPM2 could contribute to the pathophysiology of neurodegenerative disorders by interfering with vital Ca^{2+}-dependent downstream signalling pathways, particularly in cells such as microglia.

In Chapter 8 of the present study, there was a significant decrease in TRPM2 mRNA level in the SN of PD patients compared to controls. Considering that TRPM2 is expressed in microglia, and may be required for normal function of these cells (Kraft et al., 2004), this reduction could potentially have deleterious consequences, similar to those described by Hermosura et al. (2008) in relation to the loss-of-function TRPM2 variant.

In experimental PD, we demonstrated a significant increase in TRPM7 expression, as well as trends to increase in TRPM2. TRPM7 has been proposed to regulate Mg^{2+} homeostasis via Mg^{2+} influx (Wolf, 2004) and is strongly activated by low levels of intracellular Mg^{2+} (Kozak and Cahalan, 2003; Nadler et al., 2001). Considering that Mg^{2+} concentrations are reduced in PD patients (Bocca et al., 2006; Yasui et al., 1992) and in experimental PD animals (Muroyama et al., 2009; Oyanagi et al., 2006), it is possible that these increases in TRPM7 expression are an attempt to restore intracellular Mg^{2+} concentrations. However, these increases in TRPM7 (and TRPM2) could also be deleterious to dopaminergic neurons, because these ion channels provide a pathway for Ca^{2+} to enter cells. As discussed, TRPM7 is permeable to toxic trace metals, including Fe^{2+} (Monteilh-Zoller et al., 2003). Fe^{2+} influx through TRPM7 may be particularly relevant to neurodegeneration considering its association with α-synuclein deposition and oxidative stress in PD (Molina-Holgado et al., 2007; Kozlowski et al., 2009).

Changes in the expression of TRPM3 were also observed in experimental PD. The function of TRPM3 in the brain remains to be established, thus, how these changes may contribute to PD pathogenesis requires further investigation. Nevertheless, the present thesis has identified novel factors that may be associated with the molecular mechanisms underlying PD and will form the basis of future studies.

An Interrelationship Between SP and TRPM Channels?

It is also interesting to consider the potential interrelationship between SP and TRPM channel expression in acute and chronic neurological disorders.

In the present thesis as well as in our previous study (Donkin et al., 2009), we observed increases in SP mRNA level and immunoreactivity, respectively, in experimental TBI. Donkin et al. (2009) demonstrated that SP release following TBI was associated with functional deficits, BBB breakdown and oedema and contributed to poor neurological outcome in TBI animals. With regard to PD, our previous study (E. Thornton, PhD thesis) demonstrated an increase in SP expression in early PD that accelerated disease progression by promoting neuroinflammation and BBB dysfunction, thus contributing to dopaminergic cell death.

Interestingly, in the present thesis, TRPM7 expression was elevated in TBI animals as well as in 6-OHDA lesioned PD animals. As discussed, an increase in TRPM7 channels may exacerbate oxidative stress and cause unregulated Ca^{2+} influx as well as allowing the entry of toxic trace metals into neurons; these processes could have deleterious effects in TBI and PD.

Furthermore, low concentrations of Mg^{2+} are a feature of both TBI and PD, and TRPM7 is likely to be a key regulator of Mg^{2+} homeostasis in vertebrate cells. Previous studies have demonstrated that Mg^{2+} deficiency evokes an inflammatory response (Malpuech-Brugère et al., 2000), including the release of pro-inflammatory cytokines and SP (Mazur et al., 2006). Indeed, within one week of Mg^{2+} deficiency, plasma SP levels were elevated, which was associated with rises in IL-1, IL-6, TNF-α and free radical-mediated tissue injury (Weglicki and Phillips, 1992), as well as the development of neurogenic inflammation (Weglicki et al., 1994). Moreover, a SP receptor antagonist improved the functional recovery of Mg^{2+} deficient rats following cardiac ischaemia-reperfusion injury (Kramer et al., 1997). Therefore, strong evidence suggests that Mg^{2+} deficiency promotes SP release, which could exacerbate inflammatory events and oxidative and nitrosative stress (Kramer et al., 2009). As discussed, low intracellular Mg^{2+} activates TRPM7 channels, which could further enhance these processes.

Taking these factors into consideration with regard to the present thesis, the interplay between SP release, upregulation of TRPM7 channels and persistent low Mg^{2+} could represent a significant pathophysiological event in acute and chronic neurological disorders, by creating a neurotoxic environment whereby neuroinflammation, oxidative stress, excitotoxicity and other factors promote cell death (see Figure 9.1).

In addition, it is possible that the differences in SP and TRPM7 expression between the TBI cerebral cortex and hippocampus could contribute to the regional differences in vulnerability to injury. The hippocampus contains high levels of NMDA receptors (Herron et al., 1986), which is likely to influence its particular susceptibility to damage in TBI. We demonstrated increases in SP and TRPM7 channel expression in the hippocampus following experimental TBI. As shown in Figure 9.1, SP is able to activate NMDA receptors, which may lead to increased Ca^{2+} influx and production of free radicals, leading to stimu-

lation of TRPM7 channels and neuronal cell death. Given the high density of NMDA receptors in the hippocampus, this could represent one mechanism conferring high sensitivity of hippocampal neurons to injury, and is one pathway whereby SP and TRPM channels may interact to exacerbate injury. Further investigations are required to elucidate the potential molecular mechanisms of SP and TRPM channel interaction in CNS disorders.

Conclusions

The present thesis has characterised the transcript and protein expression of SP and TRPM channels in TBI and PD. We have demonstrated changes in the expression of SP and TRPM channels that may be relevant to the pathophysiology of these disorders. Furthermore, this is the first study to consider the potential interrelationship between SP and TRPM channels with regard to CNS disorders. Future studies focusing on how SP and TRPM channels may contribute to CNS pathophysiology are justified and will build on the results presented herein. Importantly, our results provide insight into the molecular processes underlying TBI and PD and will contribute to the development of effective treatments in the future.

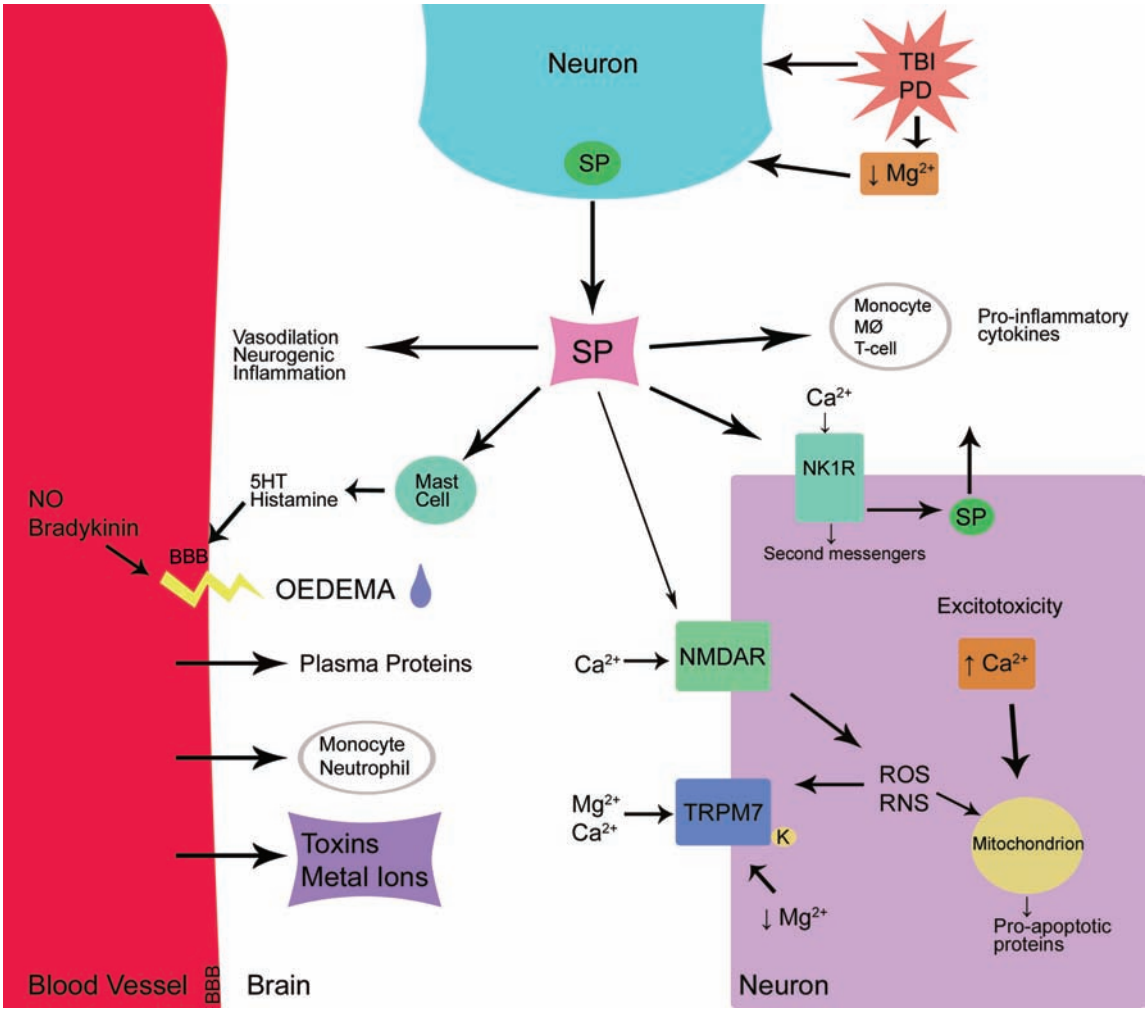

Figure 9.1: Potential interaction between SP and TRPM7 in acute and chronic CNS disorders. Our laboratory has demonstrated an increase in SP release in experimental TBI and PD. These neurological disorders are associated with low Mg^{2+} concentrations, which also triggers the release of SP. SP has a number of neuroinflammatory functions, including stimulating the release of histamine and serotonin (5HT) from mast cells, which can compromise the BBB along with nitric oxide (NO) and bradykinin. SP is a potent initiator of neurogenic inflammation (vasodilation, plasma protein extravasation and oedema) and disruption to the BBB results in the entry of toxins, metal ions and inflammatory cells into the brain. SP can also stimulate immune cells to release pro-inflammatory cytokines, resulting in further inflammation. The binding of SP to the NK-1R can promote further SP release in a positive feedback loop (autoreceptor pathway). Additionally, NK-1R activation stimulates second messenger pathways, resulting in Ca^{2+} entry to neurons. Since SP also activates NMDA receptors, Ca^{2+} influx through these channels may lead to excitotoxicity and the production of free radicals such as peroxynitrite, which can be highly toxic to cellular macromolecules. Free radicals and low Mg^{2+} concentrations activate TRPM7, leading to further Ca^{2+} influx and possibly mitochondrial dysfunction. In PD, SP also stimulates DA release (not shown), which can lead to further SP release in a positive feedback loop via the binding to DA receptors, potentially also leading to oxidative stress, which would further activate TRPM7. Finally, toxic trace metals may enter neurons via TRPM7 channels. Thus, SP release is relevant to CNS disorders and can result in inflammation, BBB breakdown, excitotoxicity and oxidative stress. These pathways are likely to activate TRPM7 channels. Overactivation of TRPM7 channel and kinase (K) activity may lead to neuronal cell death. Therefore, prolonged Mg^{2+} decline, increased SP release and TRPM7 activation may represent critical events leading to cell death in CNS disorders. Mϕ, macrophage.